Identification and characterization of novel skeletal stem cell populations in mice and humans

Stephanie Farhat

A thesis submitted in partial fulfillment of the requirements for the

Doctorate in Philosophy degree in Cellular and Molecular Medicine

Department of Cellular and Molecular Medicine

Faculty of Medicine

University of Ottawa

Table of Contents

Acknowledgements

I would like to thank my supervisor Dr. Daniel Coutu for accepting me in his lab, his guidance and mentorship have helped me grow as a scientist. I am also grateful for having the opportunity to learn his cutting edge and advanced techniques, and most importantly I thank him for his patience, constant help, and support throughout these years with my project.

A special thank you to all my TAC members, Dr. Cathy Tsilfidis, Dr. Michael Rudnicki and Dr. Jeffrey Dilworth for their constructive criticism and positive feedbacks on my project. Also thank you to Dr. William Stanford for attending some of the TAC meetings and for his guidance and input.

I would like to thank my colleague and best friend, Bahaeddine Tilouche, for all his help and support in the lab and outside of the lab. Special thanks to all previous and current members who helped with this project, especially Mariya Somyk and Francis Roy.

Also, special thanks to all the members of the Mattar lab, for their constant support and motivation and their friendship. Thank you to their technician Samuel-Clemot for all the help with running the gels for genotyping.

Thank you to my friends outside of the lab, in Canada and Lebanon for their encouragement and support.

Thank you to all my family members, living in Canada and Lebanon, and parents in Lebanon for believing in me and pushing me to achieve my goals.

Finally, I would like to thank my husband, Rami Al Haddad, for being my best friend, my support system and my rock through thick and thin. I never would have made it till the end nor had my dreams come true without him by my side!

Abstract

Treatments for skeletal tissue injuries include surgery and rehabilitation but in adult patients, the healing process is slow and incomplete, and the underlying biological mechanisms are largely unknown. Skeletal tissues contain stem cells responsible for their maintenance and repair, but the identity and location of these stem cells, and what molecular mechanisms regulate their fate decisions remain unclear. To design more effective regenerative therapies for skeletal conditions, understanding the fundamental biology of skeletal stem cells (SSC) in postnatal organisms is required.

Our project aims at identifying and characterizing these SSC populations in postnatal murine and human tissues using lineage tracing techniques, combined with multicolor 3D confocal microscopy and computational image analysis, in vitro assays, and single cell transcriptomics. We hypothesized that the postnatal skeleton contains self-renewing and multipotent Sox9+ SSCs that persist in adulthood.

We showed that the adult mouse skeleton contains Sox9+ cells self-renewing, multipotent skeletal stem cells (SSCs) with osteogenic and chondrogenic potential. They are located adjacent to the growth plates and in periosteum and persist in adulthood. Transcriptome analysis revealed that these cells express other putative SSCs markers, as well as genes involved in skeletal development, stem cell self-renewal, and fate decision. This data provides testable drug targets to pharmacologically manipulate SSCs fate decisions in situ. In addition, we showed that human tissues contain SSCs similar to murine tissues.

This is the first experimental proof of self-renewal in postnatal Sox9+ SSCs in vivo. These findings provide actionable insights for the use of culture-expanded stem cell product for

regenerative medicine product or pharmacological targeting of these stem cells in situ. We believe our data will help improve stem-cell based and tissue engineering therapies, increasing success rate of regenerative orthopaedic surgeries while reducing reoccurrence of injuries.

Abbreviations

4OHT:4-hydroxytamoxifen

BODIPY: Fluorinated Boron-Dipyrromethene

CFU-C: Colony forming unit cell

Cre: Cyclic recombinase

D: Day

DAPI: 4′,6-diamidino-2-phenylindole

DMEM: Dulbecco's Modified Eagle Medium

EdU: 5-ethynyl-2'-deoxyuridine

FACS: Fluorescence activated cell sorting

FOD: Focal osteochondral defect

hSox9: Human SRY-Box Transcription Factor 9

IP: Intraperitoneal

ITGB5: integrin β5

MFU: Mean Fluorescence Intensity

P: Postnatal day

PBS: Phopshate buffer saline

PFA: paraformaldehyde

RFU: Relative fluorescence unit

scRNA seq: Single cell RNA sequencing

Sox9: SRY-Box Transcription Factor 9

SSC: Skeletal stem cells

TDE: *2,2'-thiodiethanol*

tdT: tdTomato

Tmx: Tamoxifen

List of Figures

List of Tables

Chapter 1: Introduction

1. Skeletal system

The skeletal system is an essential part of any organism belonging to the vertebrate subphylum. The musculoskeletal system comprises skeletal muscle, bone, cartilage (growth plate, articular, menisci, etc.), tendons (connecting bones to muscles), ligaments (connecting bones to bones), the joint capsule and marrow stroma. The skeletal system is known to have diverse functions; it enables body movements such as walking, running, eating, and talking. It also forms a protection barrier for the sensitive vital organs including the brain, heart, lungs, and spinal cord. The skeletal system also plays an indispensable role in maintaining the homeostasis of mineral ions' concentrations by regulating the storage of calcium and phosphate in the bone, hormone production and secretion, as well as hematopoiesis taking place in the postnatal bone marrow [1].

1.1 Developmental origin

During early embryonic development, three germ layers are formed: the ectoderm, the mesoderm and the endoderm. The mesoderm (middle) layer, more specifically the paraxial and lateral plate mesoderm, are known to give rise to all musculoskeletal tissues of the axial and appendicular skeleton, respectively, through a process known as endochondral ossification[2]. The axial skeleton includes the thoracic cage, skull base and vertebral column[3]. It originates from the somitic mesoderm, which in turn gets divided into three parts; the myotome that forms the skeletal muscles, the dermatome that gives rise to the dermis, and the sclerotome forming the tendons and bones of the vertebral column[4]. The craniofacial part of the skull originates from the neural crest (an ectoderm derivative) through the process of intramembranous ossification. As for the lateral

plate mesoderm, it allows limbs and pelvis development, known as the appendicular skeleton[3] (figure 1).

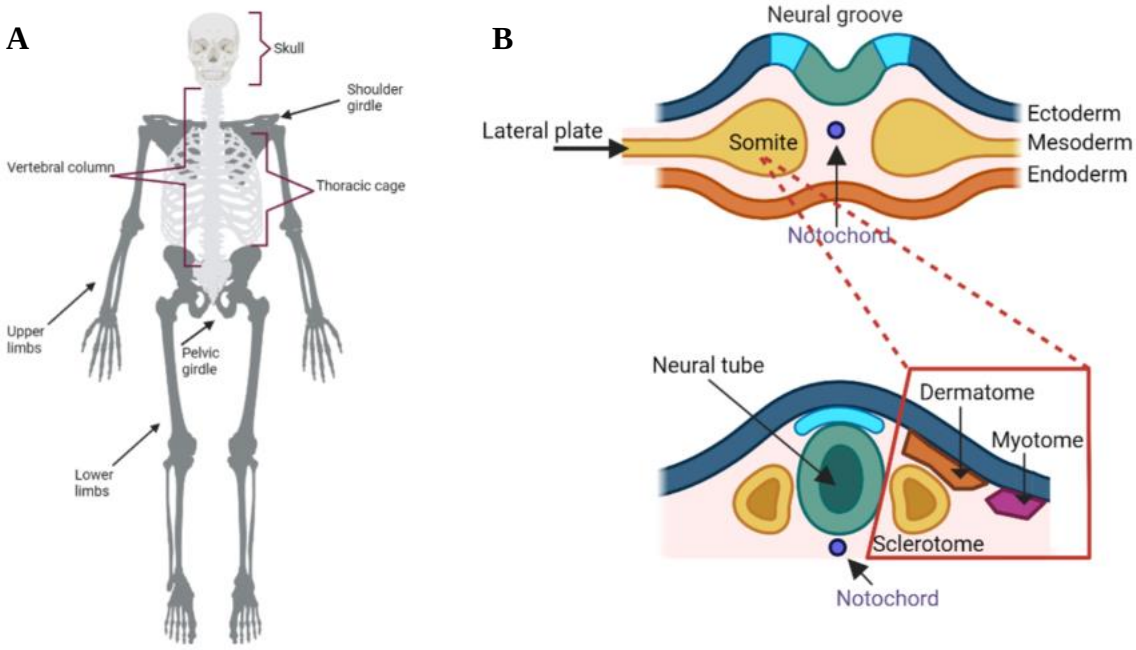

Figure 1: Developmental origin of the skeleton. A) Bones shown in white are part of the axial skeleton and bones shown in dark grey are part of appendicular skeleton. B) The three germ layers formed in early stages of embryonic development are the ectoderm, mesoderm and endoderm. The mesoderm layer has 3 subdomains; the paraxial mesoderm which is organized into somites when the neural groove is formed, the intermediate mesoderm and the lateral plate mesoderm. Somites get divided into 3 parts: dermatome, sclerotome and myotome (created on biorender).

1.2 Limb bud formation

Cells expressing fibroblast growth factor-10 (FGF-10) from the lateral plate mesoderm, called mesenchymal cells, migrate to the location of the limb bud formation and stimulate the formation of two essential signaling centers for limb patterning. The first one is the apical ectodermal ridge (AER) in the ectoderm layer, right above the distal edge of the limb bud; it secretes fibroblast growth factor-8 (FGF-8) which has been shown to be important in determining the proximal to distal axis of the bone [5]. It is believed that FGF-8 acts on the mesenchymal cells

as an antagonist, inhibiting the retinoic acid signaling pathway in the proximal end of the limb. As the cells move away from the AER due to cell proliferation and tissue expansion, they stop receiving the FGF-8 signal. The longer they receive the signal, the more proximal they will be. The second signaling center is the zone of polarizing activity (ZPA) formed within the mesenchymal cells, at the posterior side of the limb bud's distal area. ZPA produces Sonic hedgehog (SHH) that promotes anterior-posterior patterning[2,5].

1.3 Endochondral ossification

The first step in endochondral ossification is the condensation of the mesenchymal cells originating from the lateral plate mesoderm, forming the condensing mesenchyme. These cells are known to express the transcription factors Prrx-1 and Sox-9 during the early stages of limb development[1]. Sox-9 upregulates the transcription of many genes encoding for collagens and proteoglycans, largely contributing to the condensation process. The cells located in the middle of the condensation differentiate into chondrocytes that secrete type II, IX and XI collagens and aggrecan, forming a cartilaginous template, while the cells on the periphery differentiate into perichondrial cells secreting type I collagen[6–8]. Subsequently, chondrocytes start forming the growth plate and they are highly proliferative. When cells at the center of the cartilage anlagen stop receiving key signals and factors for their cell division cycle, such as FGF-8, PTHrP and BMPs, they become hypertrophic chondrocytes[1]. These cells express VEGF (vascular endothelial growth factor) that induces angiogenesis within the perichondrium, and they also express the Indian hedgehog protein (Ihh). Ihh has been shown to have several functions: 1) it acts on adjacent round chondrocytes, inducing their proliferation and differentiation into flat chondrocytes, and then stimulating their differentiation into hypertrophic chondrocytes. 2) It stimulates perichondrial

cells to differentiate into osteoblastic cells. These will express the transcription factor Runx-2 and its downstream Osterix (Osx) and start secreting bone matrix proteins (type I collagen, osteopontin and osteocalcin) to calcify the ECM, hence forming the bone collar, which will eventually become the cortical bone. 3) Ihh also induces the expression of Parathyroid hormone-related peptide (PTHrP) from periarticular chondrocytes that are responsible for the formation of joints during the process of endochondral ossification. Once PTHrP is expressed, it acts on its receptor (PTHrP-R), stimulates proliferation of flat chondrocytes and delays their differentiation into hypertrophic chondrocytes, thus forming a negative feedback-loop with Ihh that helps in regulating bone development and maintaining the epiphyseal plate[1,9] (figure 2).

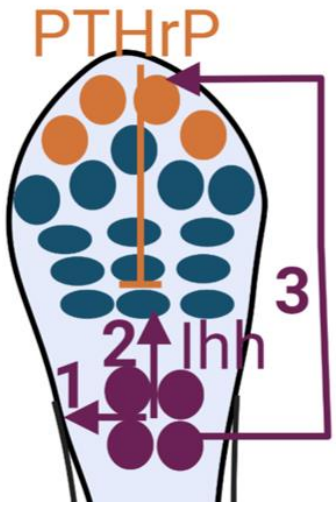

Figure 2: Ihh target cells. Ihh stimulates perichondrial cells to differentiate into osteoblastic cells **(1),** acts on adjacent round chondrocytes to stimulate their differentiation into hypertrophic chondrocytes **(2)**, and induces PTHrP expression from periarticular chondrocytes which in return forms a negative-feedback loop with Ihh **(3)** (created on biorender).

During the development of the primary ossification center, the bone marrow cavity is formed in the middle of the cartilage template. It comprises blood vessels that invade the marrow cavity due to VEGF secretion by hypertrophic chondrocytes, hematopoietic stem cells and

mesenchymal stromal cells[1]. It is thought that the mesenchymal cells originate from the inner layer of the perichondrium, also known as the groove of Ranvier. They are transported to the marrow cavity in a pericyte-like manner through blood vessels, and then can mature into osteoblasts[10].

Once in the marrow space, mesenchymal cells proliferate and differentiate into osteoblastic and stromal cells, producing the endosteum layer and trabecular bone within a condensed and complex network of blood vessels, thus forming the primary spongia[1]. The vessels that run within the center of the bone marrow cavity are the arteries, becoming arterioles as they move further away from the center, then branching out into capillaries when invading the cortical bone, which anastomose into the periosteal blood vessels on the outer surface of the bone. They then transition into sinusoids which eventually converge to the central sinus inside the cavity[11,12] (figure 4).

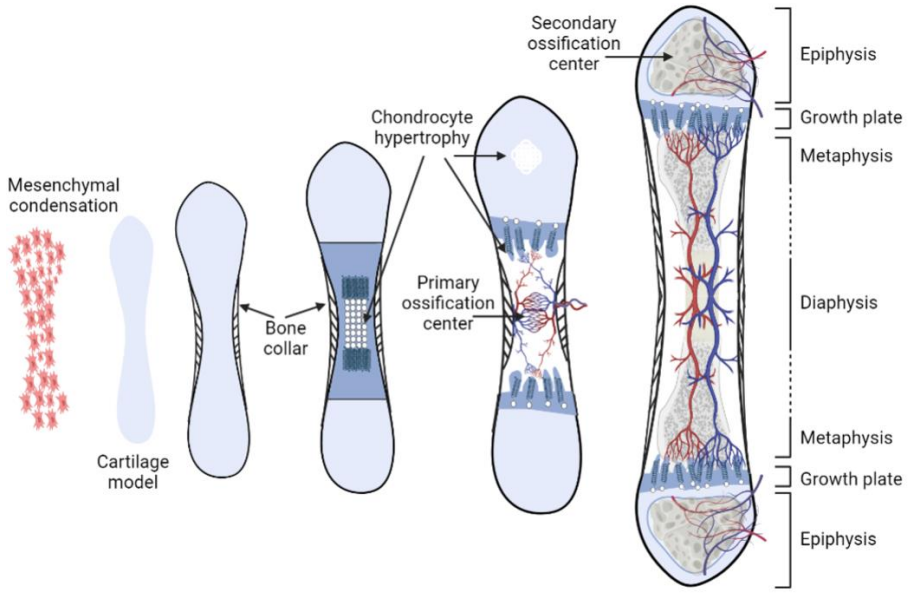

Figure 3: Different steps of the endochondral ossification. Condensation of the mesenchymal cells, cartilage is formed from the chondrocyte progenitors and bone collar is formed from the osteoblast progenitors. Growth plate appears and then chondrocytes hypertrophy, leading to angiogenesis and the appearance of the primary ossification center. After birth, the secondary ossification center appears, and the different parts of the bone become apparent; epiphysis (both ends of the bone), metaphysis and diaphysis (middle shaft) (created on biorender).

Following birth, the secondary ossification center is formed which will become the epiphysis. The round chondrocytes from the growth plate become hypertrophic chondrocytes, blood vessel invasion occurs, and mesenchymal cells migrate and start forming the trabecular bones. The ossification center is located between the articular cartilage of the joint and postnatal epiphyseal plate. The chondrocytes at the top of the cartilaginous growth plate become dormant forming the resting zone and are called resting (or reserved) chondrocytes. They are believed to act as stem-like cells that can divide and give rise to proliferating chondrocytes, thus allowing bone growth postnatally (Figure 5)[13].

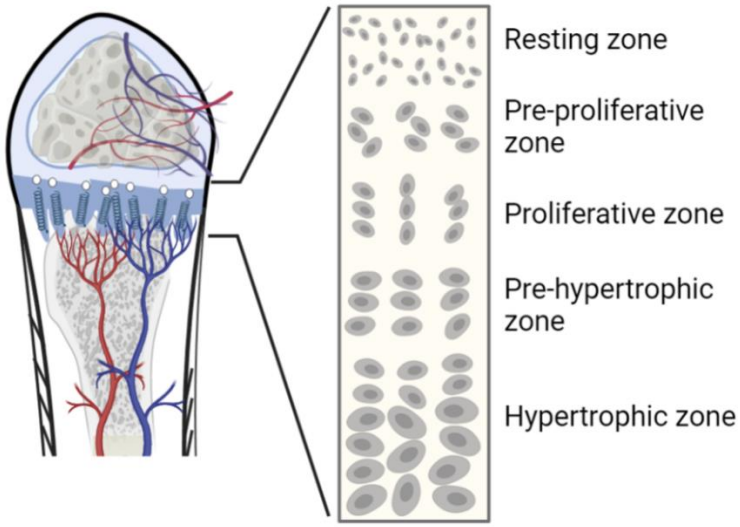

Figure 4: Detailed view of the growth plate cells. In the upper part lies the dormant or resting chondrocytes that act like stem cells, then there are the pre-proliferative and proliferative chondrocytes. The latter mature (pre-hypertrophy), then hypertrophy (created on biorender).

1.4 Intramembranous ossification

During intramembranous ossification, the mesenchymal cells condense and immediately differentiate into osteoblastic cells that start secreting the mineralized matrix, thus forming the

rigid bone while skipping the cartilage transition phase. This ossification process is relatively simple and not as well defined and characterized as the endochondral ossification process .[1]

2. Sexual dimorphism

Sexual dimorphism in the skeleton between males and females is due to differences in signaling pathways involving sex steroids (androgens and estrogen), growth hormone (GH), insulin-like growth factor 1 (IGF1), as well as mechanical loading[14–16]. These factors are key regulators of mineral bone deposition and accumulation during puberty[15,17–19]. The male skeleton is known to be bigger, stronger and establishes a higher peak bone mass than the female skeleton[15,18], however their density is similar since bone mineral acquisition, especially in long bones, is directly proportional to the bone volume[20]. Thus, no differences exist in the volumetric bone mineral density (BMD) between males and females, but only in the size and width, rendering females more susceptible to developing osteoporosis[17]. More recently, a study showed that female mice formed a higher number of osteoclast cells compared to males, which explains the lower osteogenic response in females during development[19,21].

2.1 Sex steroids

Testosterone, the most common type of male androgens, acts on the androgen receptor (AR) and the estrogen receptors α and β (ERα and Erβ) after aromatization into 17 β-estradiol[16,22]. Studies conducted in pubertal mice showed that androgens have a stimulatory effect on the radial bone expansion of periosteal and cortical bone growth in males at the latest stages of puberty. On the other hand, the female sex hormone, estrogen, had an inhibitory effect that limited the periosteal bone size expansion, but induced the endosteal bone apposition (endocortical bone expansion) in females during early puberty, as well as more trabecular bone[14]. In addition, due to

higher estrogens, female bones stop growing earlier because of "premature" epiphyseal fusion[23]. In contrast to the inhibitory effect observed of the female estrogens, the male estrogen showed a high importance in bone growth to the point where males transform some of their testosterone levels into estrogens (by aromatization of androgens into 17 β-estradiol in males). It has a contribution in the increased radial bone size[14–16], when only binding on ERα and not Erβ[24]. Thus, AR and ERα are the main receptors required in males for cortical bone formation[16].

2.2 GH-IGF1 axis

GH and IGF1 hormones are important factors for bone growth during puberty[25] and have shown to have a major role in sexual dimorphism of the bone mass[14]. During puberty, GH and IGF1 concentrations increase. These hormones have higher levels in males compared to females, and as a result, stimulate bone formation. Knockout mice models showed that GH and IGF1 hormones work simultaneously, and the absence of either one of them or both results in decreased bone expansion[25–28]. Sex steroids, specifically estrogens, show a correlation with GH-IGF axis during puberty[25,29,30]. It has been reported that male mice that lacked ERα or had low levels of 17 β-estradiol showed decreased concentrations of IGF1 hormone levels, affecting bone growth[25,31,32]. In the case of cartilage specific $ER\alpha^{-/-}$ mice, the concentration levels of GH-IG1 axis is not affected and bone growth is not altered during puberty, however it induces elongation of the bone instead of width expansion[33].

2.3 Mechanical loading

Several studies showed the effect of physical activity and mechanical loading on bone development and morphology, as increasing bone formation[34–38]. Cross-sectional studies in humans support these findings; for instance, a study showed that tennis players have a significantly

thicker cortical humerus in their playing arm versus the nonplaying one[39]. Also, it has been observed that in female players, before and during early stages of puberty, mechanical loading increases periosteal bone deposition and enhances bone strength in their dominant playing arms. If physical activity and mechanical loading start at later stages of puberty, most of the growth expansion occurs in endocortical bone area with no effect on strength[39]. In male tennis players, periosteal bone expansion in response to loading in their humerus happens before and during puberty, and no osteogenic response to loading is observed after puberty, unlike what is seen in female players[40]. These findings suggested that sex steroids might affect bone expansion in response to mechanical loading due to gender differences[16].

3. Skeletal tissue repair

Bones have a great capacity for self-repair and regeneration. Small to average fractures heal through intramembranous ossification, whereas bigger and deeper fractures require endochondral ossification. This generates a soft callus and fibrocartilage at the injury site to stabilize it and link the bone fragments to each other[41]. Cells from the marrow stroma migrate to the fracture site, proliferate extensively and differentiate into osteoblasts directly since they appear to retain osteoprogenitor properties[10,41,42], while cells from the periosteum proliferate into chondrocytes then osteoblasts followed by vascularization and mineralization[10,41–44]. A recent study used Cxcl12-CreERT2 mice for lineage tracing that labeled marrow stromal cells, and they were shown to be quiescent in the adult mice during homeostasis, while in the cortical fracture model they were involved in the repair process by differentiating into osteochondral cells[45]. On the other hand, other skeletal tissues, such as articular cartilage, tendons, ligaments and menisci, heal slowly and incompletely in adult individuals and still represent a challenge in orthopaedic

surgery[46–48]. Articular cartilage lesions show limited capacity for self-repair, and current treatments include transplantation of autologous chondrocytes or bone-marrow aspirate, or surgical treatments such as drilling, abrasion or microfracture of the subchondral bone to stimulate endogenous repair[46,48]. For tendons and ligaments repair, surgical reattachment aims at recreating the natural organization of the enthesis, where soft and elastic tendons attach to hard mineralized bone[49]. However, adult tendons heal through a fibrocartilage scar rather than regeneration of the normal tissue[50]. Similarly, meniscal tears are surgically manageable when they occur in the peripheral, vascularized region but are more challenging when occurring in the deep, avascular region[51]. Several experimental strategies for meniscus regeneration are being developed, and they involve tissue engineering and cell-based approaches[51–53]. Most of the procedures used for articular cartilage, tendons, ligaments and menisci injury treatments are not long-term solutions as they show high failure rates and often require revision surgery[46,49,50,53].

4. Stem cells in skeletal tissue

4.1 Mesenchymal stem cells in-vitro

Early studies in the 19th century attempted to identify the source of cells responsible for bone regeneration by performing transplantation assays of osteogenic cells from the periosteum and marrow[54,55]. A century later and after the identification of hematopoietic stem cells[56], transplantation of osteogenic cells was tested as an attempt to improve the efficacy of bone marrow transplants. Small fragments or cell suspensions of bone marrow isolated from femurs of mice were transplanted subcutaneously or under the renal capsule[57,58] and formation of stromal and bone tissue was observed. However, when large and intact marrow fragments where isolated and transplanted, the donor vasculature was maintained after transplantation and bone tissue was observed with a marrow cavity supporting hemopoiesis[59]. Marrow cells responsible for bone and marrow formation were next isolated based on their capacity to adhere to tissue

culture plastic and form heterogenous colonies of fibroblastic cells[60,61]. Transplantation experiments showed these cells can generate adipocytes, adventitial reticular stromal cells, bone and cartilage[60–63]. Later on, these cells were introduced in the literature as bone marrow-derived mesenchymal stem/stromal cells (MSCs) [64–66], that are isolated from bone marrow and possess osteoprogenitor properties[41,42]. They have been well characterized in vitro after culture expansion[64,67–77], and the morphology of unfractionated skeletal cells is very similar to the cells found in the bone marrow stroma [65,78–81], in addition to their capacity to adhere to plastic cell-culture dishes, and formation of heterogeneous proliferating cell colonies with osteo-, chondro-, and adipogenic potential in vitro and in vivo[60–62,82]. Also, these MSCs have a known and well established role in interacting with the hematopoietic cells and providing a suitable niche for their differentiation[83–85], yet little is known about the biology of MSCs in-vivo. Cells similar to MSCs in their morphology, marker expression and differentiation potential in vitro were isolated from various tissues and were suggested to be analogous to tissue-resident pericytes[86,87]. These are characterized by their perivascular localization, and their function and phenotype are heterogeneous and depend on the type of vasculature they are associated with as well as their tissue origin[87]. Their function in bone and marrow physiology is largely unknown since they lack direct experimental evidence using lineage tracing that pericytes are MSCs [88–94].

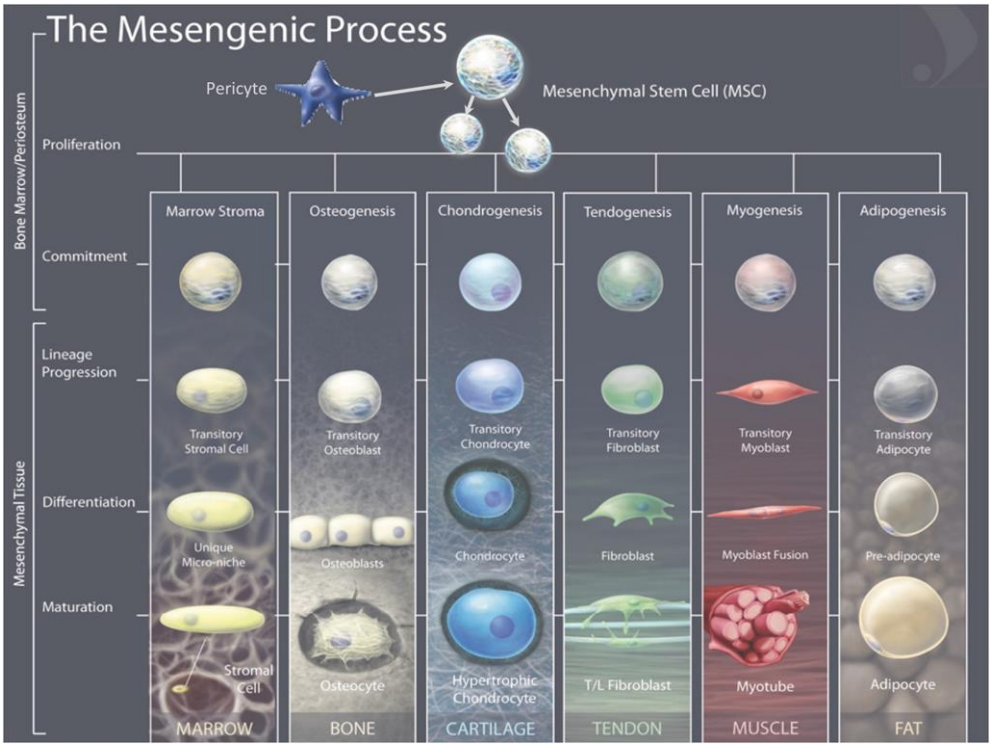

Figure 5: The central dogma of mesenchymal stem cells. A mesenchymal stem cell can self-renew and differentiate into marrow, bone, cartilage, tendon, muscle and fat cells. Also, mesenchymal stem cells can be derived from pericytes (Reprinted from Cell Stem Cell, Vol.9, Arnold I. Caplan, The MSC: An Injury Drugstore, Page No.9, Copyright (2011) with permission from Elsevier).

4.2 Skeletal stem cells in-vivo

4.2.1 Lineage tracing approach

Recent studies have aimed to study skeletal stem cells (SSCs) in-vivo, by using lineage-tracing approach through: 1) genetic labeling to study multipotency and lineage progression[95], and 2) thymidine analogues incorporation and retention, to measure cell proliferation and tissue turnover rates[96].

While using lineage tracing approach, it is assumed that all somatic cells have a finite lifespan except for the stem cells responsible for replacing them. Cells are genetically labeled using a specific system such as the Cre-LoxP system, where Cre expression is driven by a gene promoter

active in the cells of interest and induces constitutive expression of a fluorescent reporter, such as tdTomato from the Ai14 allele[97]. This reporter/label is inherited by daughter cells until cells turnover and the number of labeled cells decays as a function of cell turnover rate[95]. If progenitor cells are labeled, the number of labeled cells can increase transiently, but inevitably decays over time. In contrast, when self-renewing stem cells are labeled, the number of tagged cells remains stable or increases depending on the fraction of stem cells labeled, tissue turnover rate, and postnatal developmental stage (tissue growth, maintenance, or degeneration), over the entire lifespan until stem cells stop self-renewing[94] (figure 6).

To quantify cell proliferation and turnover rates within tissues, thymidine analogues uptake and retention assay has been used[96]. When cells divide, specifically during the S-phase of mitosis, they integrate and retain the thymidine analogue in their genetic material, during DNA replication. The dividing cell and its progeny are tagged, and their proliferation kinetics is determined by measuring dilution[99]. One type of a synthetic thymidine analogue that preserves the integrity of the cells and do not interfere with their live biochemical reactions is the 5-ethynyl-20-deoxyuridine (EdU)[100]. EdU, unlike the halogenated thymidine analogues (which includes BrdU (5-bromo-20-deoxyuridine), CldU (5-chloro-20-deoxyuridine) and IdU (5-iodo-20-deoxyuridine)), does not require the denaturation of DNA to be detected because the detection reaction does not involve antibody staining and detection. Rather, it is detected in the DNA through a chemical reaction known as the “click” reaction, where a fluorescent azide forms a covalent bond with its terminal alkyne group via Cu(I)-catalyzed reaction[99,100].

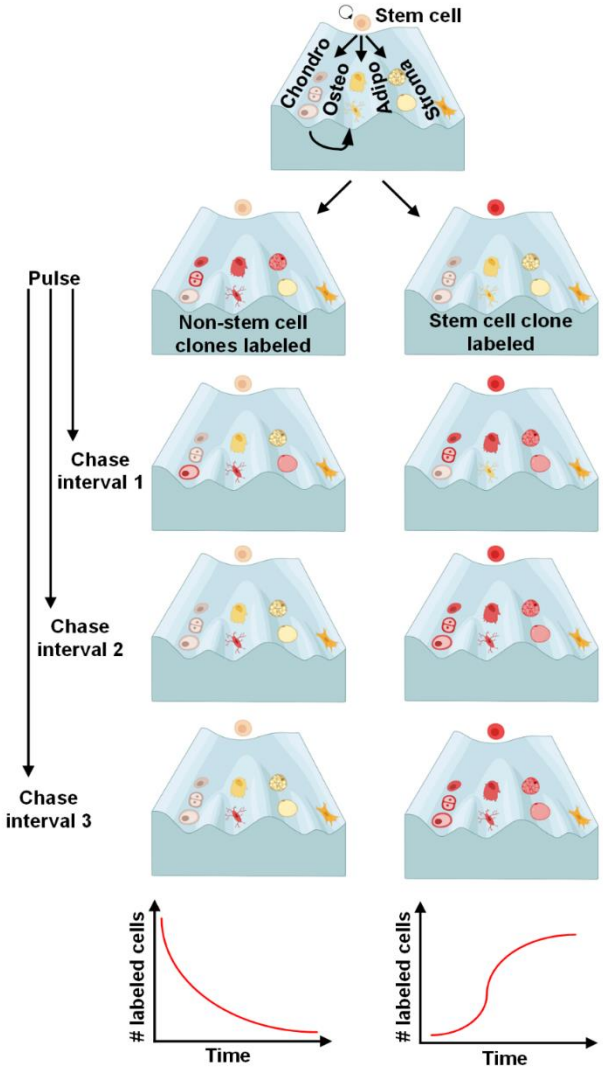

Figure 6: Stem cell lineage tracing theory. Shown are Waddington landscapes of skeletal cell differentiation downstream of self-renewing skeletal stem cells. When postnatal skeletal cells are genetically labeled using a Cre-driver not expressed in stem cells (left), cells at various points of the lineage tree are labeled. Labeled cells differentiate and are replaced but non-labeled cells derived from non-labeled stem cells. The number of labeled cells decays with a half-life depending on tissue turnover rate and where the Cre-driver was expressed down the differentiation tree. When the Cre-driver is expressed in stem cells (right), the number of labeled cells increases in all lineages downstream of this stem cell through exponential clonal expansion, until all steps of the differentiation tree are labeled. The number of labelled cells then plateaus for as long as the stem cell self-renews (figure courtesy of Dr. Daniel Coutu).

4.2.2 Cre-Lox P system

The Cre-LoxP system is a specific and powerful tool that is widely used for gene editing. Its main mechanism of action relies on the Cre recombinase enzyme (Cre) recognizing and binding to the LoxP sequences, which in turn flank a specific gene that gets excised by the Cre enzyme[101]. To generate the Cre-Lox P system in mice, two separate breeders are needed; the first mouse strain has a Cre driver line that gets expressed by a cell type-specific promoter. The second mouse strain has a LoxP flanked gene that needs to be excised. In these double mutant lines, Cre recombinase enzyme gets expressed and excises the floxed gene (flanked by LoxP sequences) only in the cells where the promoter driving transcription of the Cre transgene is active[102,103].

For a more specific and less leaky system, a mutated human estrogen receptor (ER) is fused to the Cre and has low affinity to the endogenous estrogen but higher affinity to tamoxifen; this fusion transgene is known as CreERT. This inducible CreERT is transcribed by a specific promoter and conditionally activates expression of a fluorescent protein when tamoxifen (TAM) is administered[101,102]. A common fluorescent reporter is tdTomato from the Ai14 allele; it is a bright protein that is inserted between exon 1 and exon 2 of the ROSA26 locus which is expressed in most somatic cells. In addition, tdTomato is a tandem dimer with a fast folding-maturation and high quantum yield (brightness)[97].

TAM binds to the CreERT recombinase enzyme and the complex tamoxifen-CreERT recombinase targets and binds to the LoxP sequence flanking the stop codon of the Ai14 reporter gene and excises it. Thus, tdTomato can be ubiquitously and permanently expressed in CreERT+ cells by its active CAG promoter[101,103–105], labeling cells of interest in red and mapping their cell

fate through pulse-chase experiments. More recently, an optimized version of CreERT is developed, the CreER^{T2}, that has three mutations instead of one in the human ER and has showed more sensitivity and higher efficiency in recombination rate (around tenfold higher in vivo)[105] (Figure 7).

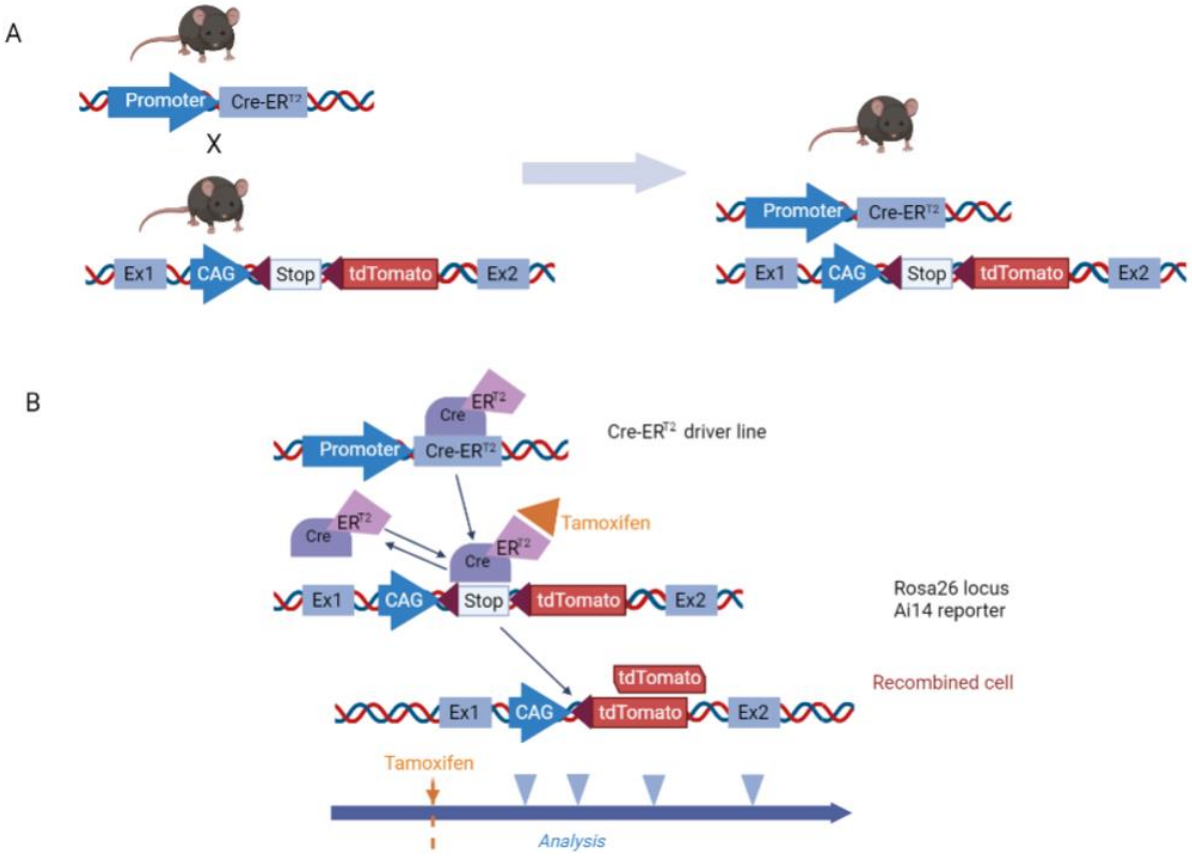

Figure 7: Cre-LoxP system. A) Two separate breeders are required to generate the double mutant mouse line. B) Upon injection of tamoxifen, it binds to the CreER^{T2} recombinase enzyme that gets expressed by a specific promoter. The complex tamoxifen-Cre recombinase targets and binds the stop codon of the Ai14 reporter gene and excises it. Thus, tdTomato can be ubiquitously and permanently expressed in the specific cells by its active CAG promoter (created on biorender).

4.2.3 Lineage tracing studies of postnatal skeletal cells using Cre-LoxP system

Some studies used ubiquitously-expressed inducible Cre lines, such as Mx1-Cre[106], Actin-CreERT[107] and Nestin-CreER[108], and they were combined with FACS purification, in vitro assays and transplantation experiments. The latter failed identifying putative SSCs with long-term multipotentiality and self-renewal capacity at the single-cell level, in addition they have been shown to be unspecific markers, where Mx1-Cre and Actin-CreERT are ubiquitously expressed and label all cell types, whereas Nestin-CreER label mainly endothelial/perivascular cells and neurons[106–109]. Other studies used constitutively-active Cre-drivers, that include LepR-Cre[89,110], cathepsin K-Cre[111], Collagen 10a1-Cre[112,113] and Prx-1-Cre[114], rendering lineage tracing experiments ambiguous since it remains unclear when during development those transgenes were expressed. Lineage tracing studies in embryos using LepR-Cre labeled mainly bone and stromal cells; when transplanted LepR+ cells gave rise to bone and adipocytes, and participated in bone fracture injury repair[89,110]. On the other hand, Cathepsin K-Cre labeled mainly periosteal cells in embryos that gave rise to bone and cartilage after transplantation under the renal capsule. Interestingly, Cathepsin K+ periosteal cells mediated intramembranous ossification during homeostasis and endochondral ossification during fracture injury repair[111]. Collagen 10a1-Cre lineage tracing studies showed evidence of transdifferentiation of hypertrophic chondrocytes into osteoblasts[112,113]. Tamoxifen injection labeled thousands of Col10a1-CreERT+ chondrocytes at embryonic or perinatal stages. After short chases, cells of the osteoblast lineage were also labeled, suggesting transdifferentiation if one assumes that Col10a1 expression is restricted to hypertrophic chondrocytes. Postnatally, when Col10a1+ cells were labeled at P5 and chased for 16 months, the entire progeny of these Col10a1+ cells consisted of a few osteocytes and marrow adipocytes, suggesting that Col10a1-expressing cells are not self-renewing long-term[113]. When Prx-1-Cre

positive cells were lineage traced in embryos, they were initially found in undifferentiated mesenchyme during limb bud formation, and were then confined to periosteum and tendons of limbs of embryos. Prx-1+ cells from periosteum exhibited chondro- osteo-differentiation in culture, and in the callus of a diaphyseal fracture model[114].

However, some studies based their research on inducible CreERT drivers, such as Osx/Sp7-CreERT[10,115–117], collagen 2a1-CreERT[118], Gremlin1-CreERT[119], or PTHrP-CreERT[120] and they were mainly conducted during embryonic or perinatal development in mice. Labeled putative SSCs in these studies showed that they were different from MSCs; they had osteo-chondro-stromal progenitor properties and were localized near the growth plate and/or in the periosteum[10,115–120], and more recently, it has been suggested that the skeletal stem cells are mainly located in the resting zone of the growth plate[107,120], but this was not confirmed in juvenile or adult animals. Moreover, these studies did not attempt to demonstrate self-renewal and multipotency at the population or single cell levels. More recently, many of these markers were shown to be either unspecific and/or labeled differentiated lineages [109,121]. A recent study identified putative human skeletal stem cell (hSSC) that can be isolated from the adult and fetal bone using fluorescence activated cell sorting[122]. When transplanted under the renal capsule of immunocompromised mice they formed ossicles containing human bone, cartilage and marrow stroma but no adipocytes. hSSCs can be isolated from these ossicles and serially transplanted, suggesting self-renewal and multipotentiality, however they lack a phenotypical analysis of cell fate at the single-cell level which can be done with a classical lineage tracing experiment and clonal analysis[10]. Moreover, Col2a1-CreERT, Acan-CreERT and Sox9-CreERT were all reported to label similar osteochondral progenitors in perinatal mice. These studies also made no attempts to study self-renewal or multipotency of the labeled cell populations[120,123,124]. To prove the stemness of these

putative SSCs populations will require a more detailed analysis to be performed in postnatal animals. Cxcl12-CreERT+ marrow stromal cells appear to be a distinct, self-sustaining lineage in postnatal mice and only contribute to bone formation during tissue repair[45]. Pericytes remain poorly studied to date largely due to the lack of specific markers that can be used for purification or lineage tracing[87], but were recently shown not to behave as stem cells in most tissues[125]. A study published recently demonstrated that stem cells residing the periosteum control the proliferation of resting zone stem cells in the growth plate postnatally via Ihh signaling. Using a $Ihh^{flox/flox}$ Cathepsin K-Cre mouse line, they show a severe aberration of bone development in adulthood that starts at P21, suggesting that Ihh signaling deriving from hypertrophic chondrocytes from growth plate decreases after birth, but bone prolonged bone maturation in adulthood is maintained by Ihh secretion derived from periosteal stem cells[126].

Most of the markers used in the previous studies to identify SSCs are proteins and transcription factors that are crucial for the skeletal development. A particular one that is present at the earliest stages of limb bud formation is the Sox9 protein and it induces the differentiation of the mesenchymal cells into cartilage, which is the first step for the long bones to form[124].

5. Sox9 protein

Sox9 is a high-mobility-group (HMG) box-containing transcription factor homologous to SRY (sex-determining region Y), and is located on chromosome number 17[127]. So far, there has been 20 human and mouse Sox proteins identified, and they are grouped from A to H, depending on the structural homology of the regions outside the HMG conserved site[128]. Sox9 is classified in the SoxE group, in which the proteins have in common the dimerization domain (DIM) near the

N terminus of the gene, and the transactivation domains where one is central (K2) and the second is near the C terminus (TA)[128,129] (figure 8).

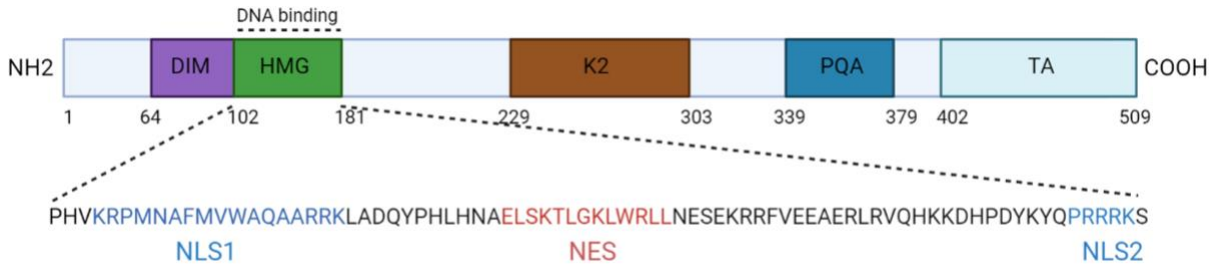

Figure 8: Sox9 gene schematic structure. It consists of the dimerization domain (DIM), high mobility group (HMG), two transactivation domains (K2 and TA) and a proline-glutamine-alanine (PQA) rich region. The nuclear export sequences (NES) in the HMG domain are the phosphorylation sites (shown in red), while the nuclear localization sequences (NLS1 and NLS2) are the ubiquination/sumolyation sites (shown in blue) (created on biorender).

Sox9 is a highly conserved protein among species with 99.61% of homology between Human (509 amino acids) and mouse (507 amino acids)[129]. The conserved HMG domain of the Sox-family proteins is composed of 70 amino acids, and they have at least 50% or more overlap with that of SRY[128–131]. For Sox9 more specifically, it is the AGAACAATGG sequence in the HMG region of the Sox9 gene structure that allows it to bend and form an L-shaped complex inside the DNA minor groove[132]. By doing so, Sox9 binds to co-factors and induces activation or repression of its target genes[128,132]. Most of the post-translational modifications of Sox9 occur at the conserved HMG region, where phosphorylation of the amino acids in the nuclear export sequence (NES) site (highlighted in red in figure 8) by protein kinase A (PKA) enhances DNA-binding affinity of Sox9 and leads to its translocation into the nucleus. SUMOylation/ubiquitination of the residues in the nuclear localization sequence (NLS) site

(highlighted in blue in figure 8) by small ubiquitin-related modifier, affects the degradation rate of Sox9 and regulates its post-transcriptional activity in the cytoplasm[128,129,131].

The role of Sox9 as a transcription factor is to either activate or repress the expression of its target genes, which is dependent on its target site and the co-repressors or co-activators that it recruits to form a dimer complex with[133]. For example, when Sox9 binds to Gli protein, this complex inhibits the transcription of Col10a1 gene that is crucial for chondrocyte maturation and hypertrophy[134]. However, when Sox9 binds to the dimer protein SoxD, also known as Sox5 and Sox6, they form a trio-complex that induces Col2a1 gene transcription which stimulates chondrocyte differentiation and ECM (extracellular matrix) deposition[135] (figure 9).

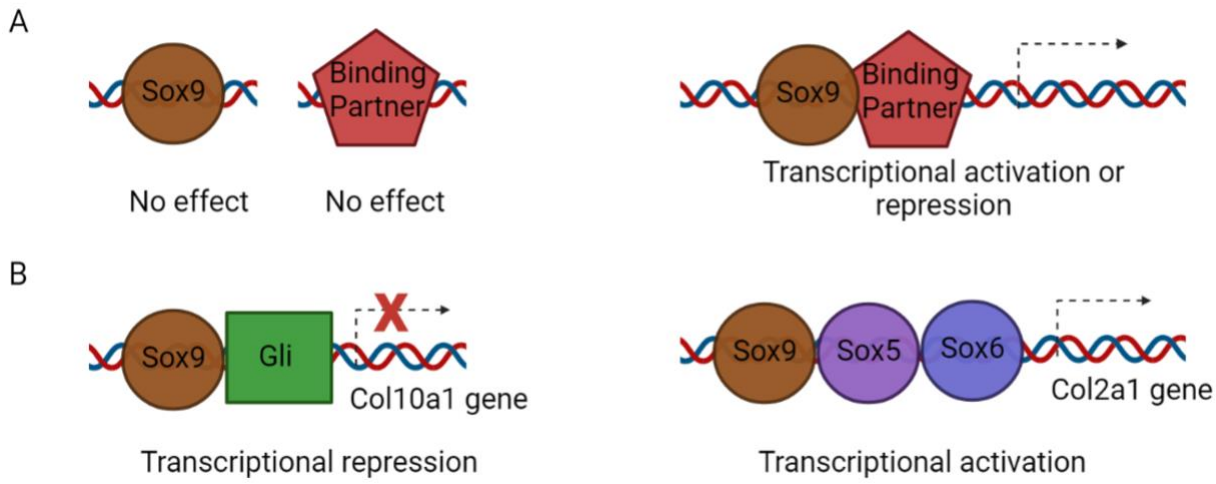

Figure 9: Mechanism of action of Sox9 and its binding partners. A**)** Sox9 requires a binding partner to activate or repress transcription of its target genes. B) Transcription activation or repression depends on the binding partner of Sox9 and target genes; when Sox9 binds with Gli, it represses Col10a1 expression, however when binding to Sox5/6 dimer it activates Col2a1 expression (created on biorender).

Sox9 is widely expressed in all the embryonic germ layers (mesoderm, ectoderm and endoderm layers), regulating the development of most tissues, and rendering it present in most of the somatic progenitor cells[128]. These include neural stem cells[136,137], liver/intestine/pancreatic

progenitor cells[138–144], cardiac cells[145,146], male gonads[147,148], hair follicle stem cells[97,149,150], retinal progenitor cells[151–153] and mesenchymal cells that condense and differentiate into chondrocytes[6,7,154,155]. In adulthood, Sox9 expression is still maintained in most of these tissues[128].

5.1 Mutations of Sox9 and associated disorders

Mutations can happen either within the coding region of Sox9 or in the regulatory non-coding region. When the mutations are in the coding region, Sox9 protein function and structure is affected, resulting in an altered, complete, or partial loss/gain of function. However, mutations within the non-coding region of Sox9 gene affect mainly its expression (overexpression or downregulation)[129]. The main disorders caused by mutations in the Sox9 gene/expression include cancer, sex-reversal and campomelic chondrodysplasia.

5.1.1 Sox9 and cancer

It has been suggested that Sox9 plays a role in tumorigenesis, metastasis and drug resistance in several types of human cancers[130,131]. It acts as an oncogene in breast[156], pancreatic[157], prostate[158,159], gastric[160], renal cancer[161] and others, where Sox9 expression is upregulated and overexpressed and most of the mutations are in the non-coding region of Sox9. Whereas, in other types of cancers, like the case of cervical[162] and colorectal cancer[163], Sox9 behaves as a tumor suppressor gene, and when mutated in its coding region, its function is repressed, and cancer is developed.

5.1.2 Sox9 and sex-reversal

During embryonic development, Sox9 plays the role of a sex determining gene, downstream of SRY (sex-determining region Y). SRY protein binds to Sf1 (steroidogenic factor-1),

forming a complex that activates Tesco (Testis Specific Enhancer of Sox9 core), a Sox9 enhancer. Tesco activation induces Sox9 protein expression in male gonads that allows Sertoli cells differentiation, and through a positive feedback loop, Sox9 maintains its expression by forming a complex with Sf1 and activating Tesco[98,129,164–166]. Mutations in Sox9 lead to sex reversal cases seen in humans, as well as in mice[147,148,167,168] . Studies showed that when Sox9 is overexpressed in XX mice[169], male testis developed, and in Sox9$^{-/-}$ mice models, their sex reversed; from male to females despite having the XY chromosomes[167]. Mutations in SRY and Tesco can also cause gonad dysgenesis, however, a more detailed genetic diagnosis for sex reversal cases is required for a better understanding of the mutation types and location[129].

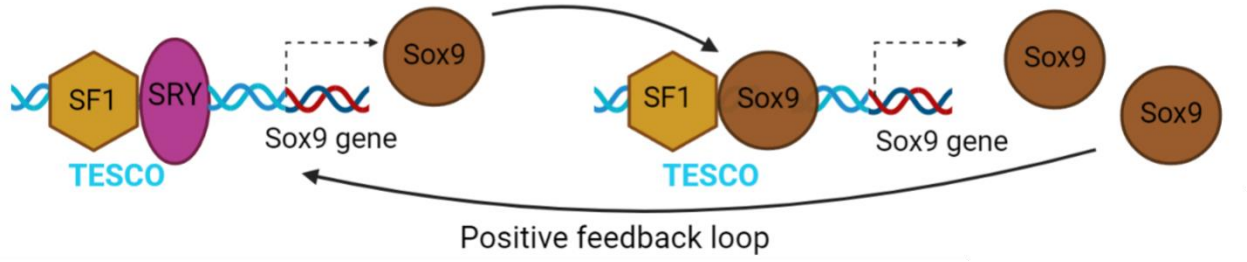

Figure 10: Sox9 expression. SRY protein binds to SF-1 protein, and the complex induces Sox9 expression in Sertoli cells by activating TESCO (sox9 enhancer). Through a positive feedback loop, Sox9 maintains its expression by binding to SF-1 and the dimer complex activates TESCO, which induces more Sox9 protein transcription (Positive feedback loop) (created on biorender).

5.1.3 Sox9 and campomelic chondrodysplasia

Sox9 is one of the first genes expressed in limb bud development[170–172] in embryos, and its deletion before the mesenchymal condensation stage of limb bud formation leads to complete absence of cartilage and bone, a severe and fatal skeletal disorder in humans known as Campomelic Chondrodysplasia (CCD). Its main cause is a heterozygous mutation in Sox9 leading to a loss of

function of the protein. Sox9$^{+/-}$ mice die around birth with a similar phenotype[170–172]. When the mutation is in the coding region of Sox9, individuals are born with a hypoplastic scapulae, bowed lower limbs, non-mineralized thoracic pedicles and narrow iliac wings (132). These mutations could be in the HMG-box domain of Sox9, NLS or TA domain[147,173–176]. In case of a mutation in the upstream non-coding region of Sox9, similar phenotypes are presented minus the bowed limbs[154]. Since Sox9 is widely expressed in many somatic tissues, malfunctions of other organs are also presented in CCD patients, such as the heart, brain, lungs and Kidneys[177], in addition to sex reversal conditions where the majority of XY patients develop female gonads and XX patients develop testis[173].

5.2 Sox9 in skeletal tissue

Sox9 is a regulator gene expressed early in skeletal development, it is required for chondrogenesis during the mesenchymal condensation step in limb bud formation, where mesenchymal cells differentiate into chondrocytes[7]. Sox9 expression is present in chondro-progenitors, proliferative and mature chondrocytes and absent in pre-hypertrophic/hypertrophic chondrocytes, thus inducing proliferation and inhibiting hypertrophy[6,7]. However, downregulation of Sox9 expression in hypertrophic chondrocytes is crucial for bone marrow formation and blood vessel invasion during endochondral ossification step[127,178]. Studies showed that Sox9 regulates the expression of several genes involved in skeletal development. Deletion of the Sox9 gene completely inhibits the expression of Sox5 and Sox6, two genes coding two proteins required for chondrogenesis, it also eliminates the expression of Runx2, a crucial transcription factor for osteoblast differentiation[154,155,172]. In addition, it upregulates the expression of several extracellular matrix genes, such as aggrecan, and many collagens including Col2a1, Col9a2 and Col11a2, all of

which are highly expressed in proliferative chondrocytes[7,155,171,172,179], while downregulating Col10a1 expression which is observed in hypertrophic chondrocytes[134,178]. In addition, Indian Hedgehog (Ihh), Patched-1, parathyroid hormone-related peptide and its receptor expression are all downregulated when Sox9 is not present[172]. As for ß-catenin, Sox9 stimulates its degradation via the ubiquitination/proteasome pathway and inhibits its expression during chondrogenesis[180]. In later embryonic skeletal development, Sox9 remains expressed in various progenitor cells for tendons, ligaments, marrow stroma, bone and cartilage tissues[124,181–183]. In adult mice, Sox9 is reported to be expressed by proliferative chondrocytes and their progenitors[123,184], but little is known about the property of Sox9 in postnatal skeleton.

6. New cutting-edge imaging technique

The study of postnatal skeletal tissue has been hindered by technical difficulties; these include processing hard and thick bone tissues for histology while conserving their morphology, and the issue of high auto-fluorescence of bone and marrow, rendering imaging studies difficult. A newly developed multicolor, three-dimensional confocal imaging method has been recently published for whole postnatal mice bones, in addition to XiT software for unbiased quantitative image analysis of large datasets[109,185,186]. This cutting-edge technique addresses these technical challenges by preserving bone tissue integrity, imaging the entire organ at a high resolution and using a multiplexed immunostaining, allowing proper lineage tracing and fate analysis[185]. This method was used to map the expression of the various putative SSCs markers in bones, and it was found that most of these markers were non-specific and labeled various differentiated cell lineages[109]. Briefly, mice are injected with 4OHT then femurs are collected at different timepoints post-injection. Bones are fixed, decalcified with EDTA and >300mm thick sections are produced on a vibratome.

Immunofluorescent staining and optical clearing for deep imaging is then performed. Samples are mounted and imaged on a Leica TCS SP8 spectral confocal system equipped with five detectors, AOBS, virtual filters and eight laser lines during an average of 12h/sample, generating datasets of 20-100GB. Images are then compressed (lossless), cell types of interest expressing tdTomato are segmented with Imaris, and further quantified using Xit software[185] which allows FACS-like gating on populations based on staining controls (fluorescence minus one), automated phenotype analysis, mapping of cell types within the sample, fluorescence bleed through compensation, and other functions.

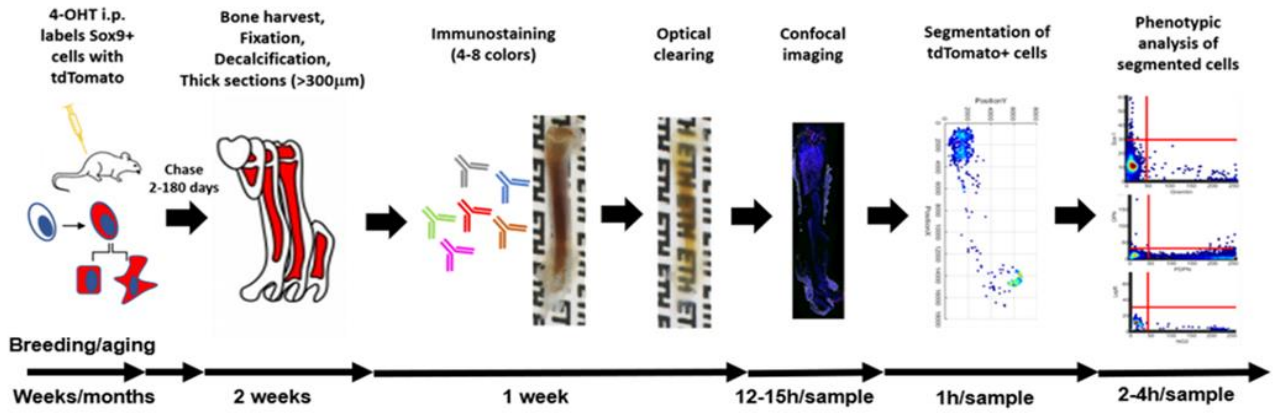

Figure 11: Lineage tracing analysis pipeline. CreERT2 driver lines are crossed with the Ai14 tdTomato Cre-reporter lines. Mice are injected with 4-hydroxytamoxifen (4OHT) inducing tdTomato expression in Cre+ cells. After a chase period, bones are processed, immunostained, optically cleared and imaged by confocal microscopy. tdTomato+ cells are segmented, and their phenotype quantified using imaging cytometry (gated according to staining controls). Adapted from Coutu et al., Nature Methods (2018) (figure courtesy of Dr. Daniel Coutu).

7. Rationale

The studies cited above provide little or no data about the existence of these stem cell populations in juvenile or adult organisms. Also, they lack self-renewal and multipotency assays at the single cell level. While all these populations are found near the growth plate cartilage and in the periosteum, it is important to understand whether these cells persist or not in adulthood, and what could explain the blunted regenerative capacity of skeletal tissues with age. Answering these questions will help design more effective regenerative therapies for orthopedic conditions. We performed lineage tracing of Sox9+ cells in whole adult mouse femurs using multicolor 3D confocal microscopy and quantitative imaging cytometry[109,185]. By using this newly described method and software, the study and characterization of the molecular and cellular biology of SSCs in-vivo becomes possible.

8. Hypothesis

We here hypothesize that the postnatal skeleton contains self-renewing multipotent Sox9-expressing skeletal stem cells that persist in adulthood, with osteochondral potential and regenerative capacity.

Chapter 2. Methods and materials

2.1 Animals

All experiments in mice were performed in accordance with the Animal Care and Veterinary Service (ACVS) guidelines at University of Ottawa and approved by the institutional ethics review board. The Sox9-CreERT;Ai14 double mutant mouse line used in this study was obtained by breeding two mouse strains, both in the C57Bl/6 background: 1) an inducible Cre driver line in which expression of the CreERT2 BAC transgenic is driven by the Sox9 promoter (Sox9-cre/ERT2)1Msan/J; MGI: 5009223)[139], and 2) a Rosa26 LoxP-STOP-LoxP fluorescent Cre-reporter mouse line in which expression of the tdTomato (Ai14) reporter is induced by Cre activation (B6.Cg-*Gt(ROSA)26Sor*$^{tm14(CAG-tdTomato)Hze}$/J; MGI : J:155793)[97]. Both strains were purchased from the Jackson Laboratory.

Experiments were conducted using both males and females because of sexual dimorphism in skeletal physiology. Two age groups of male and female mice were used for this study, juvenile mice (P56) and adult mice (P180). Once they reached their appropriate age, they were injected 1-3 times with 75mg/kg body weight 4-hydroxytamoxifen (4OHT) or tamoxifen (TAM), as indicated in the text/figures, at 24h intervals intraperitoneally (i.p) to activate CreERT and induce the expression of tdTomato in Sox9+ cells. At several time-points following 4OHT/TAM administration (TAM at P56 or P180, timepoints P58 or P182, P86 or P210, and P236 or P360), the mice were euthanized by CO_2 inhalation followed by cervical dislocation[139,187].

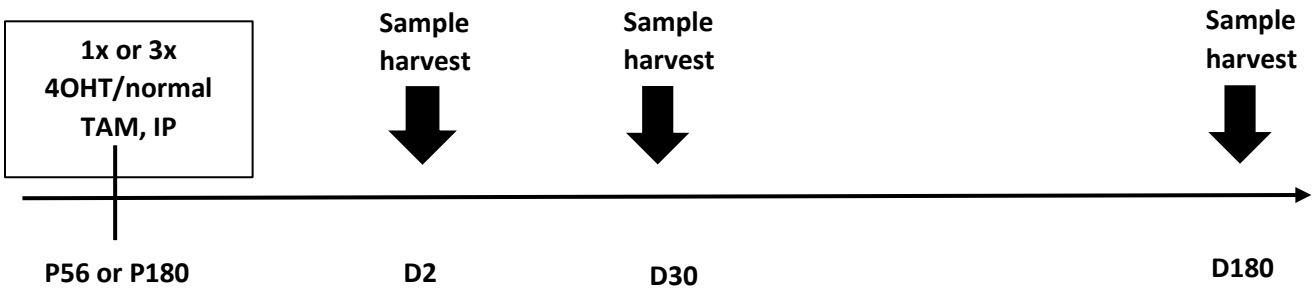

2.2 Genotyping

Mice were genotyped to test for the presence and/or homo-/heterozygosity of the Cre and Ai14 alleles. Genomic DNA extraction was performed by adding 120uL of lysis reagent (50mM NaOH) to mouse ear punches. The samples were heated to 95°C by using the heat block for 20 min, then 30uL of neutralization buffer (1 M Tris-HCl, pH 7.4) was added. Samples were then centrifuged at 14800 rpm using a microcentrifuge (Thermo Fischer, Sorvall legend XtR) for 5 min to pellet hair and debris and stored at 4°C. PCR mix consisted of 2x Taq FroggaMix (FroggaBio), nuclease-free water, extracted DNA template and specific primers for each gene as per the table below[188,189]:

Gene	**Orientation**	**Sequence (5' -> 3')**
Cre	Forward	AGGTGTAGAGAAGGCACTTAGC
	Reverse	CGGCGGCGGTCACGAACTCC
Ai14 Wildtype	Forward	AAG GGAGCTGCAGTGGAGTA
	Reverse	CCGAAAATCTGTGGGAAGTC
Ai14 Mutant	Forward	GGCATTAAAGCAGCGTATCC
	Reverse	CTGTTCCTGTACGGCATGG

PCR reaction was performed using the following thermal cycling conditions[188,189]:

Steps	**Temperature**	**Time**	**Cycles**
Pre-denaturation	94°C	3 min	1
Denaturation	94°C	30 sec	30
Annealing	Cre: 54°C Ai14 WT: 60°C Ai14 MT: 62°C	30 sec	
Extension	72°C	1 min	
Hold	72°C	10 min	1
Hold	12°C	Infinite	

2.3 Skeletal cells isolation

Sox9-CreERT;Ai14 mice were injected at P56 or P180 (as indicated in text/ figures) with a single dose of 4OHT, then femurs or joints were harvested after 48h. Epiphyses were cut, marrow was flushed out using 25G needle filled with PBS, then mechanically dissociated by passing through 25G needle. Bone was cut in small pieces, enzymatically dissociated, then crushed using a sterile mortar and pestle under the cell culture hood. Stemxyme (Worthington Biochemical Corp.) was used for enzymatic digestion. Alternatively, a custom enzymatic cocktail (as indicated in text/ figure) was used containing PBS with 2% FBS, 2.5 mg/mL of collagenase I (Worthington), 0.7 mg/mL of collagenase II (Worthington), 1 U/mL of dispase (Worthington) and 5uM of Ca2+(Sigma-Aldrich).

The samples were then placed on a shaker for 45 min at 37°C. Cells were filtered using a 100um cell strainer, then plated in cell culture dishes with murine Mesencult expansion medium (StemCell Technologies). Skeletal cells were passaged biweekly or when they reached 80% confluency, whichever came first. For enrichment, negative selection was used where CD31+ endothelial, Ter119+ erythroid, and CD45+ hematopoietic cells were magnetically depleted using the EasySep™ Mouse Mesenchymal Stem/Progenitor Cell Enrichment Kit StemCell Technologies (customized by adding a biotinylated CD31 antibody)[187,190].

2.4 LIVE/DEAD assay

After skeletal cell isolation, a viability assay was performed to measure the ratio of live cells versus dead/dying cells using the LIVE/DEAD™ Cell Imaging Kit (488/570) (Invitrogen)[191], as per the manufacturer's instructions.

2.5 Antibodies

The list of primary and secondary antibodies used for staining in this study are summarized in the tables below. All primary and secondary antibodies were reconstituted according to manufacturer's instructions (when required), then diluted 1:1 in glycerol, and stored at -20^{O}C.

Table 1: Primary antibodies

Catalog number	Target	Clone	Company	Host Species	Dilution
AF2910	alkaline phosphatase	poly	Cedarlane/R&D	Goat	1/400
AF497	lepR	poly	Cedarlane/R&D	Goat	1/100
AF808	OPN	poly	Cedarlane/R&D	Goat	1/200
MAB808-100	OPN	2139B	Cedarlane/R&D	Rabbit	1/200
108102	Sca1	D7	Cedarlane/BioLegend	Rat	1/400
AF1226	Sca1	poly	Cedarlane/R&D	Goat	1/50
ab209484	Osterix	EPR21034	abcam	Rabbit	1/200
ab-23750	Fibronectin	poly	abcam	Rabbit	1/100
CL50151AP	collagen type 1	poly	Cedarlane	Rabbit	1/100
5012587	CD45	30-F11	FisherScientific/eBioscience (OH Store)	Rat	1/50
5011513	CD31-biotin	390	FisherScientific/eBioscience (OH Store)	Rat	1/50
AF3628	CD31	poly	Cedarlane/R&D	Goat	1/25
5013211	Endomucin	V.7C7	FisherScientific/eBioscience (OH Store)	Rat	1/50
AB14106	SM22	poly	Abcam	Rabbit	1/400
AB8874	CD271	poly	Abcam	Rabbit	1/50
AB5320	NG2	poly	Millipore	Rabbit	1/50
600-401-379	RFP	poly	Rockland	Rabbit	1/50
14-0731-82	CD73	TY/11.8	FisherScientific/eBioscience (OH Store)	Rat	1/50
AF2067	CD90	poly	Cedarlane/R&D	Sheep	1/200
ab203676	tenomodulin	poly	abcam	Rabbit	1/50

Catalog number	Target	Clone	Company	Host Species	Dilution
AF3615	collagen type 2	poly	R&D/Bio-techne Canada	Sheep	1/50
LS-C359243	Aggrecan/ACAN	poly	LSBio	Rabbit	1/50
AF956	Gremlin	poly	R&D/Bio-techne Canada	Goat	1/50
ab263898	THBS4	EPR22922-232	abcam	Rabbit	1/50
AF3244	Podoplanin	poly	R&D/Bio-techne Canada	Goat	1/50
ab19027	Cathepsin K	poly	abcam	Rabbit	1/50
ab81443	Fibromodulin	poly	abcam	Rabbit	1/50
LS-C160144-400	TPPP3	poly	LSBio	Rabbit	1/50
ab185966	Sox9	EPR14335-78	abcam	Rabbit	1/50
NB300-144AF488	Laminin a1	poly	Novus Biotechnology	Rabbit	1/50
AF3075	hSOX9	poly	R&D systems	Goat	1/50
14-5698-82	Ki-67	SolA15	Fisher Scientific	Rat	1/50
sc-65495	Endomucin	V.7C7	Santa Cruz	Rat	1/50
AF806	CD31	poly	R&D Biotechne	Sheep	1/50
OAAB18141	GLI2 C terminal	poly	Aviva System Biology	Rabbit	1/50
14-0441-82	CD44	IM7	eBio/Fisher Scientific	Rat	1/50
PA5101921	Tbx18	poly	Thermofisher	Rabbit	1/50
600-901-379S	anti-RFP	poly	Rockland	chicken	1/50
BS-0709R	collagen 2	poly	Thermofisher	Rabbit	1/50
14-9771-82	collagen X	X53	Thermofisher	Mouse	1/50

Catalog number	Target	Clone	Company	Host Species	Dilution
MA517687	CD45	YAML501.4	Thermofisher	Rat	1/50
17399-1-AP	Peripherin	poly	Thermofisher	Rabbit	1/50
ab189034	P16	poly	abcam	Rabbit	1/50
AF853	GDF5	poly	R&D/Bio-techne Canada	Goat	1/50
sc-130428	Tbx18	CD-21	Santa Cruz	Mouse	1/50
ab213723	Bmi1	EPR19848	abcam	Rabbit	1/50

Table 2: Secondary antibodies

Catalog number	Fluorophore	Company	Host species	Dilution
A21208	Alexa Fluor 488	Thermofisher	Rat	1/200
A21206	Alexa Fluor 488	Thermofisher	Rabbit	1/200
S32354	Streptavidin Alexa Fluor 488 Conjugate	Thermofisher	N/A	1/200
A31572	Alexa Fluor 555	Thermofisher	Rabbit	1/200
A21432	Alexa Fluor 555	Thermofisher	Goat	1/200
S32355	Streptavidin Alexa Fluor 555 Conjugate	Thermofisher	N/A	1/200
A21082	Alexa Fluor 633	Thermofisher	Goat	1/200
S21375	Streptavidin Alexa Fluor 633 Conjugate	Thermofisher	N/A	1/200
A10043	Alexa Fluor 680	Thermofisher	Rabbit	1/200
A21084	Alexa Fluor 680	Thermofisher	Goat	1/200
S32358	Streptavidin Alexa Fluor 680 Conjugate	Thermofisher	N/A	1/200
A32814	Alexa Fluor Plus 488	Thermofisher	Goat	1/200
D1306	DAPI (4'6-Diamidino-2-Phenylindole Dihydrochloride)	Thermofisher	N/A	1/500

2.6 Skeletal Cell staining

Skeletal cells were immediately fixed after isolation with 16% methanol-free paraformaldehyde (Electron Microscopy Sciences) diluted to 4% in PBS, for 15 min at room temperature. Cells were then stained with primary antibodies (1/200 dilution from stock concentration) for 15 min at room temperature on a shaker, then washed with 1x PBS. Cells were then stained with DAPI (1/500 dilution from stock concentration of 2mg/mL prepared in DMSO) and secondary antibodies (1/200 dilution from stock concentration) for 15 min at room temperature on a shaker, then washed with 1x PBS and finally mounted between microscope slides and coverslips, with 80% glycerol mounting medium with 0.1 M N-propyl gallate (Sigma) and a pH of 8.5, for confocal imaging[187].

2.7 CFU-F assay

Sox9-CreERT;Ai14 mice were injected at P56 or P180 (as indicated in text/ figures) with a single dose of 4OHT. Femurs or joints were harvested two days post-4OHT, and cells were isolated as described in section 2.3. Cells were then counted and seeded at densities of 1.2×10^5 cells/cm2, in triplicates, in 24 well-plates. After 10 days in culture, cells were fixed and stained with 0.5% crystal violet in methanol. The total number of colonies and the number of tdT+ colonies were counted (colonies containing >20 fibroblastoid cells were counted) using an Epifluorescence microscope (Nikon eclipse TE2000-E, filter B-2E/C , DM:505, Excitation: 465-495 and Emission: 515-555, CFI Plan Fluor 10X Dry N.A 1.3)[187].

2.8 *In vitro* differentiation

Sox9-CreERT;Ai14 mice were injected at P56 or P180 (as indicated in text/figures) with a single dose of 4OHT, then femurs or joints were harvested two days post-4OHT, and cells were

isolated as described in section 2.3, then cultured in Mesencult medium (StemCell Technologies). Cells were expanded until confluence in 9 wells (three biological replicates with three technical replicates each) of 24-well plates. Adipogenic, chondrogenic and osteogenic differentiation was induced in three wells each. For chondrogenic differentiation, cells were pelleted by centrifugation at 1200RPM using a centrifuge (Eppendorf, 5810 R, v8.4) in 15 mL falcon tubes to promote aggregation. Serum-free chondrogenic medium contained 10ng/mL TGF-β1, 100nM dexamethasone, 50 µg/mL ascorbic acid-2-phosphate, 100 µg/mL sodium pyruvate, 40 µg/mL L-proline, 1X ITS+3 (Sigma) and 1.25mg/mL Bovine Serum Albumin. For osteogenic and adipogenic differentiation, cells were differentiated using mouse MesenCult™ Adipogenic and Osteogenic Differentiation Kits from StemCell Technologies. Cells were differentiated for 3 weeks and then fixed, immunostained, as described in section 2.6, for differentiation markers and imaged using confocal microscopy. Alternatively, mineralized matrix was stained with 2% m/v alizarin Red diluted in ddH_2O, and adipocytes with 2uM BODIPY™ 493/503 (4,4-Difluoro-1,3,5,7,8-Pentamethyl-4-Bora-3a,4a-Diaza-*s*-Indacene) (Invitrogen)[187].

2.9 FACS sorting (flow cytometry)

To sort tdT+ cells, Sox9-CreERT;Ai14 mice were injected at P56 with a single dose of 4OHT, then joints were harvested two days post-4OHT. Joints were digested and depleted from hematopoietic and endothelial cells as described in section 2.3. tdT+ cells were isolated from both distal femurs and proximal tibias using a MoFlo XDP flow cytometer and sorter located at the Flow cytometry and Cell sorting facility of the Ottawa Hospital Research Institute, as described[121].

2.10 Single-cell RNA sequencing

Sox9-CreERT;Ai14 mice were injected at P56 with a single dose of 4OHT, then femurs were harvested two days post-4OHT. Femurs were digested and depleted from hematopoietic and endothelial cells as described in section 2.3. The 10X Genomics Chromium Single Cell 3' Assay was used with library preparation and sequencing performed at the genomics core facility in Ottawa Hospital Research Institute. 10^4 cells were sequenced at a depth of 25K reads/cell and the data was analyzed at the bioinformatics core facility and with the help of our collaborator Dr Theodore Perkins (Ottawa Hospital Research Institute). Genes identified had variable expression based on dispersion of binned variance to mean expression ratio. A dimensionality reduction method (principal component analysis, PCA) was then used on this subset of genes after filtering out ribosomal and mitochondrial genes. The data was reduced to the top PCA components and performed graph-based clustering (FindNeighbors and FindClusters functions in Seurat). The clusters were visualized on 2D map computed by t-SNE and UMAP approaches. Finally, genes differentially expressed between clusters were identified[190].

2.11 Focal osteochondral defect injury model (FOD)

Sox9-CreERT;Ai14 mice were injected at P56 or P180 with one or three injections of 4OHT or normal tamoxifen (as indicated in text/figures) at 24h intervals. P58 or P182, P86 or P210, and P236 or P360 post-4OHT, a FOD injury was created in the distal femur by doing an incision, revealing the knee joint and luxating the patella laterally. Once the distal femur was exposed, a full-thickness defect penetrating cartilage and subchondral bone was made by drilling a hole in the femoral trochlear groove using a 25G needle. The contralateral leg was sham operated as a control; the same surgery was performed except no hole was drilled in the femur. Joint samples were then collected at day two, seven, and 30 post-FOD injury and processed for imaging[192,193].

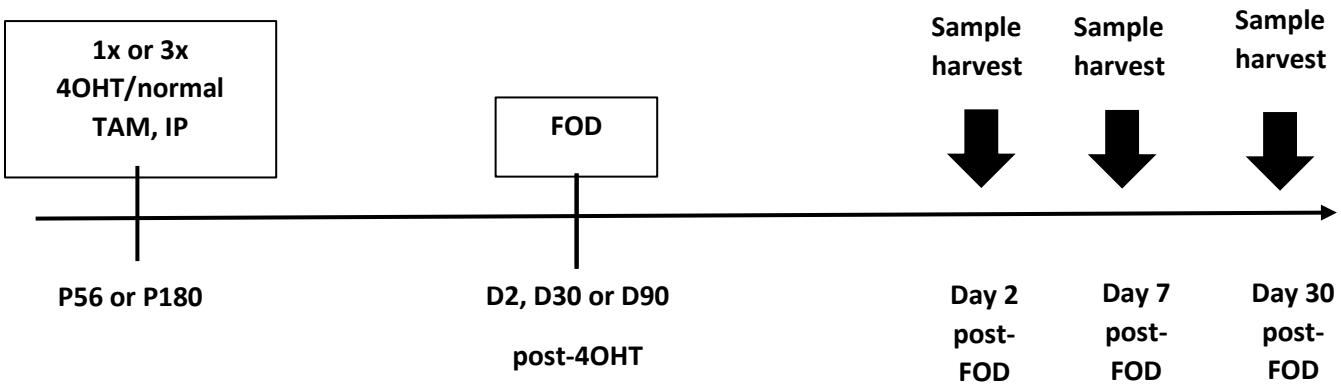

2.12 Tissue harvesting and processing for immunofluorescence

Sox9-CreERT;Ai14 mice were injected at P56 or P180 with one or three injections of 4-OHT (as indicated in text/figures), and femurs or joints were collected at specific timepoints (two, 30 and 180 days post-4OHT injection), for both conditions (healthy versus FOD injury) and both gender (three males and three females/condition). Femurs and joints were cleaned from muscle tissue then fixed overnight in 4% methanol-free paraformaldehyde (Electron Microscopy Sciences) diluted in PBS at 4°C with rotation. This was followed by decalcification for two weeks in 10% EDTA (Sigma) diluted in PBS, pH 8, at 4°C with stirring[194].

2.13 Vibratome sectioning

Decalcified bones/joints were embedded in 4% low-temperature gelling agarose (high gel strength grade, Bioshop, CAS#9012-36-6), and then cut into 250 µm-thick sections for femurs and 400 µm-thick sections for joints, using a Leica VT1200S vibratome with low profile, injector-type Endurium zirconia ceramic blades (Cadence Inc.). These femur/joint sections were then probed by immunofluorescence staining and processed for confocal microscopy[194].

2.14 Immunofluorescence

Femur/joint sections were blocked and permeabilized for 1h with blocking buffer made from TBS (final concentration 0.1M Tris, 0.15 M NaCl, pH 7.5), 0.05% Tween-20, 20% DMSO (all from Sigma), 5% donkey serum (Jackson ImmunoResearch) and 0.3% Triton X-100 (Sigma). Sections were then stained with primary antibodies (refer to section 2.13 table x for working dilutions) in blocking buffer overnight. Sections were washed 5x60 minutes with TBS containing 0.05% Tween-20, stained with fluorophore-conjugated secondary antibodies (1:200 dilution) and counterstained with DAPI (1:500 dilution of a 2mg/mL stock solution), in blocking buffer, overnight. The fluorophores used were AlexaFluor 555, 488, 633, 680, Biotin-Streptavidin amplifications plus DAPI (Thermo). The samples were then washed 5x60 minutes as above, then optically cleared (see below). All steps were done at room temperature with gentle shaking[109].

2.15 EdU proliferation assay

Sox9-CreERT;Ai14 mice were injected with one or three injections of 4OHT, and simultaneously with one, three or five EdU injections (2.5mg/mL) at 24h interval (as indicated in text/figures). Femurs were harvested and processed as described in section 2.12. Femur sections were blocked then stained with Click-iT EdU Alexa Fluor 488 imaging kit (Invitrogen) overnight[124]. The next day, sections were stained as described in section 2.14.

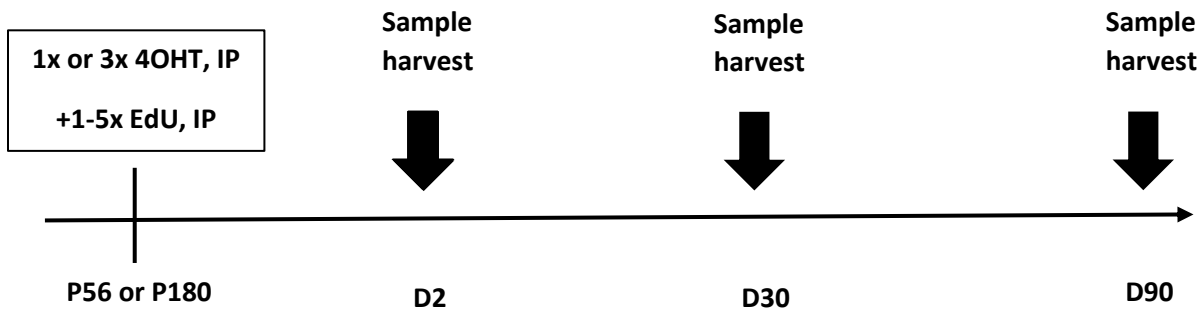

2.16 Optical clearing and mounting of sections

Femur samples were optically cleared with either TDE, glycerol or histodenz (Sigma). For TDE clearing, a graded series of TDE (2,2-thiodiethanol) diluted in TBS was used. Sections were incubated in 25%, 50%, 75%, 90% and 97% TDE, 4x60 minutes each at room temperature with gentle shaking. The final mounting medium consisted of 97% TDE with 0.1 M N-propyl gallate (Sigma) with a pH of 8.5. The refractive index was measured using a handheld refractometer (Atago) and adjusted to 1.518 with TDE or TBS[194].

For glycerol clearing, a graded series of glycerol diluted in TBS was used. Sections were incubated in 20%, 60% and 80% glycerol, 1x20 minutes each at room temperature with gentle shaking. The final mounting medium consisted of 80% glycerol with 0.1 M N-propyl gallate (Sigma) with a pH of 8.5. The refractive index was measured using a handheld refractometer (Atago) and adjusted to 1.467 with glycerol[194].

For histodenz clearing, no graded series was used. Sections were incubated in 88% histodenz overnight at room temperature with gentle shaking. The final mounting medium consisted of 88% histodenz dissolved in TBS with 0.1% tween-20, 0.01% NaN3 and a pH of 8.5. The refractive index was measured using a handheld refractometer (Atago) and adjusted to 1.467 with histodenz[195].

Sections were then mounted on Superfrost microscope slides using custom-designed silicone spacers (Grace Biolabs) and size 1.5 coverslips[194].

2.17 Confocal microscopy

Imaging was performed on a confocal microscope (Leica TCS SP8) equipped with three PMTs (photomultiplier tubes), two HyD detectors and five lasers: blue diode (405 nm), argon (458,

476, 488, 496 and 514 nm) and three helium neon (543, 594 and 633 nm). For TDE cleared samples, type F immersion liquid (Leica) was used with an RI of 1.518, and for glycerol/histodenz cleared samples, type G immersion liquid (Leica) was used with an RI of 1.467. Image acquisition was done using a 20× multiple immersion lens (NA 0.75, FWD 0.680 mm). All scans were acquired at room temperature with a speed of 600 Hz, in the bidirectional mode and with z-spacing of 2.5 um. Images were acquired in 8-bit format with a 1.0× zoom at 1,024 × 1,024 resolution[194].

2.18 Analysis and statistics

Images were compressed (lossless), visualized, and segmented using Imaris v9.8.2 (Bitplane) and segmentation data were exported for downstream analyses using XiT software. For statistical analyses, gated data was exported from XiT and analyzed using GraphPad Prism v9. For statistical analyses, data from all technical and biological replicates was compiled for each age, sex group and condition, and plotted (mean +/- SD). For each cohort, an outlier analysis was performed, and normality tested using the Shapiro-Wilks test. Each age, sex group and condition were compared using two-way ANOVA with significance threshold set at p=0.05. All figure legends contain the *n* and *P* value where relevant[194]. N number used was determined by performing a post-hoc power analysis.

Chapter 3: Determination of Sox9+ cells stemness

According to the most recent literature, Sox9+ cells give rise to osteochondral cells in postnatal animals. In long lineage tracing studies (up to 18 months) using Sox9-Cre mouse lines, as well as in three months old mice, Sox9+ cells showed progenitor properties for bone and cartilage in postnatal femurs. However, these studies failed to demonstrate self-renewal and multipotency at the population or single cell level, thus failing to prove the stemness of these Sox9+ cells[118,123,196]. In addition, Sox9 gene is known to be expressed in mesenchymal cells at the earliest stages in limb formation and appendicular skeletal development in embryos and is an important regulator of chondrogenesis[128,147,159,178,179,197]. In embryos, Sox9+ cells participate in the mesenchymal condensation leading to long bone development. In addition, recent and strong evidence show the persistence of these Sox9+ cells postnatally which retain osteochondro-progenitor properties. Taken together, these studies suggest that Sox9 could be a potential putative marker of SSCs.

To test if Sox9+ cells contain self-renewing and multipotent SSCs, we performed lineage tracing using the Sox9-CreERT;Ai14 BAC transgenic mouse line (Ai14 being a tdTomato fluorescent Cre-reporter allele). Experiments were conducted using both males and females because of sexual dimorphism in skeletal physiology[16,18], and sex was analyzed as an independent variable for statistical purposes. Two age groups of male and female mice were used for this study: juvenile mice postnatal day 56 (P56) in which bones as still actively growing, and skeletally mature adult mice postnatal day 180 (P180)[198]. Once they reached their appropriate age, they were injected 1-3 times with 75mg/kg body weight 4-hydroxytamoxifen (4OHT) or tamoxifen (TAM), as indicated in the text/figures, at 24h intervals intraperitoneally (i.p) to activate CreERT and

induce the expression of tdTomato (tdT) in Sox9+ cells. At several time-points following 4OHT/TAM administration (day two, 30, 90 and 180), the mice were euthanized, femurs were collected and processed for multicolor immunostaining, optical clearing, spectral confocal imaging, and image analysis (figure 12)[109,185].

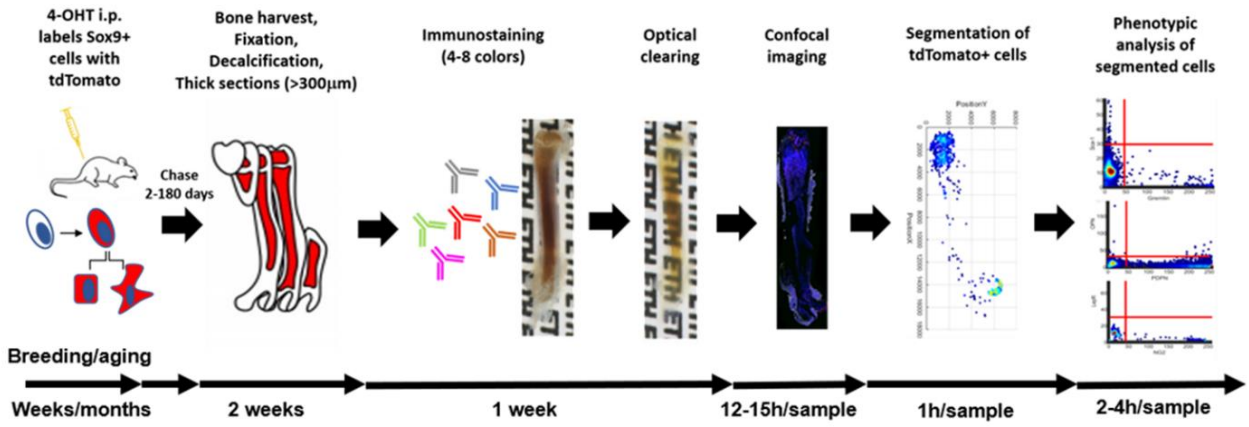

Figure 12: Experimental workflow for lineage tracing. Mice are injected with tamoxifen intraperitoneally to activate Cre-ERT and induce the expression of td-Tomato in Sox-9^{+} cells. Then they are euthanized at the appropriate timepoints (2 days, 1 month, 3 months and 6 months post-4OHT) with CO_2 followed by cervical dislocation, femurs are dissected and cleaned from muscle tissue then fixed overnight in 4% methanol-free paraformaldehyde at 4°C with rotation. This is followed by a decalcification step for 2 weeks in 10% EDTA at 4°C with stirring. The decalcified femurs are then embedded in 4% low-melting agarose, and then cut into 250 µm-thick sections using a LeicaVT1200S vibratome with ceramic blades. These femur sections are used for sample analysis by immunostaining them with different markers of differentiation for chondrocytes and osteoblasts, followed by fluorescence imaging with a confocal microscope. Young mice (between the age of 8 and 9 weeks) and adult mice (between the age of 5 and 6 months) will be compared while separating males and females and the healthy versus the injured model.

3.1 Optical clearing optimization

Several optical clearing solutions were tested; Glycerol, TDE and Histodenz (Figure 13A). For glycerol clearing, sections were incubated in 20%, 60% and 80% glycerol, 1x20 minutes each at room temperature with gentle shaking[194]. For TDE clearing, a graded series of TDE (2,2-thiodiethanol) diluted in TBS was used. Sections were incubated in 25%, 50%, 75%, 90% and

97% TDE, 4x60 minutes each at room temperature with gentle shaking[194]. For histodenz clearing, no graded series was used. Sections were incubated in 88% histodenz overnight at room temperature with gentle shaking[195].

When samples are cleared with glycerol, the depth of imaging (Z position) reaches around 600 µm however, the mean fluorescence intensity (MFI) of tdT is low (~70 relative fluorescence unit (RFU)), as well as the total number of tdT (~ 100 cells). With TDE and histodenz clearings, the depth of imaging is similar to glycerol but the signal of tdT is the strongest (255 RFU) and the number of tdT+ cells detected is five to six-fold higher (Figure 13B). Given the fact that histodenz was the most time efficient in comparison to TDE (overnight clearing with histodenz versus 16 hours of graded series in addition to an overnight with TDE), it was used for optical clearing in the following experiments (Figure 13C).

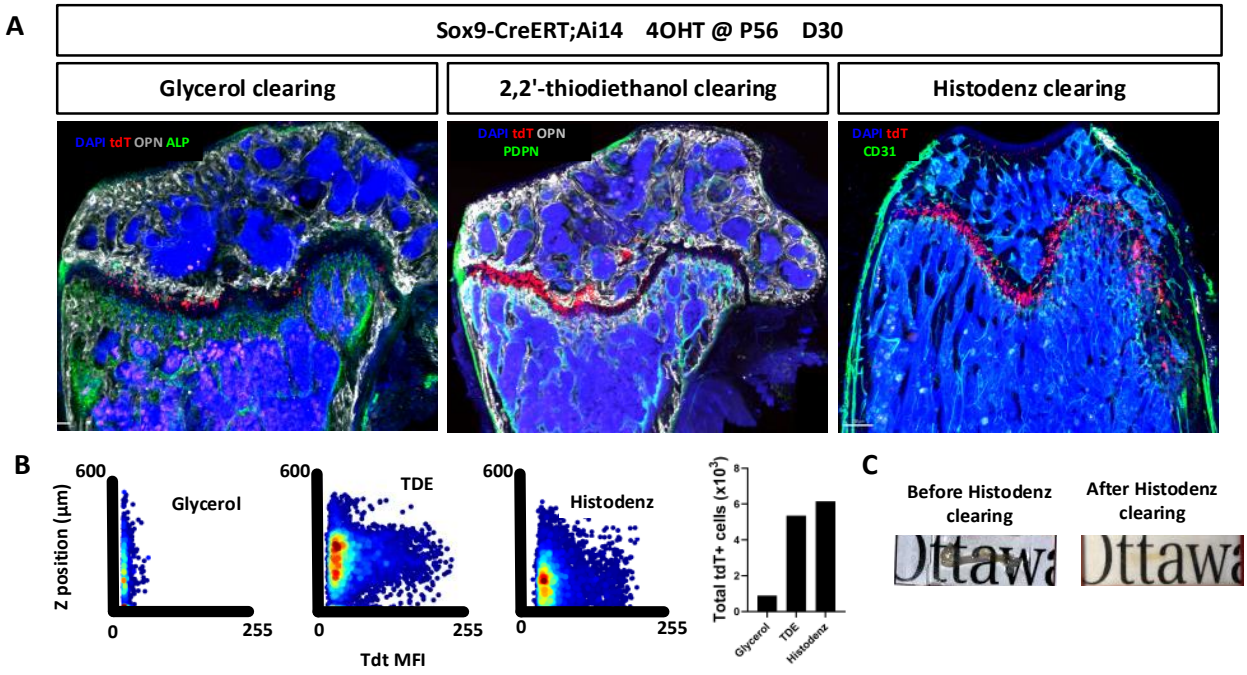

Figure 13: Comparison of different clearing solution. A) Sox9-CreERT;Ai14 mice received 4OHT injection at P56, femurs were then collected at D30 post injection and processed by confocal microscopy and imaging cytometry.

B) Xit plots showing the depth of imaging (position) versus mean fluorescence intensity (MFI) of tdT for each clearing solution. C) Thick section of a mouse femur before and after optical clearing with Histodenz.

3.2 Controls

For all staining, fluorescence minus one (FMO), which is a sample where a single primary antibody is omitted, were used as controls to calibrate laser powers, detectors' (PMTs or HyDs) gain and offset, and virtual filters' bandwidth. This is done by having a fully stained femur sample visualized under the microscope with the appropriate settings for imaging: the lasers are set at the highest intensity possible where no photobleaching occurs, the virtual filters and detectors are set at their maximal bandwidth and sensitivity, allowing visualization of all fluorophores without obvious bleed through between channels. Then, the FMO controls were used to fine tune settings and ensure no bleed through was detected in any channels.

In addition, three different controls were used; sections from Sox9-CreERT;Ai14 mice injected with corn oil as a control for the Cre-LoxP system (test if it is leaky or not). Sections from mice negative for the Cre reporter gene but positive for Ai14 gene, injected three times with 4OHT at 24h intervals to test if tamoxifen injections affected our tdT signal in our images, and sections from C57Bl/6 mice to calibrate 561 laser power, gain settings and decrease background signal (Figure 14).

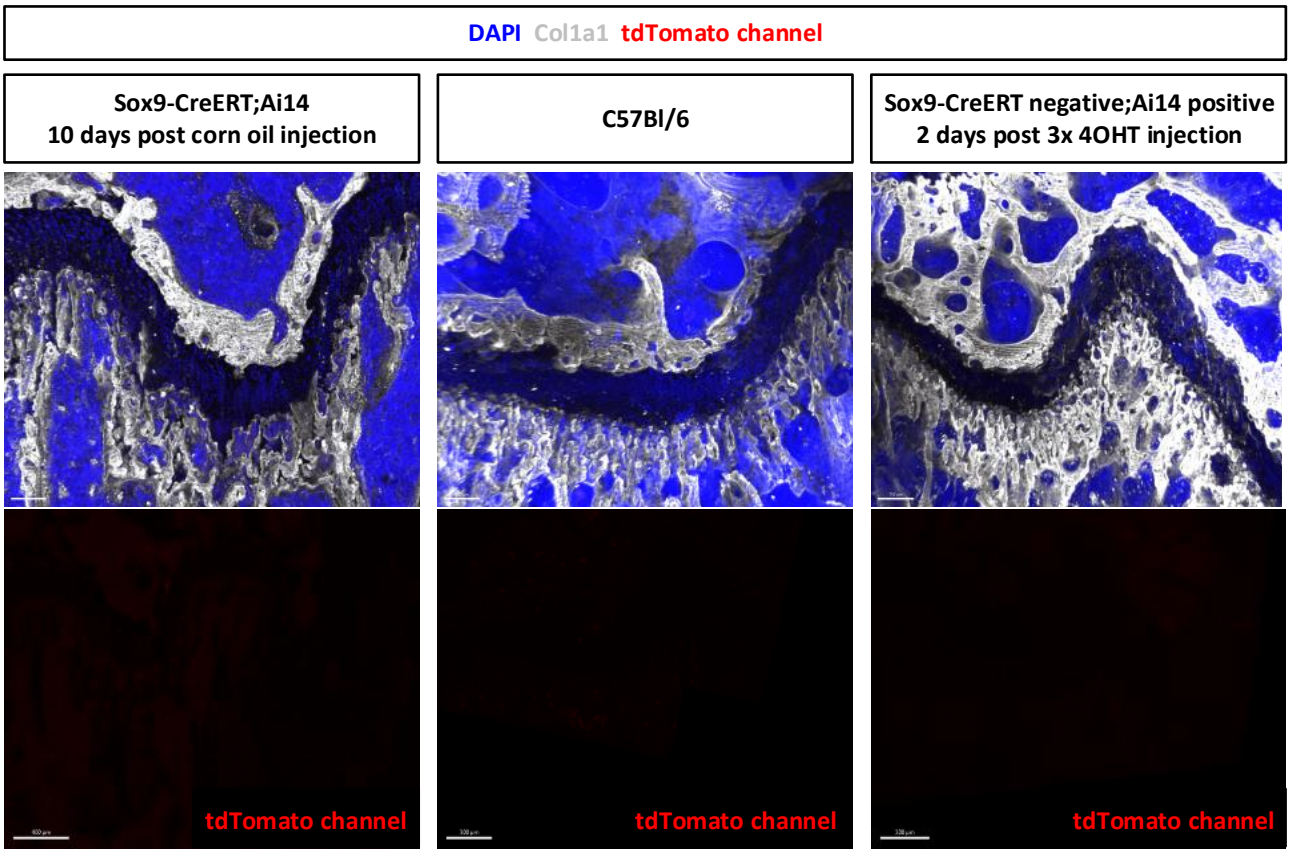

Figure 14: Controls used for staining, gating and imaging. Sox9-CreERT;Ai14 were pulsed with corn oil and femurs were collected 10 days post injection. C57 Black6 mice femurs were collected without any injections, and Sox9-CreERT positive;Ai14 negative mice were pulsed with three 4OHT injected and femurs were retrieved two days later. All femurs collected were then processed by confocal microscopy and imaging cytometry.

3.3 Dual lineage tracing of Sox9+ SSCs in juvenile mice

To track the fate of Sox9+ cells and measure their proliferation rate, we performed dual lineage tracing by pulsing mice at P56 with TAM and the thymidine analogue EdU, respectively, for three consecutive days, and retrieved femurs at day two, 30 and 90. Femurs were harvested, fixed, decalcified, sectioned around 250μm in thickness (representing 30% of the entire bone volume), stained with Sox9 antibody and Click-IT EdU detection, counterstained with DAPI, optically cleared with Histodenz, and then the entire sections were scanned using spectral confocal imaging. We next performed 3D segmentation (Bitplane Imaris) to identify tdT+ cells in the

resulting images, and quantified fluorescence intensity mean of Sox9 and EdU within tdT+ cells using XiT[35].

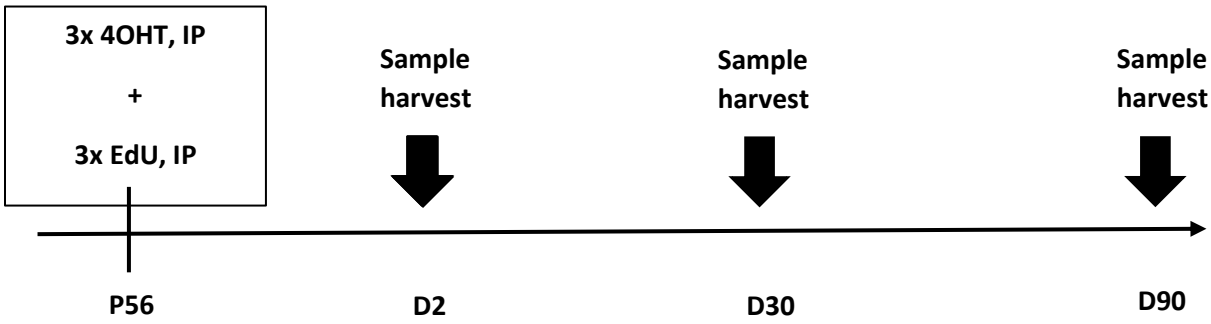

At day two post-labeling, we observed abundant tdT+ chondrogenic cells in the physes of the femur (Figure 15A). We also observed tdT+ osteogenic cells in trabecular and cortical bone, as well as periosteum. These cells were more abundant close to the physes. To quantify the expression of Sox9 protein and EdU incorporation by tdT+ cells, we excluded segmented cells without a detectable DAPI signal, as well as large cells resulting from segmentation errors (Figure 15B, left), then selected gating thresholds based on staining controls (Figure 15B, right). tdT+ cells with detectable Sox9 protein and/or EdU incorporation were found mainly in the resting zone of the physes (Figure 15A) but also in the periosteum and cortical bone, where their abundance negatively correlates with their distance from the physes (Fiure 15A, black arrowheads). We confirmed that our gating thresholds accurately identified Sox9+ and EdU+ cells within the tdT+ population (Figure 15A,i). In the physes, most of the tdT+ cells were found in the resting zone and appeared as flat, mostly Sox9+ cells. Only a few resting zone cells had incorporated EdU during cell division (Figure 15C, left panel). Columns of proliferating chondrocytes were largely EdU+ but tdT-, despite showing detectable levels of Sox9 protein. In contrast, tdT+ osteogenic cells in metaphyseal trabecular and cortical bone were Sox9-EdU- (Figure 15C, left and middle panels).

We also observed abundant tdT-EdU+ cells in the periosteum, throughout the metaphysis and diaphysis (Figure 15C, middle and right panels).

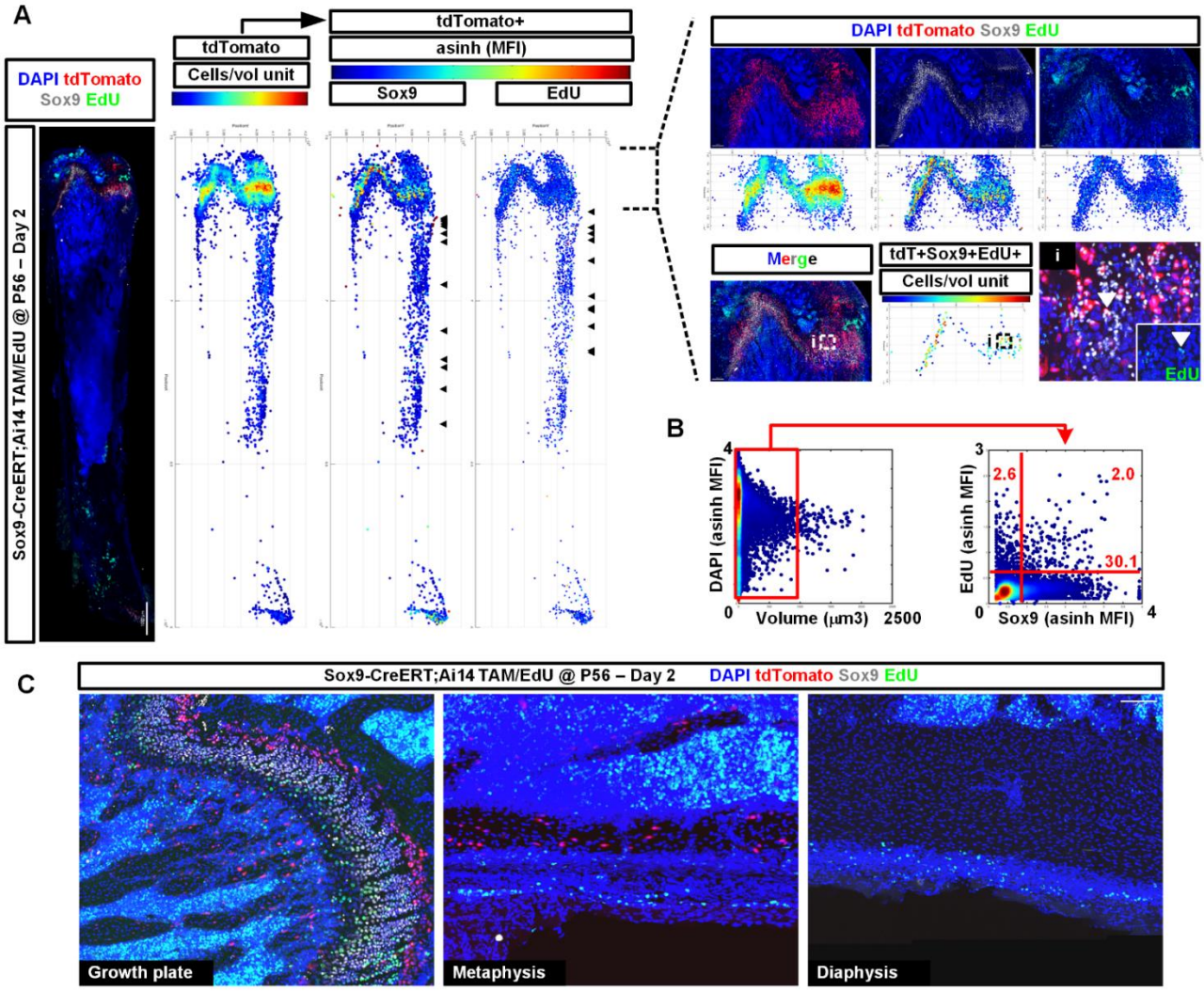

Figure 15: Location of Sox9+ and proliferative cells in the postnatal mouse skeleton. Sox9-CreERT;Ai14 mice received TAM and EdU injections for three consecutive days (P54, P55, P56) and the anatomical location of the tdT+, Sox9+ and EdU+ cells was assessed by confocal microscopy and imaging cytometry two-days post-labeling. A) Left panel: overview of the entire fluorescent image dataset showing a 250µm-thick femur section spanning the entire bone. Second to left panel: Heatmap showing the position and density of each segmented tdT+ cells (each point indicates the center of mass of a cell). Right panels: The expression of the Sox9 protein (based on antibody staining) and incorporation of EdU (detected using Click-IT chemistry) in tdT+ cells is quantified and displayed as the asinh of the mean fluorescence intensity (MFI), to better visualize small and large difference in MFI. Using staining controls, we automatically identify tdT+ cells that are also Sox9+ and/or EdU+. We validate gating thresholds by identifying the same cells in the original images. B) Example of gating strategy using XiT to quantify Sox9+ and EdU+ cells within the tdT+ compartment (each dot represents a tdT+ cell). C) Distribution of tdT+, Sox9+ and EdU+ across the femur (20 optical sections shown, representing 10% of the total volume imaged).

At day 30 post-labeling, most of the chondrogenic cells in the physes were tdT+ (Figure 16A,i) and we also observed an increase in the number of tdT+ osteogenic cells in trabecular and cortical bone (Figure 16A, ii-iii). Only few rare cells retained EdU in the physes and these were largely tdT+. tdT-EdU+ cells were still detectable in the metaphysis and diaphysis, but were now found deeply embedded in cortical bone, suggesting they had differentiated into post-mitotic osteocytes. This further indicates rapid osteogenic cell turnover in growing bones, with a large fraction of osteocytes being replaced by periosteal progenitors within 30 days. At day 90 post-labeling, the mice were skeletally mature, and their bones had stopped growing. In the physes, columns of proliferating chondrocytes were no longer visible but tdT+ cells were still abundant (Figure 16B,i). In addition, rare tdT+Sox9+EdU+ cells were still observed in the resting zone, often appearing as doublets of cells that had just divided (Figure 16B,ii, white arrowheads). In cortical bone, no EdU+ cells were observed but tdT+ cells remain abundant (Figure 16B,iii). In 30- and 90-day chases, we also observed the appearance of tdT+ osteogenic cells in the epiphysis and subchondral bone, structures that were tdT- in shorter chases (not shown).

As a summary, we detected an average of 4.58+/-1.5x10^3 tdT+ cells per section (n=9) at day two post-labeling (Figure 16C). Of these, 37.2+/-5.5% had detectable Sox9 protein, 2.89+/-0.04% had incorporated EdU, and 1.82+/-0.26% were tdT+Sox9+EdU+ (Figure 16D, n=3 for each lineage trace). During bone growth, the number of tdT+ cells increased to 11.7+/-0.7x10^3. When bones entered the homeostatic maintenance phase and stopped growing, the number of tdT+ cells stabilized to the same levels observed in short chases, i.e. 4.62+/-1.4x10^3. The fraction of tdT+Sox9+ also stabilized over time at 13.1+/-2.1% and 12.2+/-3.6%, 30 and 90 days post-labeling, respectively. However, the fraction of tdT+EdU+ and tdT+Sox9+EdU+ continuously decreased over time.

Taken together, these results indicate that Sox9 is expressed by both chondrogenic and osteogenic cells in postnatal bones. Most of these cells are highly proliferative to sustain bone growth and elongation, as well as rapid skeletal tissue turnover. However, a subpopulation of Sox9+ cells residing in the resting zone of the physes are slow-cycling and appear to give rise to both osteogenic and chondrogenic cells in the metaphysis, diaphysis, and epiphysis. Some of these cells persist for months in the resting zone until skeletal maturity, maintain expression of both tdT and Sox9 protein, and retain proliferation capacity. Hence, these display features of self-renewing osteochondral stem cells.

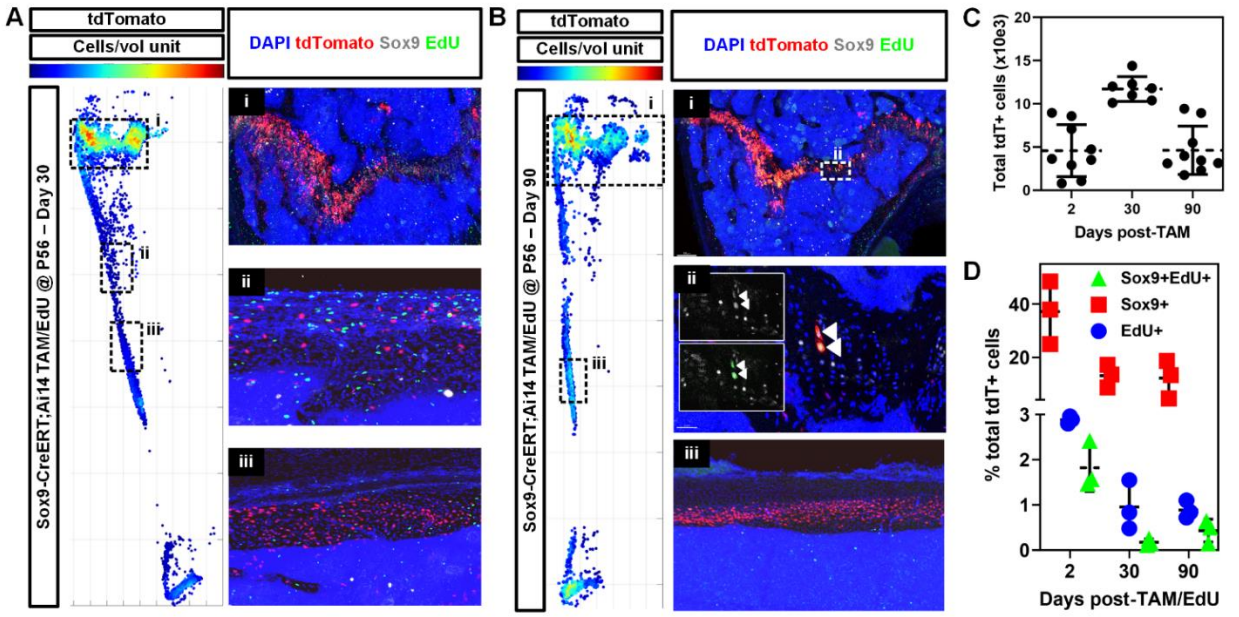

Figure 16: Dual lineage tracing of Sox9+ and proliferative cells in the postnatal mouse skeleton. Sox9-CreERT;Ai14 mice received TAM and EdU on three consecutive days (P54-P56), femurs were retrieved on days 30 and 90 post-labeling to assess the fate of Sox9+ and proliferative cells. A) Anatomical distribution of tdT+, Sox9+ and EdU+ cells, 30 days post-labeling. B) Anatomical distribution of tdT+, Sox9+ and EdU+ cells, 90 days post-labeling. C) Quantification of total tdT+ cells detected per section in each of the three lineage traces (days 2, 30 and 90 post-labeling, n=9 sections from three males and four females for each trace). D) Quantification of Sox9+, EdU+, and Sox9+EdU+ cells in the tdT+ populations, expressed as the percentage of total tdT+ cells (individual values are shown as well as mean +/-SD. n=3 (males only) for each data point).

3.4 Multipotency and self-renewal of Sox9+ SSCs in postnatal mice

To confirm that Sox9+ SSCs persist in the mature skeleton and remain multipotent and self-renewing, we performed longer chases up to six months (D180) after labeling Sox9+ cells in juvenile mice at P56 and in adult mice at P180 that are skeletally mature with a single dose of 4OHT injection.

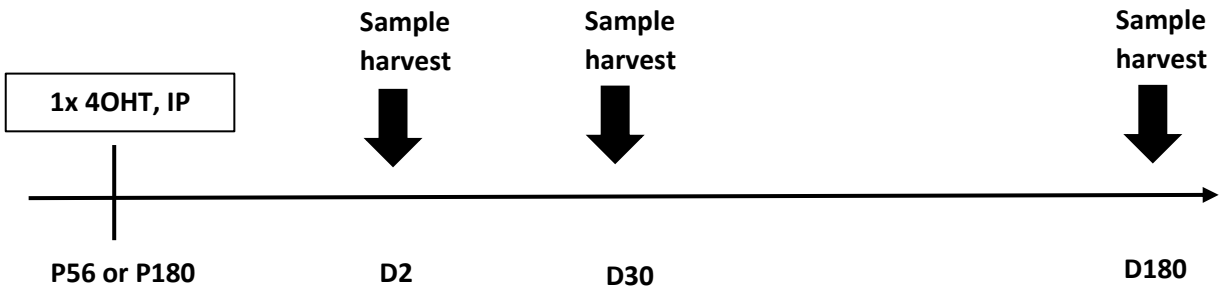

3.4.1 Single injection versus multiple injections of tamoxifen

When Sox9-CreERT;Ai14 mice were injected with TAM on three successive days (P54-P56) and femurs collected two days after the last injection, an average of 6.21+/-3.17 x 10^3 cells were labelled with tdT and these were mainly differentiated chondrocytes in the growth plate (figure 17A, left panel). The high number of labeled cells made lineage tracing results difficult to interpret. In contrast, a single injection of 4OHT (an active metabolite of TAM that is only bioavailable for two hours in mice[36]) at P56 led to a 50% decrease in the number of labeled cells at day two post-4OHT (figure 17B), labeling only the cells in which the Sox9 Cre-reporter transgene was being highly transcribed. These cells were primarily located around the growth plate (perichondrial location) (figure 17A, right panel). To facilitate data interpretation, in the following experiments (unless otherwise specified) we opted for a single 4OHT injection to perform lineage tracing of the few cells that actively transcribed Sox9.

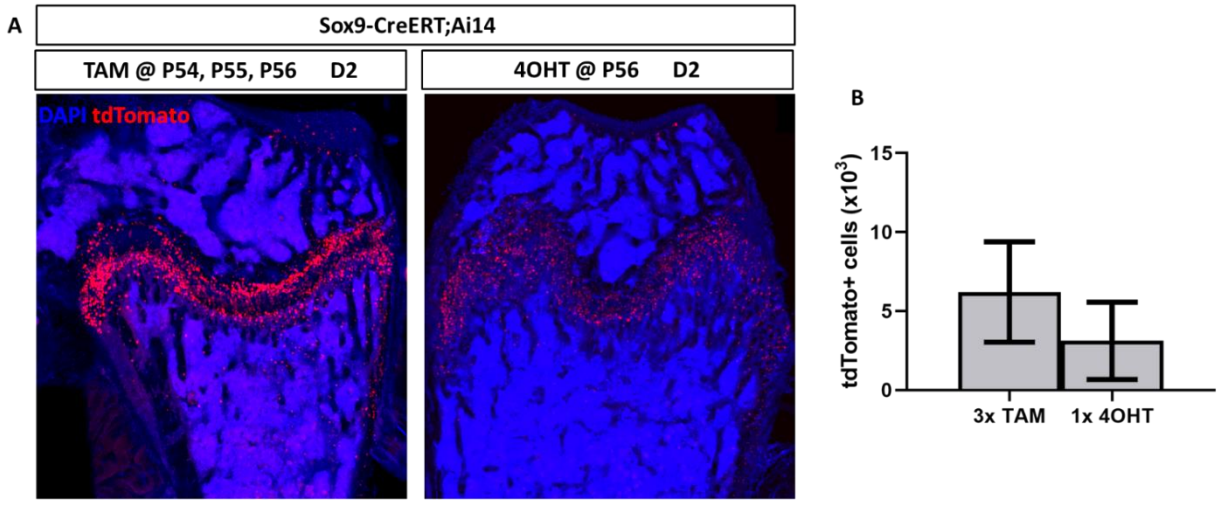

Figure 17: Comparison between two tamoxifen regimens. A) Female Sox9-CreERT2;Ai14 mice were injected at P56 with a single dose of 4OHT injection or were injected at P54, P55 and P56 with three TAM injection at 24-hour interval. Femurs were then collected at D2 post last injection and processed for immunostaining and confocal imaging. B) Quantification of segmented tdT+ cells at D2 post injections (n=6 for 1x 4OHT data set and n=3 for 3x TAM data set).

3.4.2 Lineage tracing of Sox9+ SSCs in juvenile mice

When BAC transgenic CreERT was driven by the Sox9 promoter, a lower number of cells were labeled by a single 4OHT injection in juvenile mice at D2 post-4OHT (figure 18B). They were mainly observed around the distal growth plate (figure 18A and 19), in periosteum/cortical bone, subchondral bone, and the proximal growth plate (figure18A, 19A and B). Their population increased by fivefold at D30, then at D180 their number decreased back to the original number of tdT+ cells observed at D2 (Figure 18B). tdT+ cells were giving rise to cortical and trabecular osteoblasts, periosteal cells, growth plate chondrocytes and marrow adipocytes. (Figures 18 and 19A and B). Given the short lifespan of these differentiated cells (12-30 days in mice)[106,199,200], we assumed a large proportion of the tdT+ cells progeny have already turned-over. In contrast, when BAC transgenic CreERT expression was driven by Osx/Sp7 promoter (marker expressed in committed multipotent progenitors and differentiated osteoblasts/osteocytes), tdTomato

expression was observed in various cells of the osteoblast and chondrocyte lineages in mice injected at P56 and their femurs collected at D2 post-4OHT injection (Figure 18A). After a short chase, some marrow adipocytes were also observed, and the number of labeled cells decreased because of tissue turnover (Figure 18B). This suggests that Osx-CreERT and Sox9-CreERT label the same lineage but that Sox9+ cells are upstream of Osx+ cells.

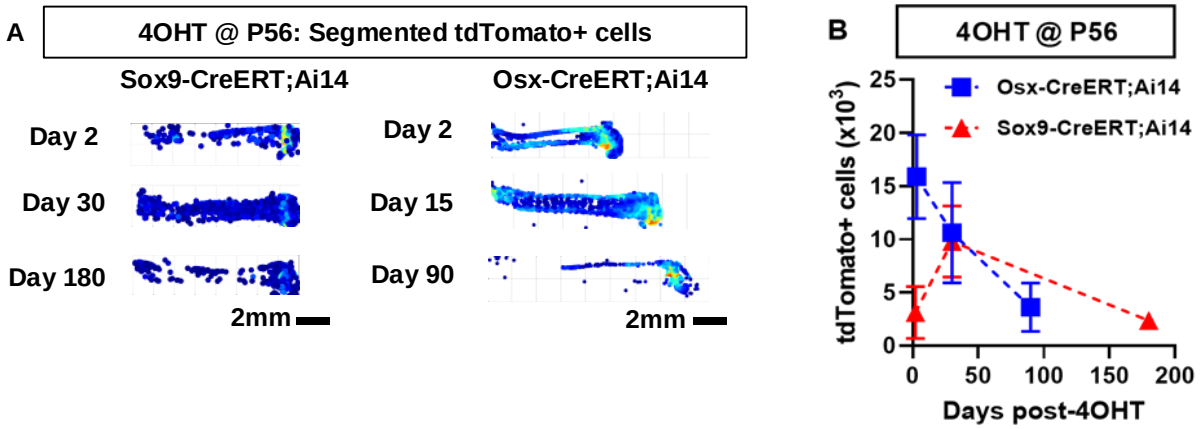

Figure 18: Comparison of lineage tracing of skeletal cells using two different Cre-driver lines. A) 4OHT was administered at P56 in female mice, inducing constitutive expression of tdTomato in Osx-CreERT+ (left) or Sox9-CreERT+ (right) cells and their progeny upon cell division. Shown are heatmaps of segmented tdTomato+ cells' position and density. B) Quantification of segmented tdT+ cells over time (n=3 for each data point).

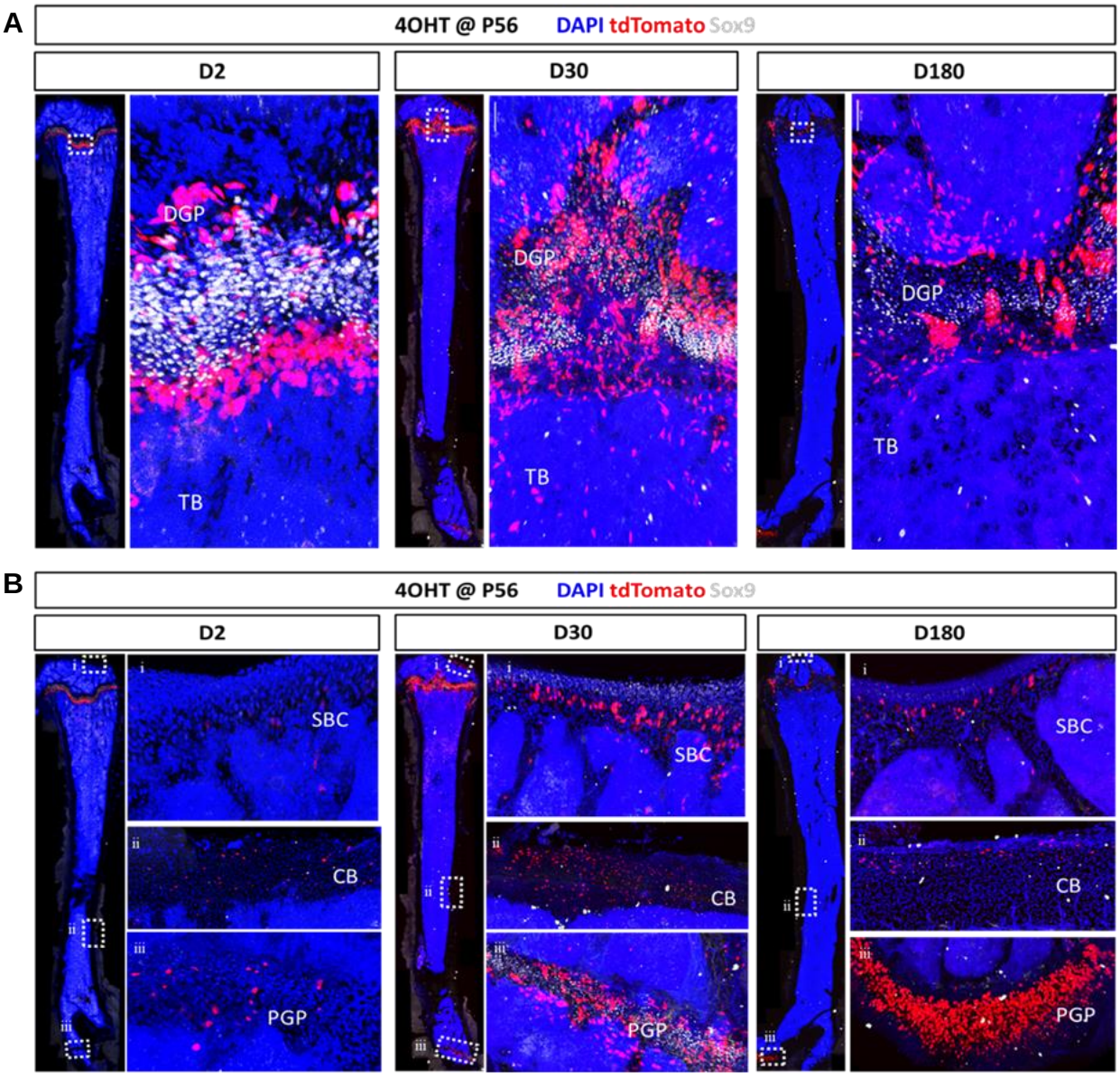

Figure 19: Lineage tracing in juvenile mice. A, B) 4OHT was administered at P56 in female mice inducing constitutive expression of tdTomato in Sox9-CreERT;Ai14 mice. tdT+ cells were chased at D2, D30 days and D180 post-4OHT injection, then immunostained and analyzed by confocal microscopy and imaging cytometry. SBC: Subchondral bone; CB: Cortical bone; PGP: Proximal growth plate; DGP: Distal growth plate; TB: Trabecular bone.

3.4.3 Lineage tracing of Sox9+ SSCs in adult and aged mice

When we labeled Sox9+ in P180 adult animals with a single dose of 4OHT, the expression of tdT+ cells was similar to that observed in juvenile animals. Labeled cells were observed near

the physes (both distal and proximal), in periosteum and cortical bone, trabecular bone, and subchondral bone (Figures 20A and B).

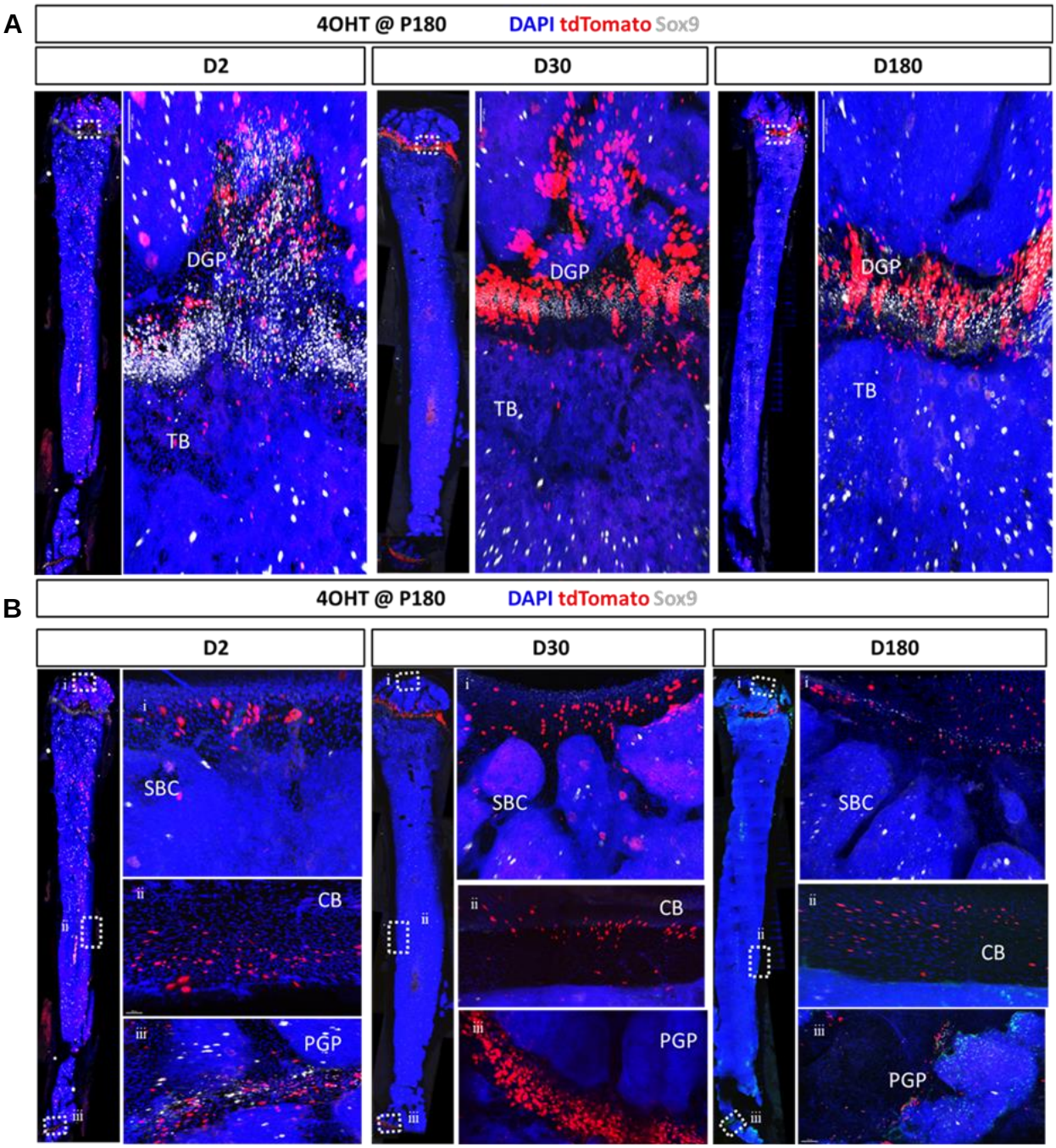

Figure 20: Lineage tracing in adult mice. 4OHT was administered at P180 in female mice inducing constitutive expression of tdT in Sox9-CreERT;Ai14 mice. tdT+ cells were chased at D2, D30 days and D180 post-4OHT injection, then immunostained and analyzed by confocal imaging. SBC: subchondral bone; CB: cortical bone; PGP: proximal growth; DGP: Distal growth plate; TB: Trabecular bone.

When aged mice were injected at P300 with a single dose of 4OHT, and the femurs were harvested then processed at D7 and D30 post 4OHT-injection, labelled cells were detected mainly in the physis, with very few cells present in the subchondral and trabecular bone. This indicates the tdT+ cells maintain their phenotype (multilineage and location) and keep proliferating over time (Figure 21).

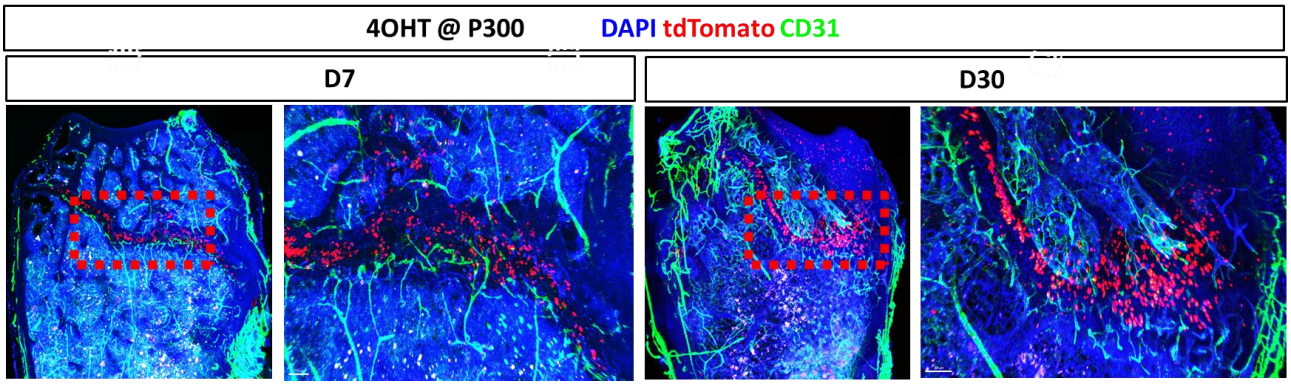

Figure 21: Lineage tracing in aged mice. 4OHT was administered at P300 in female mice inducing constitutive expression of tdT in Sox9-CreERT;Ai14 mice. tdT+ cells were chased at D7 and D30 post-4OHT injection, then processed by confocal imaging and imaging cytometry. CD31: Endothelial cells marker.

3.4.4 Comparison between juvenile and adult mice

As a summary, when Sox9+ cells were labeled in P56 mice, the anatomical distribution of tdT+ cells over time was similar to that observed in longer pulses (Figure 22A). The number of cells initially labeled was lower (2.62+/-1.2x10^3 cells/section, n=12) but reached similar levels as with longer pulses after 30 days (9.11+/-3.2x10^3) (Figure 22B, G). In 180-day chases, the number of tdT+ cells was also similar to that observed in 90-day chases with longer pulses (3.75+/-1.7x10^3). The number of tdT+ chondrogenic and osteogenic cells followed a similar kinetics over time. We however observed a sharper decrease in the fraction of tdT+Sox9+ cells (presumably self-renewing SSCs) from 12.9+/-3.3% of total tdT+ cells at day two post-labeling, to 2.2+/-1.5% at day 180 (Figure 22C, G n=6 each).

When skeletally mature mice receive a short 4OHT pulse at P180, the mice skeleton is fully mature, the anatomical distribution and number of tdT+ cells at D2 were very similar to that observed in younger animals (Figure 22D, E and G), with 1.8+/-0.4x10^3 tdT+ cells observed per section (n=12). At D30, number of tdT+ cells increased in young mice, but significantly less than in adult mice (figure 22G) , suggesting that these cells proliferate less in adulthood and is consistent with the lower growth rate in older animals[198]. Thus, instead of a biphasic population kinetics (increase in cell number followed by a decrease) as seen in the juvenile mice, we observed a gradual increase in the number of tdT+ cells, that is not statistically significant, reaching 3.9+/-1.2x10^3 by day 180, which is again similar to the number of cells observed in younger animals after 180-day chases (Figure 22E, G). The fraction of tdT+Sox9+ cells observed was highly variable in two-day chases (11.97+/-5.21%) but remained mostly constant in longer chases in juvenile mice (3.78+/-2.78% and 2.19+/-3.03% after 30 and 180 days, respectively) (Figure 22C). In adult mice, the percentage of tdT+Sox9+ cells was conserved at day two and day 30 (3.43+/-1.5% and 6.03+/-4.26%, respectively) then decreases slightly to 2.20+/-1.65% at day180 post injection (Figure 22F). However, when comparing the percentage of double positive tdT+Sox9+ cells between juvenile and adult mice, it was significantly higher in young animals at two-days chase (11.97+/-5.21% in juvenile and 3.43+/-1.5% in adult), but then remained constant between both age groups in longer chases (Figure 22H). In summary, our data indicates that self-renewing and multipotent Sox9+ SSCs persist in the skeleton throughout postnatal development and in mature bones. For each cohort, an outlier analysis was performed, and normality tested using the Shapiro-Wilks test. Each age condition (young versus adult) was compared using two-way ANOVA with significance threshold set at p=0.05 (Figure 22C, F, G and H).

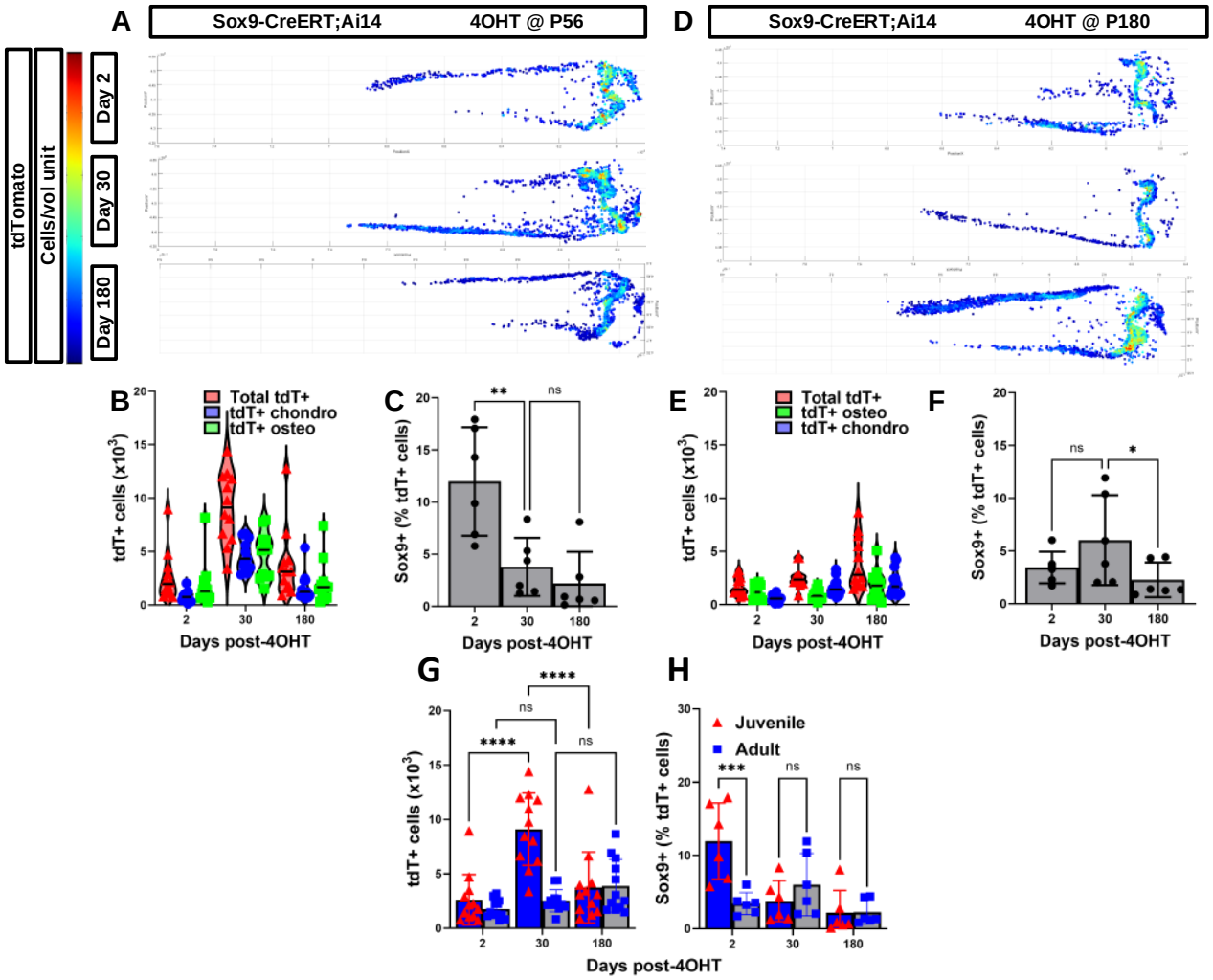

Figure 22: Persistence of self-renewing Sox9+ SSCs in skeletally mature mouse bones. Sox9-CreERT;Ai14 mice were pulsed with a single injection of 4OHT at P56 or P180 and chased for up to 180 days post-labeling. A) Anatomical distribution of tdT+ cells over time when P56 mice were pulsed. B) Quantification of total tdT+ cells, tdT+ osteogenic cells, and tdT+ chondrogenic cells, per section, over time in mice pulsed at P56. Osteogenic and chondrogenic cells were identified by anatomical location using spatial gating. N=12 (six males, six females) for each trace. C) Quantification of Sox9 protein expression in tdT+ cells over time in mice pulsed at P56. N=6 (three males, three females) for each trace. D, E, F) The same analyses were performed in mice pulsed at P180 (N numbers equal to those in panels B and C). G, H) Statistical analysis performed for each cohort; an outlier analysis was performed, and normality tested using the Shapiro-Wilks test, and adult and young conditions were compared using two-way ANOVA with significance threshold set at p=0.05.

3.4.5 Sexual dimorphism between males and females

To study the sexual dimorphism between males and females[16,18], pulse chase experiment was performed in both male and female mice. tdT+ cells distribution is similar for both males and females, young and adult; these cells are found in the growth plate and periosteum, also in trabecular/cortical bone, as well as subchondral bone (Figure 23A and B).

For each cohort, an outlier analysis was performed, and normality tested using the Shapiro-Wilks test. Each age condition (young versus adult) was compared using two-way ANOVA with significance threshold set at p=0.05 (Figure 23C and D). At D30 post-4OHT injection, the number of tdT+ cells in young females reached $12.30+/-1.27x10^3$, which was significantly higher than what was seen in young males $7.41+/-1.61x10^3$. As for tdT+ Sox9+ double positive cells, it was significantly higher in young males 18.24+/-4.12% than young females 7.51+/-2.11% at day two, but constant at D30 and D180 chases (Figure 23C). When comparing adult females and males, the main difference was observed at D180 post injection for the total number of tdT+ cells, reaching $5.62+/-2.37x10^3$ in adult males and $2.12+/-0.59x10^3$ in adult females. As for the fraction of tdT+Sox9+ cells observed, it remained constant between male and female mice at all timepoints. (Figure 23D).

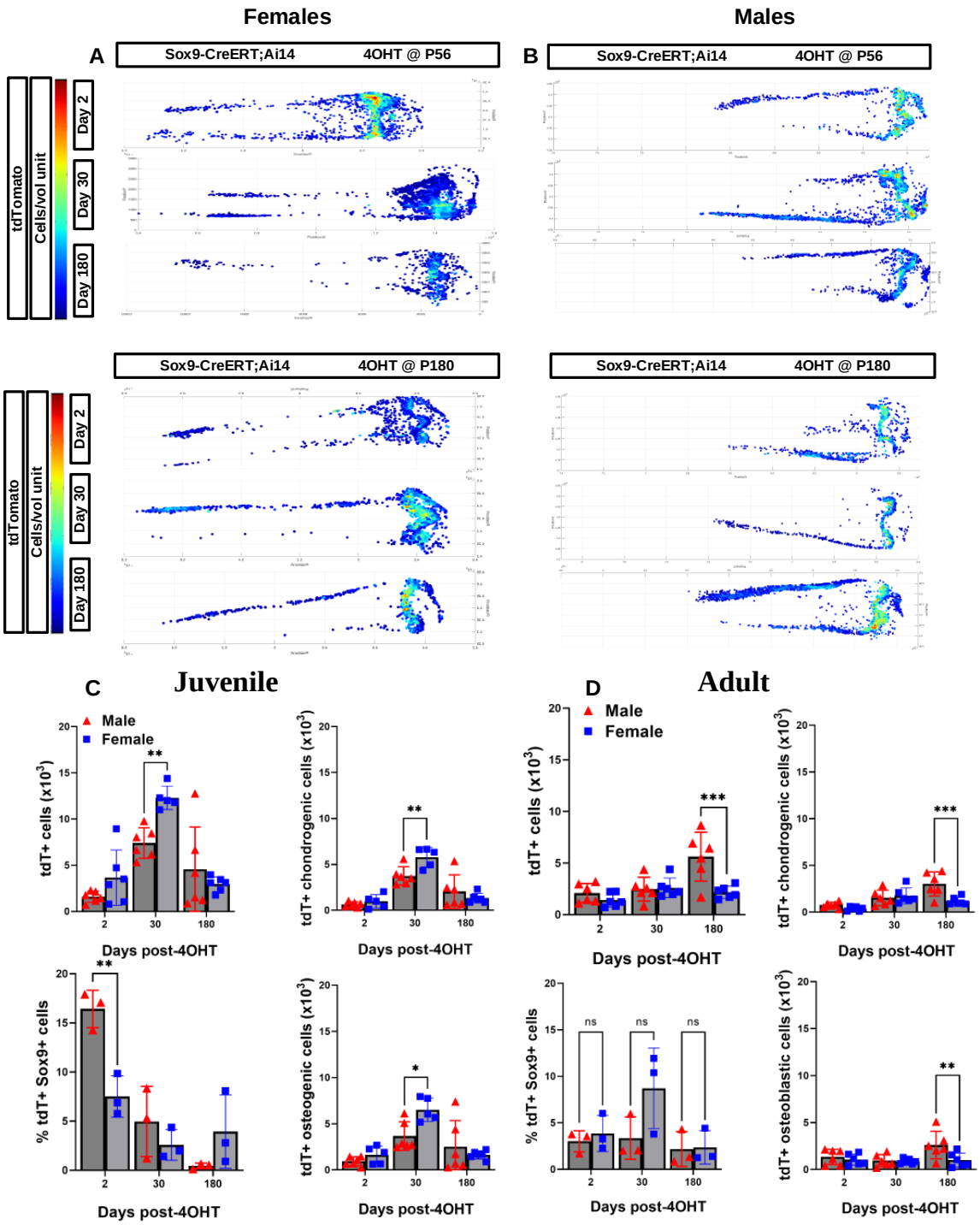

Figure 23: Expression of Sox9+ SSCs in male and female mice. Sox9-CreERT;Ai14 mice were pulsed with a single injection of 4OHT at P56 or P180 and chased for up to 180 days post-labeling. A, B) Anatomical distribution of tdT+ cells over time when P56 and P180 female and mice were pulsed, respectively. C, D) Quantification of total tdT+ cells, tdT+ osteogenic cells, and tdT+ chondrogenic cells, per section, over time in female and male mice pulsed at P56 and P180, respectively. Osteogenic and chondrogenic cells were identified by anatomical location using spatial gating. (N=6, six females/males) for each trace. Statistical analysis performed for each cohort; an outlier analysis was performed, and normality tested using the Shapiro-Wilks test, and adult and young conditions were compared using two-way ANOVA with significance threshold set at p=0.05.

In addition, another main discrepancy detected was that we observed tdT+ adipocytes in the bone marrow of female mice but not in the bone marrow of males at P56, day two chase. 30 days post-injection, adipocytes of juvenile females turnover and are replaced by non-labeled cells (same at longer chases and in the adult animals). Whereas in male mice, we start detecting adipose tissue at P86, but no tdT, and the latter is consistent in longer chases and the adult animals (Figure 24). In summary, these differences can be attributed mainly to the sex steroids in males and females and their effect on the growth rate and timing of the skeleton development.

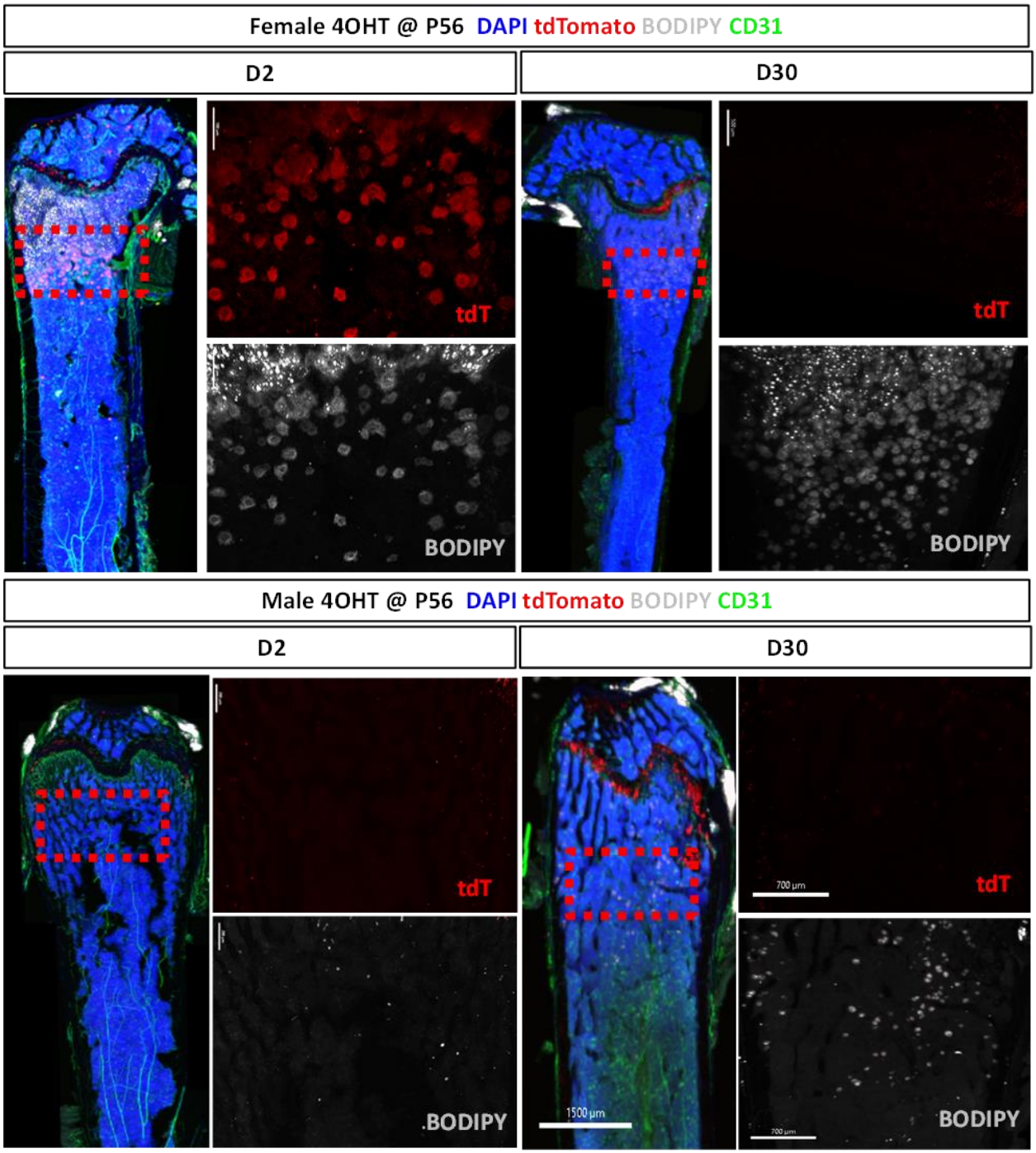

Figure 24: Comparison of marrow adipocytes between males and females in juvenile mice. Sox9-CreERT2;Ai14 mice were injected with 4OHT at P56, femurs were then collected at D2 post injection and processed for immunostaining then analyzed by confocal imaging. BODIPY: Stain for adipocytes, CD31: marker for endothelial cells.

3.5 Isolation of skeletal cells from postnatal bones

To assess if Sox9+ SSCs could be purified and expanded ex vivo for further characterization and transplantation assays, we tested three isolation procedures involving enzymatic and mechanical dissociation, for their capacity to isolate all skeletal (or non-hematopoietic / CD45-) cell types with good viability (figure 25). Isolated SSCs cells were stained using Live/Dead assay showing a viability of 80% (figure 25A), then analyzed by immunostaining where we observed a significant depletion of hematopoietic cells (CD45+) after magnetic cell separation and an increased yield of live marrow stromal cells (Lepr+CD45-), pericytes (SM22+), endothelial cells (CD31+), chondrocytes (CD73+CD31-) and osteoblast progenitors (OB prog, Sp7+CD73-) when enzyme mix 3 was used (figure 25B and C).Thus, we opted for an enzymatic dissociation using collagenases and neutral protease followed by gentle mechanical dissociation.

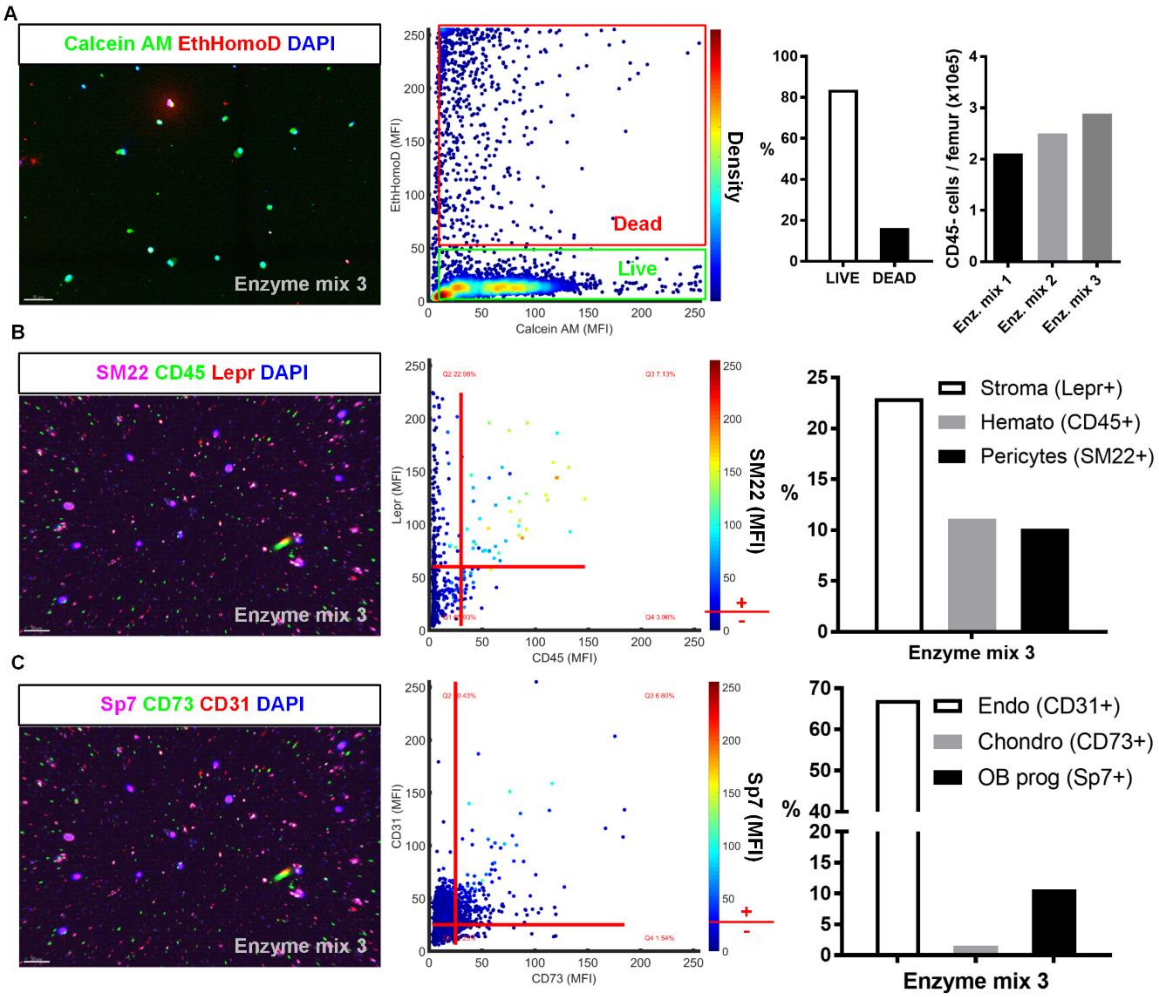

Figure 25: Optimization of skeletal cell types of isolation for RNAseq. A) Skeletal cells were isolated from P56 female C57Bl/6 mice. Isolated cells were stained using Live/Dead assay (calceim AM and ethidium homodimer for live and dead cells, respectively) and then imaged using confocal microscopy and imaging cytometry. B) and C) Isolated cells were immunostained, then imaged using confocal microscopy, and quantified with imaging cytometry. The middle column shows mean fluorescence intensity (MFI) of 2-3 fluorescent channels for all cells analyzed (each dot represents a cells). Only segmented objects containing a DAPI+ nucleus were analyzed. The gating thresholds for fluorescent channels are shown as boxes or red lines. Quantification results are shown in the right columns.

3.5.1 Optimizing colony forming unit cell (CFU-C) assay and comparing male versus female, and young versus adult mice

When we pulsed P56 mice with 4OHT and purified tdT+ cells using FACS or cultured them in individual wells, they failed to form colonies. However, when unfractionated skeletal cells were seeded at clonal densities in large cell culture vessels, we observed the formation of several tdT+ colonies (Figure 26C). Briefly, 4OHT was administered to Sox9-CreERT;Ai14 mice at P56 and P180 and femurs were enzymatically digested with mechanical dissociation[187], at D2 post-4OHT. The enriched cell suspension was magnetically depleted of CD45+ and CD31+ cells, while the non-enriched cell suspension was not. Then the isolated cells plated in 24-well plates at a density of $1.2x10^5$ cells/cm^2 for total colony counting and red colony counting (figure 26A and B). We then quantified the total number of colonies formed and the fraction of tdT+ colonies, in young and adult mice, as well as in female and male mice.

When comparing enriched versus non-enriched isolated skeletal cells, the total number of colonies obtained was higher for the enriched samples versus non-enriched at both P56 and P180 (figure 26A), and only 1-3% of these colonies were tdT+ (figure 26B). Red colonies derived from the enriched samples were noticed to be smaller in size compared to the ones derived from non-enriched samples (figure 26C). A probable explanation could be that the latter expanded on a large surface area, leaving less space for other colonies to grow, thus the higher number of colonies obtained with the enriched femur samples.

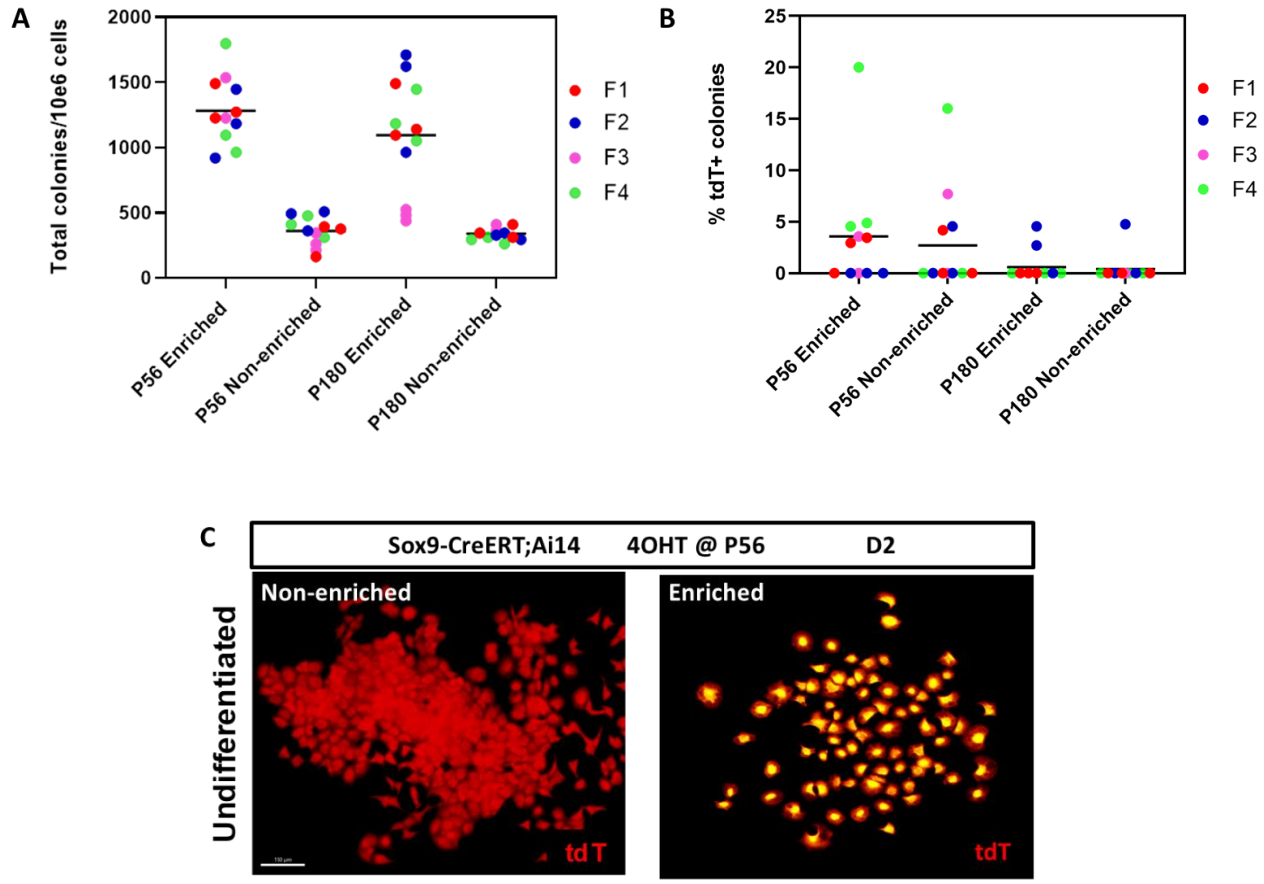

Figure 26: Isolation and culture expansion of Sox9+ SSCs. Sox9-CreERT2;Ai14 female mice were inject with 4OHT at P56 and P180, as indicated. Two days later, femurs were collected, and skeletal cells were isolated with enrichment (depletion of hematopoietic CD45+ cells and endothelial CD31+ cells) or without enrichment using the optimal enzyme mix with mechanical digestion. A) Isolated skeletal cells were plated in 24-well plates at a cell density of 120000cell/cm^2, cultured for 11 days then fixed with 4% methanol- free formaldehyde. Total colony count was done by staining the cells with 0.5% crystal violet, then the data were quantified (Shown are 4 biological replicates (color coded) with three technical replicates each (dots)). B) Quantification of percentage of tdT+ colonies (Shown are 4 biological replicates (color coded) with three technical replicates each (dots)). C) Red colonies were counted and imaged by using the red filter of a bright field inverted microscope.

In female mice, the total number of colonies obtained did not vary significantly between young and adult mice (360.4+/-54 and 341.3+/-25 colonies per 10^6 skeletal cells, respectively, n=12) (Figure 27A). In young females, 3.6+/-2.75% of the colonies were tdT+, but this fraction decreased to 0.6+/-0.7% in adult females. In young male mice, we obtained significantly more colonies compared to females (1535+/-220 colonies per 10^6 skeletal cells) (Figure 27B, n=9). This

number decreased but remained elevated in adult males (517+/-108 colonies per 10^6 skeletal cells). The fraction of tdT+ colonies was also higher in young males compared to females (8.8+/-2.0% of total colonies) but also decreased significantly in older males (1.01+/-1.5%). As a summary, the total number of colonies obtained in culture and percentage of tdT+ colonies were higher in younger animals, specifically in males.

3.5.2 Testing Sox9+ SSCs proliferation and multilineage differentiation potential in vitro

The enriched cells did not survive after passage one, and this could be caused by the lack of certain growth factors secreted by the magnetically removed hematopoietic cells in the medium, that are potentially crucial for their survival and expansion in vitro. Thus, the differentiation assay was pursued only with the non-enriched cells, where isolated tdT+ cells were plated for culture-expansion in 10 cm plastic dishes for multilineage differentiation potential.

Mice were pulsed with 4OHT at P56 and skeletal cells were isolated from femurs 48h later. We monitored the heterogenous cultures for the presence of tdT+ colonies. Wells that contained tdT+ colonies were selected and further expanded for three passages to obtain enough cells for differentiation assays. The cells were placed in osteogenic or adipogenic media, for two and three weeks, respectively, or they were aggregated and placed in chondrogenic medium for three weeks[187].

Differentiation was assessed by immunostaining for specific markers and differentiated cells were assayed for their expression of tdT. tdT+ cells were positive for Sox9 and NG2 markers (chondrocyte markers), also they were positive for Col1a1 marker (osteoblast marker), as well as BODIPY positive (adipocyte specific stain) (figure27C).

Our results indicate that tdT+ cells derived from Sox9+ cells maintain their multilineage differentiation potential in vitro after extensive proliferation and expansion.

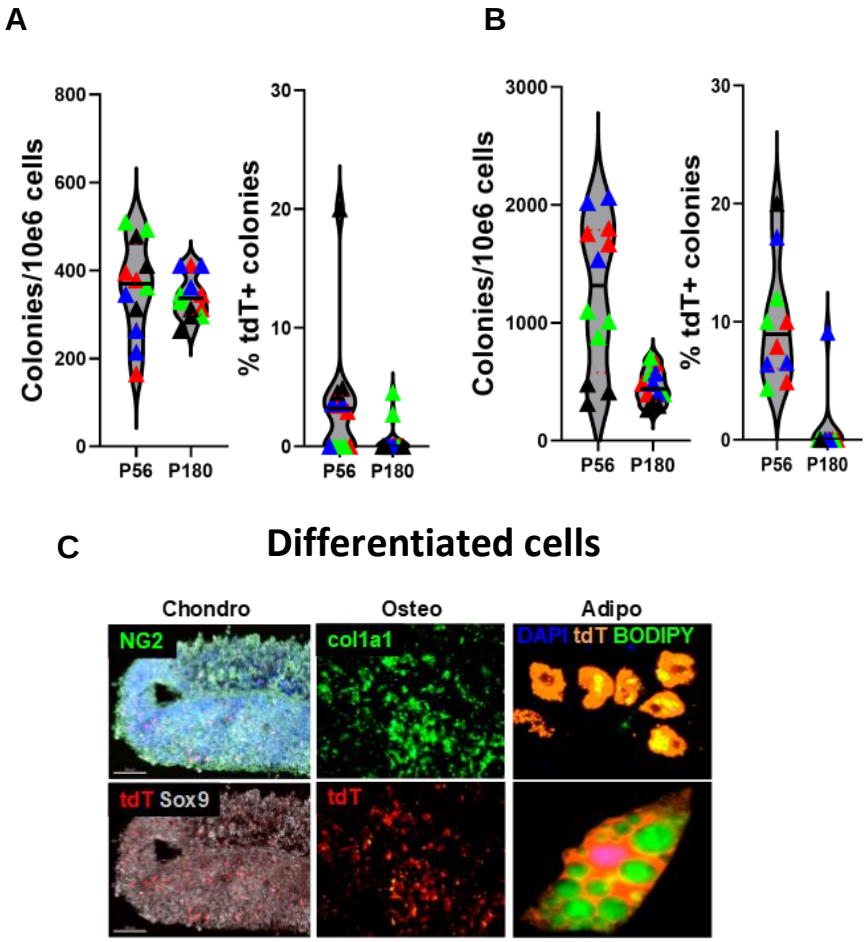

Figure 27: Culture expansion and in vitro multilineage differentiation of Sox9+ SSCs. Sox9-CreERT;Ai14 mice were pulsed with a single 4OHT injection at P56 or P180, as indicated. Femurs were harvested two days post-labeling and skeletal cells were isolated using enzymatic and mechanical dissociation, followed by magnetic removal of endothelial and hematopoietic cells through negative selection. After isolation, tdT+ cells in vitro formed colonies of cells with varying morphologies and cell numbers. A, B) Quantification of the total number of colonies obtained per 10^6 skeletal cells seeded and the fraction of these colonies that were tdT+, expressed as the percentage of total colonies. The analysis was performed in young (P56) and adult (P180) female and male mice (A and B, respectively). Shown are individual values and median. N=12 for females and N=9 for males. The biological replicates are color coded, and each was performed in three separate technical replicates. C). Mixed populations of skeletal cells (tdT+ and tdT-) were culture expanded for three passages then subjected to differentiation into chondrocytes, osteoblasts, and adipocytes. Differentiation was assessed using immunostaining and the presence of differentiated tdT+ cells was qualitatively assessed. Representative images shown. The assay was performed on three biological replicates, each in three separate technical replicates.

3.6 Detecting Sox9+ putative SSCs from postnatal human bones and assessing their multilineage differentiation potential in vitro

To determine if postnatal human bones also harbor Sox9+ SSCs, we obtained samples from a pediatric polydactyly patient undergoing amputation of the extra digits. We processed the bones for imaging as for mouse bones. We observed human Sox9 (hSox9) expression in a limited number of cell nuclei in the physeal cartilage surrounding the secondary ossification center. hSox9+ nuclei were enriched in the resting zone of the physis, in subchondral bone, and in articular cartilage (Figure 28A). hSox9+ cells in subchondral bone and articular cartilage also expressed integrin β5 (ITGB5), which we also observed in some chondrogenic lineage cells in mice (Figure 32B in chapter 4). The fraction of cells positive for hSox9 in the physeal cartilage was measured at 6.1%, and approximately 30% of those also expressed ITGB5 (Figure 28B). We next obtained pediatric physis samples from patients undergoing epiphysiodesis for minor limb length discrepancy. Skeletal cells were isolated by enzymatic dissociation, and we performed single cell transcriptomics and analysis as described in the materials and methods chapter of this thesis (Chapter2 section 2.10), confirming that ITGB5 could be used as a surrogate marker to purify at least a subpopulation of Sox9+ cells from human postnatal bones (Figure 28C). However, when they were purified by FACS based on ITGB5 expression and culture expanded, they did not survive. Skeletal cells from human tissues of three different pediatric patients were isolated and plated for culture expansion and differentiation. After three passages, the human cells were placed in osteogenic or adipogenic media or aggregated and then placed in chondrogenic medium. We stained only the chondrogenic ossicles with hSox9 antibody and showed that hSox9+ cells maintained their differentiation potential as chondrocytes. The next step will be to stain for the

hSox9 protein after adipogenic and osteogenic differentiation, but our results so far indicate that cells isolated from postnatal human bones can be purified and expanded ex vivo while maintaining their multilineage differentiation potential, at the population level (Figure 28D).

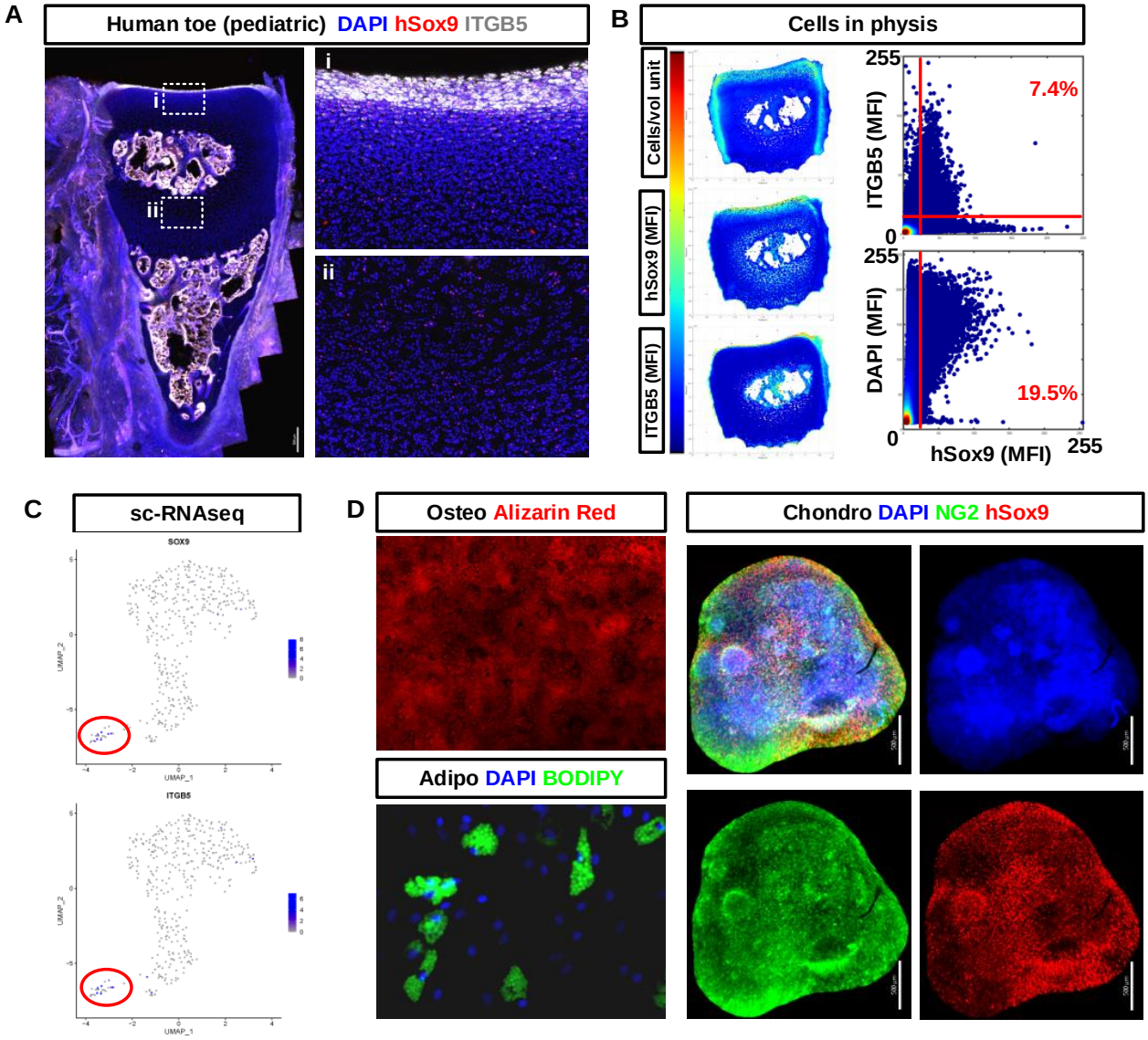

Figure 28: Sox9+ putative osteochondral SSCs in human postnatal skeletal tissue. A) Phalanx of a toe obtained from a pediatric patient with polydactyly whose toe was surgically amputated. The bone was processed similarly to mouse bones, immunostained for hSox9 and ITGB5, and counterstained with DAPI. B) Quantification of hSox9 and ITGB5 in cells located in the physis of the bone shown in A. C) Single cell transcriptomics of skeletal cells isolated from the physis of patients who underwent epiphysiodesis to correct minor limb length discrepancy, showing overlap between Sox9+ and ITAGB5+ cells. D) Skeletal cells isolated from patient undergoing epiphysiodesis were expanded for three passages in vitro and subjected to multilineage differentiation assay.

3.7 Summary

In this chapter, we showed that the resting zone of the postnatal mouse physis harbors multipotent osteochondral Sox9+ cells, and that these putative Sox9+ SSCs self-renew over the lifespan of the animal driving postnatal bone growth, as well as persist in skeletally mature mice to maintain skeletal tissue homeostasis. Our lineage tracing of Sox9-CreERT expressing cells combined with analysis of Sox9 protein expression and EdU incorporation/retention provides the first tangible experimental evidence of in vivo self-renewal in any type of SSCs identified to date. When tdT+ cells were isolated and plated for in vitro assays, they retained their multilineage differentiation potential after culture-expansion. And finally, we showed that human skeletal tissue harbors Sox9+ cells with similar properties as the putative Sox9+ SSCs characterized in mice.

Chapter 4: Molecular characterization of Sox9+ SSCs

It is well established that with age, the regenerative potential of the skeletal tissues decreases, and it has been associated with age-related stem cell exhaustion and/or loss of function. Whether SSCs become senescent or proliferate less in aged organisms is not well understood. In addition, what molecular pathways are activated or inhibited during homeostasis versus injury repair, in juvenile versus adult and aged animals is also ambiguous. Thus, it is important to understand the genetic profile and molecular regulation of fate decision of these putative SSCs in postnatal animals of different ages and conditions to enable pharmacological manipulation for therapeutic purposes.

We sought to understand the molecular mechanisms for the self-renewal and differentiation of Sox9+ SSCs, so we aimed to perform transcriptome profiling using single cell-RNAseq (scRNAseq). This would enable the identification of putative subpopulations of Sox9+ cells and comparing their gene expression to their differentiated progeny (osteoblasts and chondrocytes). In addition, this could help identifying genes specifically expressed in self-renewing stem cells or differentiated cells, including markers that will facilitate FACS isolation of Sox9+ SSCs.

4.1 Preliminary transcriptome profiling data

A preliminary single cell RNA-seq experiment and analysis has been performed using the 10X Genomics Chromium Single Cell 3' Assay. A whole femur bone from a young female Sox9-CreERT2;Ai14 mouse was enzymatically digested and hematopoietic cells were depleted by magnetic separation, two days post-4OHT injection. The freshly isolated skeletal cells were brought to our genomics core facility for library preparation and sequenced (10e4 cells) at a depth of 25,000 reads/cells. The results were analyzed with the help of Dr. Theodore Perkins using the

Seurat pipeline. Principal component analysis (PCA) was used to identify the genes contributing most to heterogeneity within the data. Graph-based clustering was then performed using these genes and visualized on 2D t-SNE maps.

Our preliminary data in figure 29 showed that some clusters have high expression of Pecam1/CD31, with cluster 6 being double positive for Pecam1 and Emcn (markers for sinusoidal endothelia cells). However, we noticed that most of these cells were CD45-, Ter119-, but Gypa+, CD71+, Gata1+. This means they are likely erythroid progenitors that lost CD45 expression but did not upregulate Ter119 yet (not shown), despite performing the magnetic cell separation to remove hematopoietic cells by negative selection.

In addition, we detected some stromal cells (Cxcl12+Lepr+/-) and osteoblasts (Runx2+Thy1+/-), and very few pericytes (Acta+, Tagln+) and chondrocytes (Cspg4+ cells). Cells of osteoblastic (Runx2), stromal (Cxcl12) and pericytic (SM22) lineages were also observed.

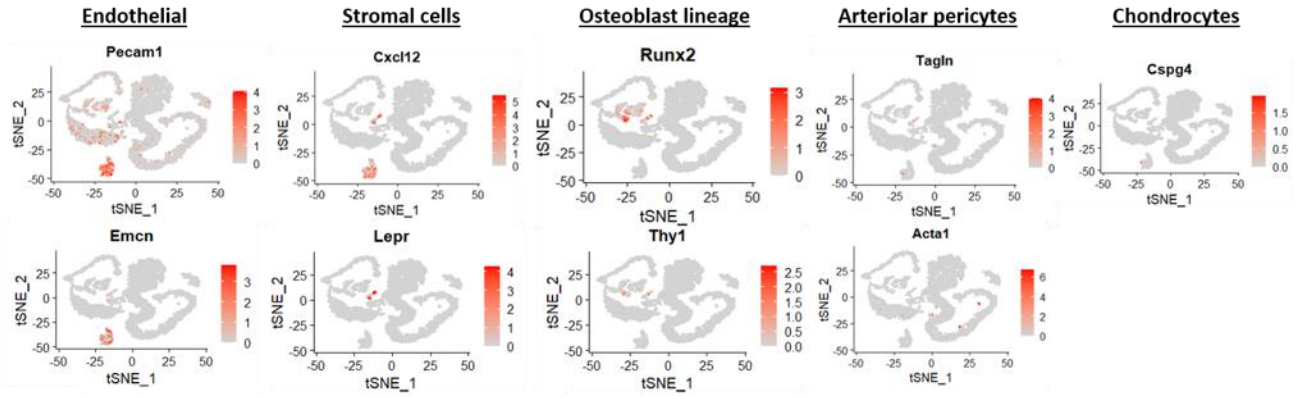

Figure 29: Preliminary scRNAseq of skeletal cells depleted of hematopoietic cells. Femurs harvested from Sox9-CreERT;Ai14 mice 48h post-4OHT injection at P56 were enzymatically and mechanically dissociated, magnetically depleted of CD45+ hematopoietic cells and used for scRNAseq. >80% cell viability was obtained, and 10^4 cells were sequenced at 10K reads per cells. Expressed genes that were highly enriched in this cluster are labeled in red.

70% of detected Sox9+ cells clustered with other cells expressing SSCs markers (Ctsk, Grem1, Pthlh, Lepr, Prrx1, Ly6a/e, Pdpn), as well as genes involved in skeletal development (Fgfr1/2, Pdgfra, Osx/Sp7, Runx2), stem cell self-renewal (Bmi1), planar cell polarity (Fzd1/2, Vangl1/2, which may be involved in asymmetric cell division), Hedgehog (Hh) signalling (Smo) and early mesoderm development (Twist1/2). Furthermore, we have identified a surface marker (Itgb5) highly specific to this cluster which may be useful for purification of Sox9+ cells (genes highly enriched in this cluster are labeled red in Figure 30). In conclusion, our preliminary scRNA seq experiment sequenced mainly erythroid progenitors and needs further optimization.

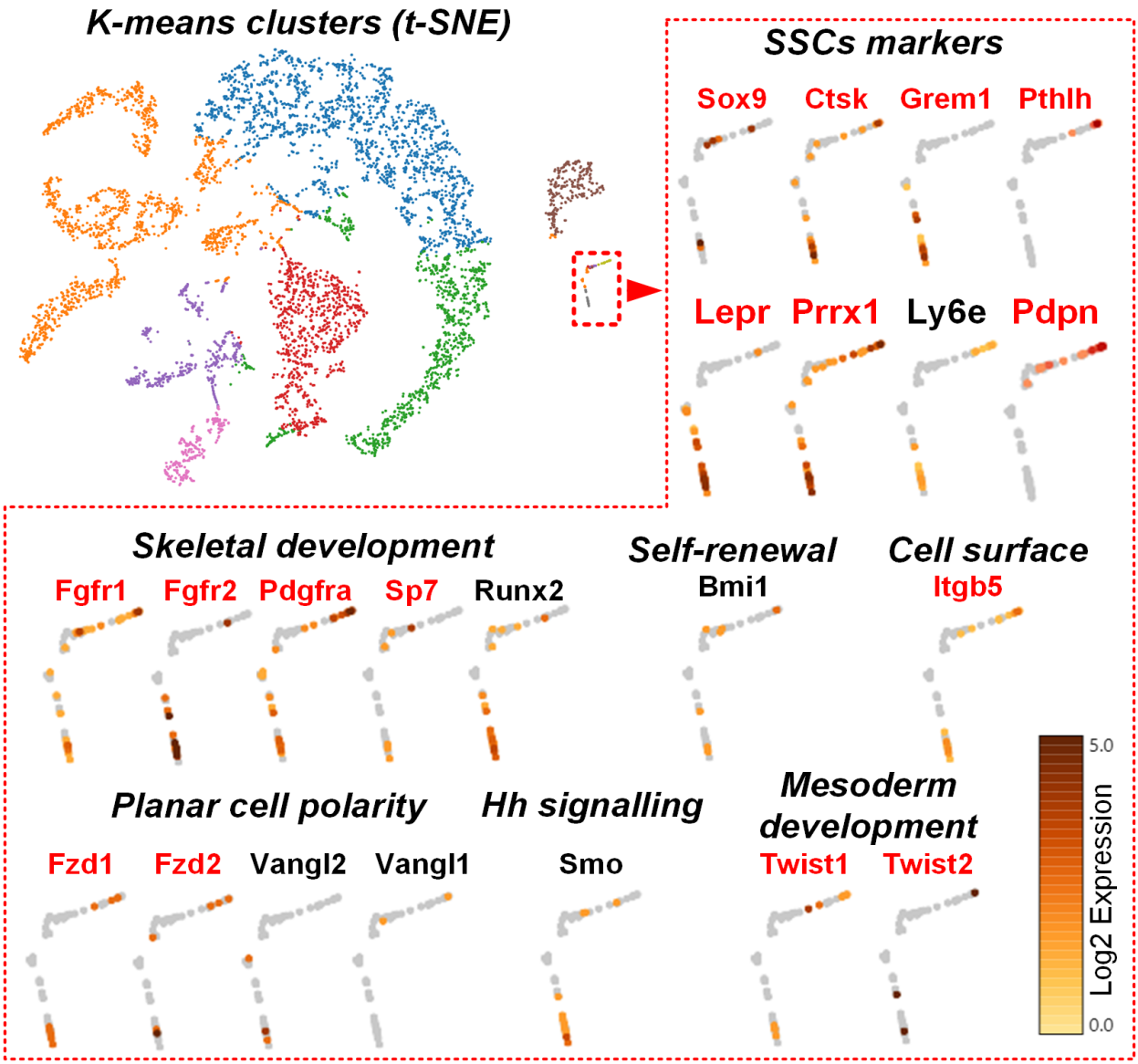

Figure 30: scRNAseq of skeletal cells depleted of hematopoietic cells. Femurs harvested from Sox9-CreERT;Ai14 mice 48h post-4OHT injection at P56 were enzymatically and mechanically dissociated, magnetically depleted of CD45+ hematopoietic cells and used for scRNAseq. >80% cell viability was obtained, and 10^4 cells were sequenced at 10K reads per cells. Expressed genes that were highly enriched in this cluster are labeled in red.

4.2 FACS sorting of tdT

Because of low abundance of Sox9+ cells and other skeletal cell types observed in our preliminary analysis, we optimized our cell separation technique and checked for the purity of skeletal cells using flow cytometry. 4OHT was administered to Sox9-CreERT;Ai14 mice at P56 and joints were enzymatically and mechanically dissociated at D2 post injection. We then used magnetic cell separation (negative selection) to remove contaminating endothelial (CD31+), hematopoietic (CD45+) cells and erythroid cells (CD235a+). Using this method, we typically achieve a cell viability of 67.7% (Figure 31, middle panel). However, flow cytometry analysis demonstrated that <0.1% of these skeletal cells expressed tdT (Figure 31, right panel).

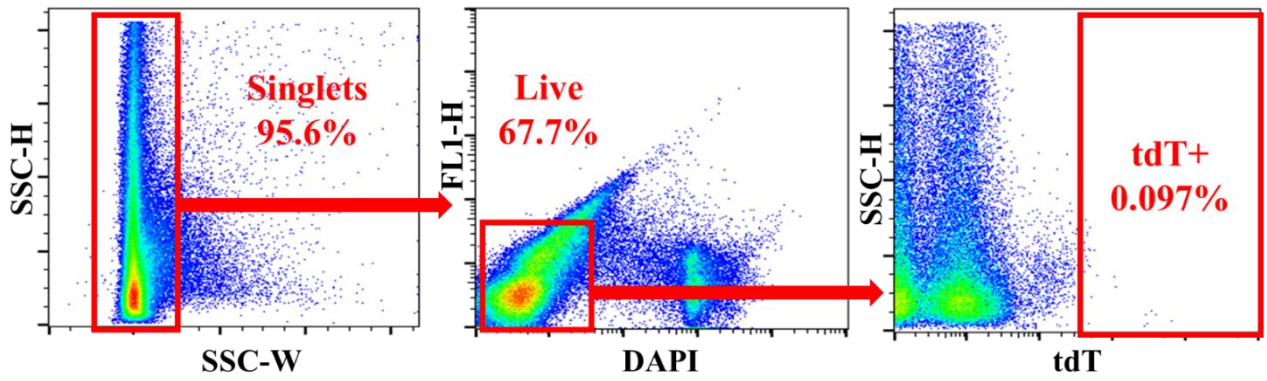

Figure 31: Isolation and purification of Sox9+ SSCs by flow cytometry. *Sox9-CreERT;Ai14* mice were pulsed with a single 4OHT injection at P56. Joints were harvested two days post-labeling and skeletal cells were isolated using enzymatic and mechanical dissociation, followed by magnetic removal of endothelial and hematopoietic cells through negative selection. Flow cytometry of freshly isolated skeletal cells was performed to sort tdT+ cells. We normally obtain around 150 tdT+ cells per animal (proximal tibias and distal femurs only).

4.3 Molecular characterization of postnatal Sox9+ SSCs

Since we lacked time and funding to repeat our scRNAseq experiments with our optimized isolation protocol, we decided to take advantage of an open-access dataset published in 2019 by Baryawno et al. from the Scadden lab at Harvard, that performed a similar analysis to study the bone marrow hematopoietic niche in normal and leukemic mice[190]. Their data contains mostly

Sox9+ and Runx2+ cells, indicating they mainly sequenced cells of the chondrogenic and osteoblastic lineages. A small cluster of Sox9+ cells also expressed many genes involved in skeletal development, planar cell polarity, stem cell self-renewal, SSCs markers, and others. After clustering the cells using the Louvain algorithm, we performed a pseudotime analysis using the Palantir algorithm, which supported our lineage tracing data and indicated that Sox9+ cells could give rise to cells in the chondrogenic and osteogenic lineages (Figure 32A). Differential gene expression between clusters indicated that Sox9+ cells also express several genes involved in chondrogenesis including Acan, Cspg4 (NG2), and Col2a1 (Figure 32B). $Sox9^{high}$ cells also express low levels of genes involved in early osteogenesis such as Runx2 and Sp7, but not genes expressed in more differentiated osteogenic cells (Spp1, Alpl, FGFR1, FGFR2, Bglap, and Col1a1). In addition, $Sox9^{high}$ cells also expressed genes involved in early skeletal development, stem cell self-renewal, and asymmetric cell division (Ptch1, Smo, Pth1r, Gli2/3), cell surface marker (Itgb5), as well as Nt5e (CD73), which was recently shown to be upregulated by Col2a1+ SSCs in the resting zone after the formation of the secondary ossification center[201].

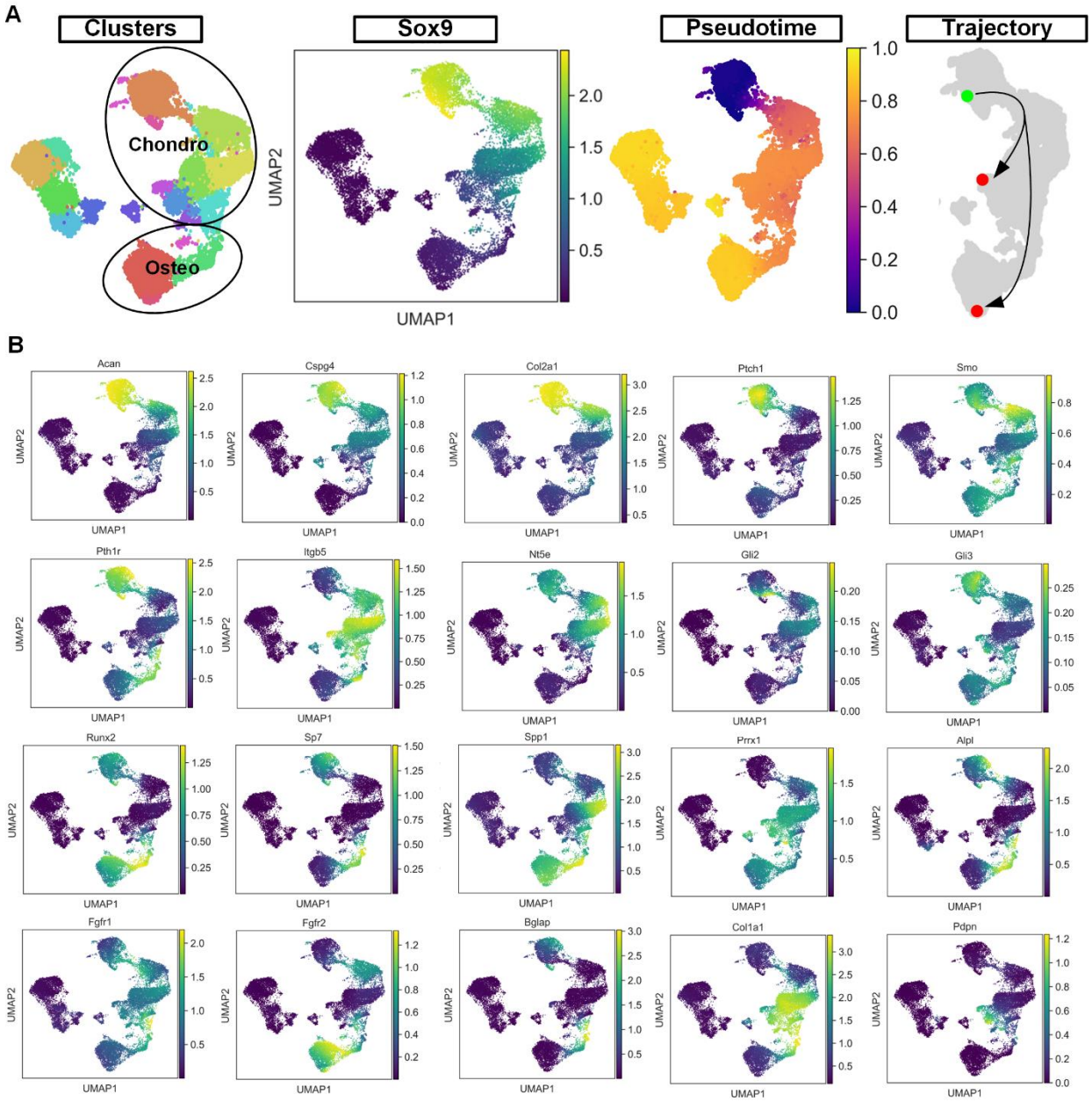

Figure 32: Single cell transcriptomics and pseudotime analysis of mouse postnatal skeletal cells. Open-access single cell transcriptomics raw data of postnatal mouse skeletal cells was obtained from ref.37. A) We performed graph-based clustering using the Louvain algorithm and pseudotime analysis using the Palantir algorithm. The cellular trajectory computed between $Sox9^{high}$ cells and differentiated osteochondral cells is shown. B) Expression of genes involved in chondrogenesis, osteogenesis, early skeletal development, and stem cell self-renewal across the different clusters.

4.4 Summary

In this chapter, we showed that although our preliminary scRNAseq experiment sequenced mainly erythroid progenitors, a small cluster of cells contained few Sox9+ cells that expressed SSCs markers, genes involved in skeletal development, stem cell self-renewal and ITGB5 cell surface marker, similar to the one identified in the scRNAseq data of Sox9+ human cells. In addition, the Pseudotime analysis performed on the open-access dataset published in 2019 by the Scadden lab supported our lineage tracing data and indicated that Sox9+ cells could give rise to cells in the chondrogenic and osteogenic lineages, and the differential gene expression between clusters indicated that Sox9+ cells also express several genes involved in early skeletal development, stem cells, and asymmetric cell division.

Chapter 5: Assessment of the regenerative potential of Sox9+ skeletal stem cells

My working hypothesis is that endogenous SSCs repair tissues in younger organisms but show blunted regenerative capacity in older ones, where pharmacological manipulation or stem cell transplantation may be required. In addition, in chapter 3 of my thesis, I showed that tdT+ cells give rise to most bone (compact, trabecular, and subchondral bones) and growth plate cartilage produced after tamoxifen injection, hence expecting them to have a role in cartilage and bone repair in injury models. Since Sox9+ SSCs possess osteochondral potential, to investigate their role in tissue repair and how aging affects their regenerative potential, I developed a focal osteochondral defect (FOD) injury model[192,193] of the knee joint, where an injury is created in the femoral articular cartilage and subchondral bone.

5.1 Creating the FOD model

FOD injury was performed by making an incision to expose the knee joint and then the patella was luxated laterally. Following that, a full-thickness defect penetrating cartilage and subchondral bone was made by drilling a hole in the femoral trochlear groove using a 25G needle (figure 33). Figure 34 show test samples when I was still developing the FOD injury model in test mice and optimizing the sectioning and imaging methods.

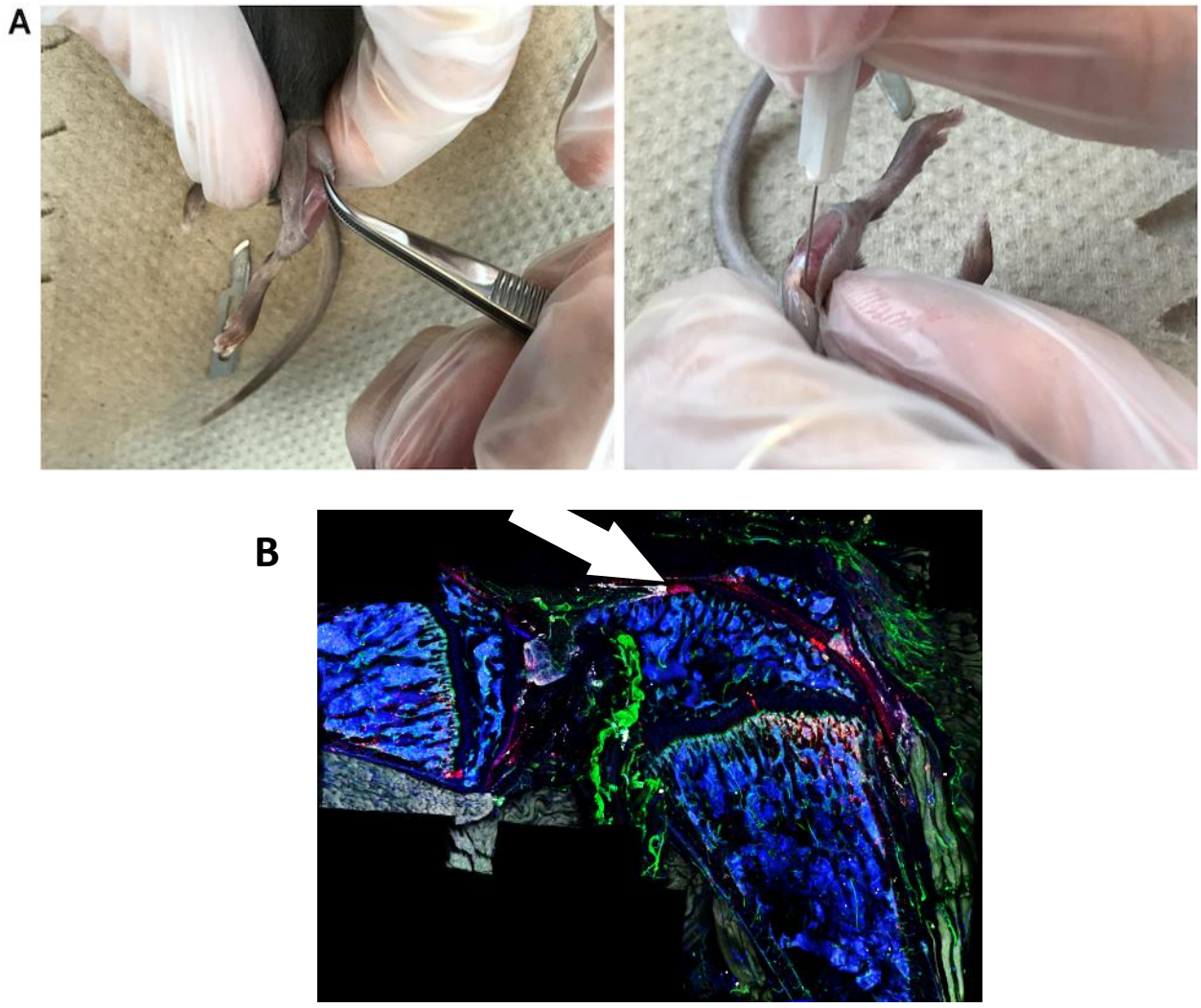

Figure 33: Injury models creation and analysis. A) Osteochondral defect is created by making an incision and exposing the knee joint and patella (left). The defect penetrating cartilage and subchondral bone is made by drilling a hole in the trochlear groove using a 25G needle (right). B) White arrow indicates the trochlear groove where the defect is created.

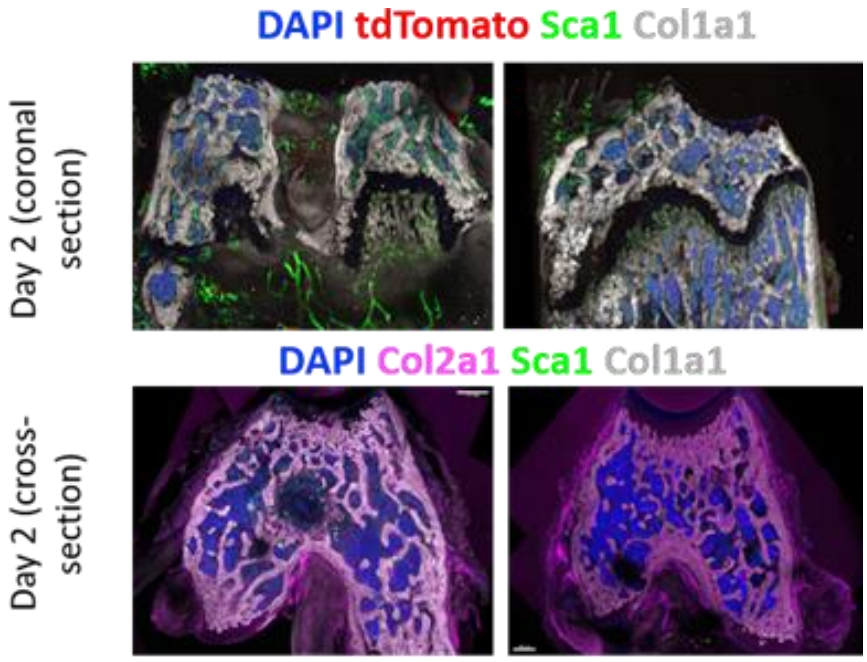

Figure 34: Focal osteochondral defect injury model. Top panel: a focal osteochondral defect is created in the distal femur of anesthetized mice by drilling a hole in the articular cartilage of the trochlear grove down to the subchondral bone. The lesion can be observed in sagittal (middle panel) or cross- (lower panel) sections, demonstrating the injury reached subchondral bone (left injured bones, right healthy bone).

5.2 Lineage tracing of Sox9+ cells in FOD mice

Figures 35 and 36 show images of the FOD injury model performed in juvenile and adult mice, respectively. Sox9-CreERT2; Ai14 mice were injected with a single dose of 4OHT at P56 or P180, at D2 post injection FOD injury was created, and then lineage tracing was performed at several timepoints (D2, D7 and D30 post FOD induction).

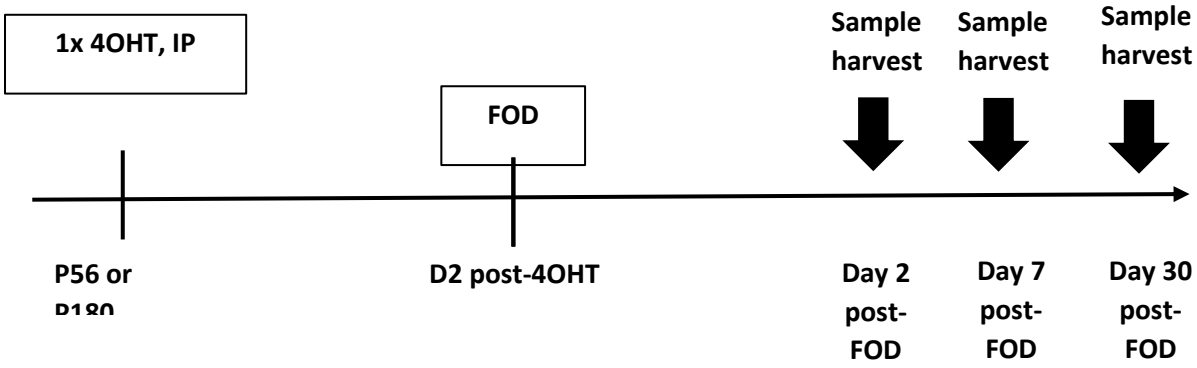

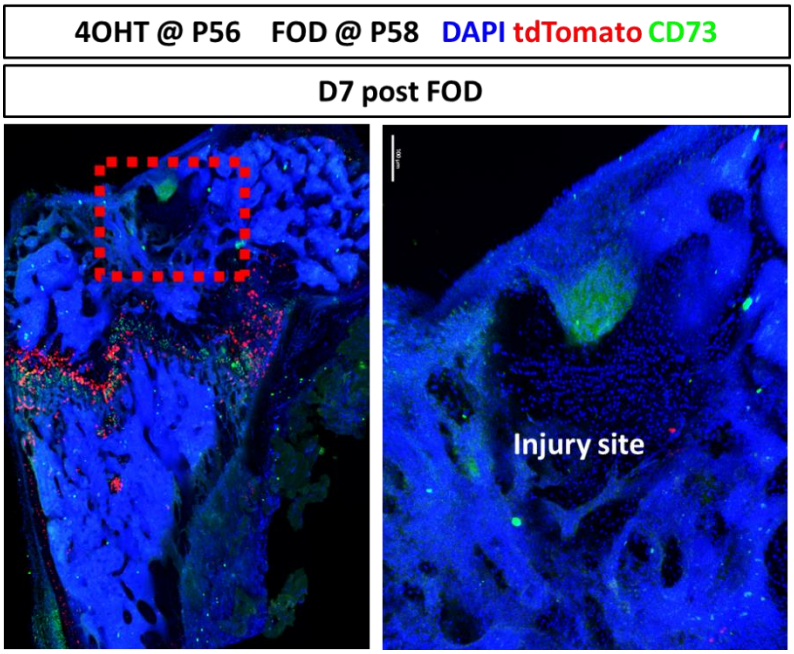

Figure 35: FOD injury performed two days post-4OHT in juvenile mice. Sox9-CreERT;Ai14 male mouse was injected with 4OHT at P56. Injury site created at P58. Femur were collected at D7 post FOD, then processed for immunostaining and confocal imaging (N=3 for females and N=4 for males).

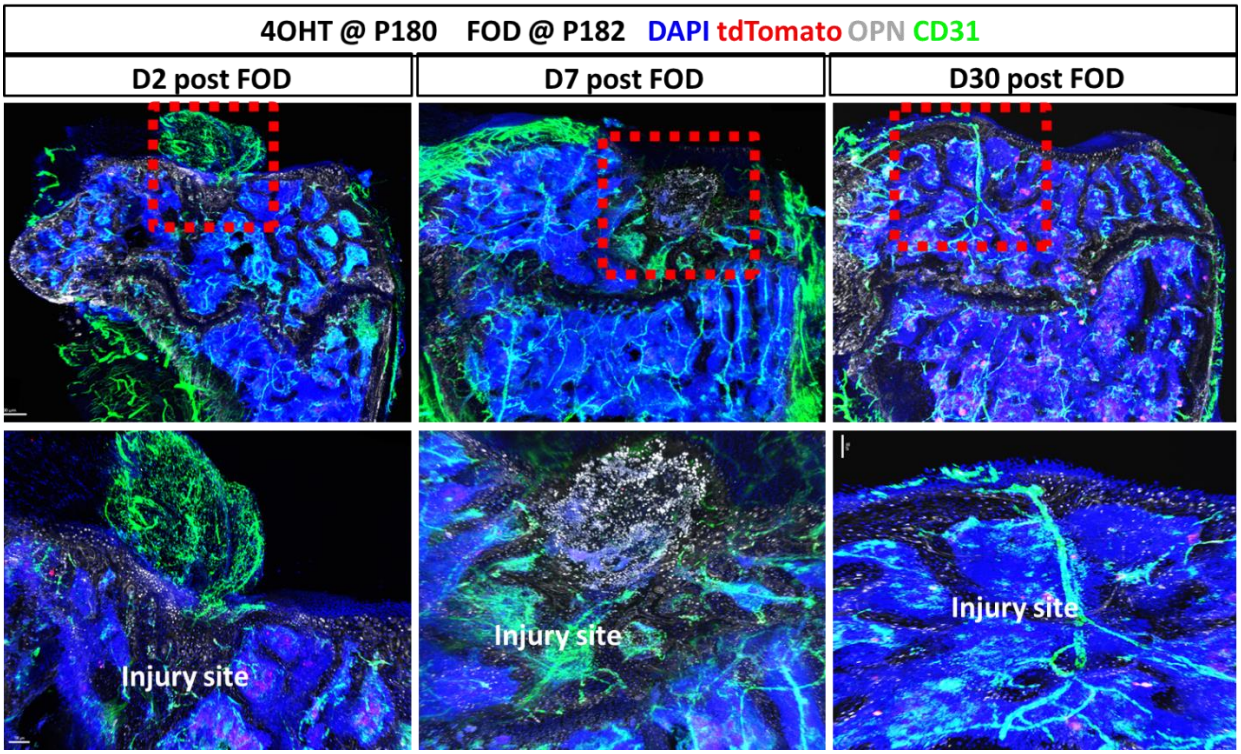

Figure 36: FOD performed two days post-4OHT in adult mice. Sox9-CreERT;Ai14 male mice were injected with 4OHT at P180. Injury site created at P182. Femurs were collected at A) D2, B) D7 and C) D30 post FOD, then processed for immunostaining and confocal imaging (N=3 for males and females at each timepoint D2, D7 and D30).

No tdT+ cells were observed at the injury sites. We hypothesized that the cells that participated in the injury repair might not have been labeled due to the short bioavailability of 4OHT (two hours in vivo), and a single dose might not have been enough to reach the avascular cartilage where Sox9 is detected in tdT negative cells (as seen in chapter 3). To address this, we decided to inject the mice with multiple doses of normal tamoxifen (instead of 4OHT), since it has a longer bioavailability in vivo, as well as wait for the number of tdT+ labeled cells to increase before performing the injury (as described below).

5.3 Lineage tracing of Sox9+ cells in FOD mice after multiple injections and longer chases

It is possible that Sox9+ SSCs do not directly contribute to tissue repair but that their downstream progeny are the actual effector cells. To test this, Sox9-CreERT;Ai14 mice received three injections of tamoxifen (TAM) (75mg/kg body weight) i.p., at 24h interval to maximize labeling of Sox9+ cells, since tamoxifen has a longer bioavailability than 4OHT in vivo. At day 30 post-TAM injection (after most Sox9+ SSCs have divided at least once and most differentiated chondrocytes have hypertrophied and died), a FOD injury was created in the distal femur and samples were collected at D2 and D7 post FOD induction. To our surprise, we still observed no participation of tdT+ cells in tissue repair (figure 37).

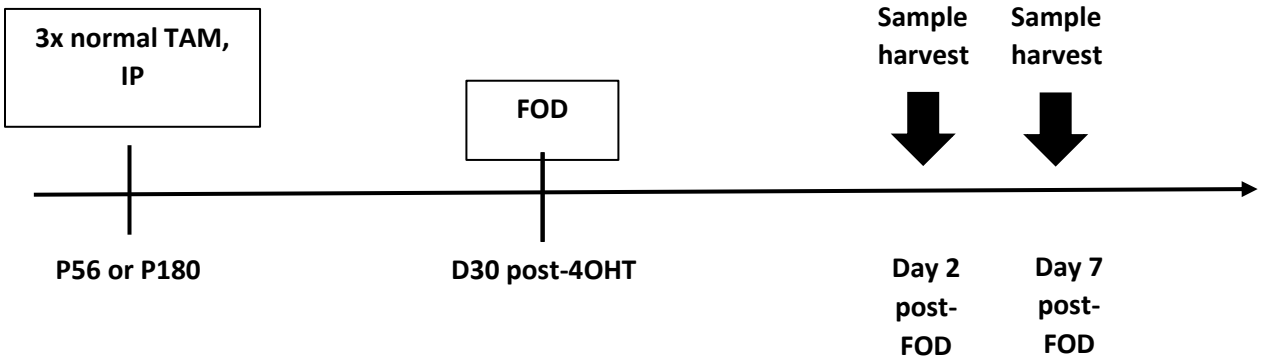

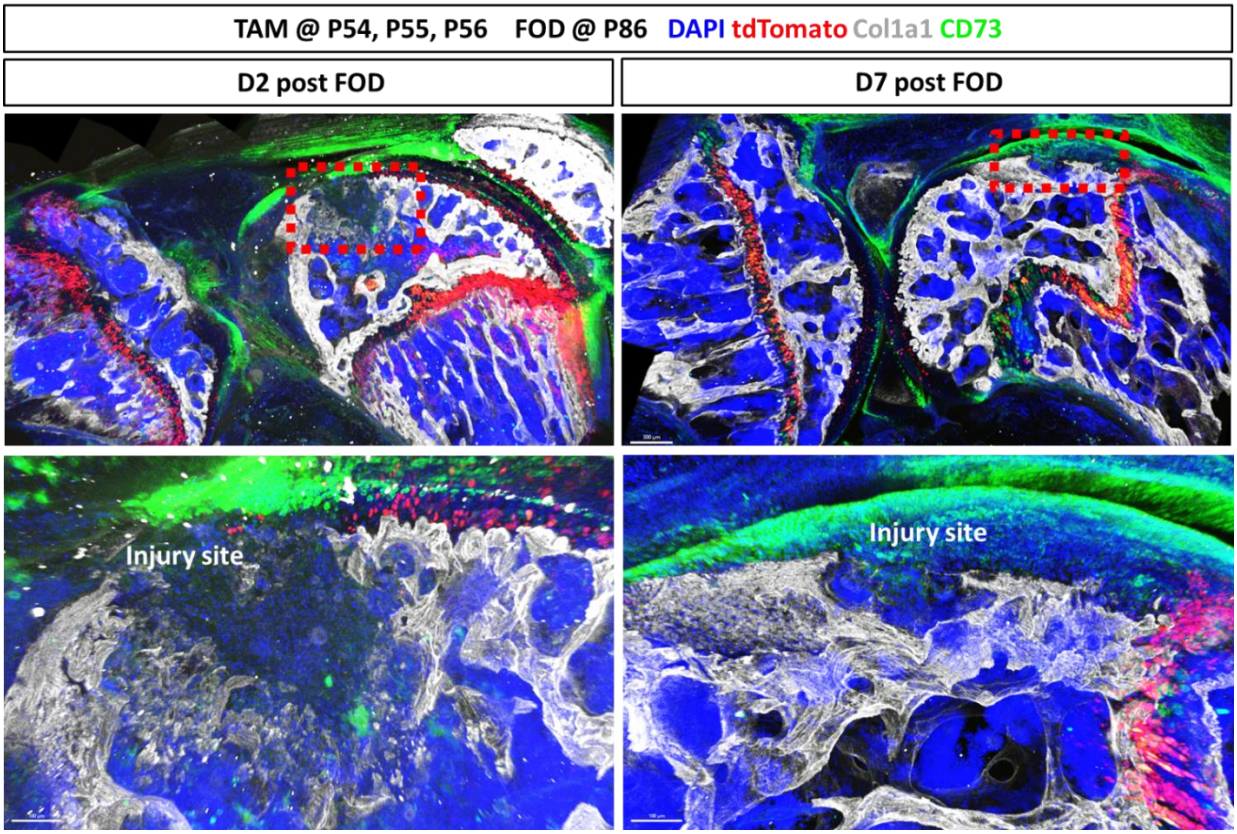

Figure 37: FOD performed one month after the last TAM injection in juvenile mice. Sox9-CreERT;Ai14 female mice were injected three times with TAM at P54, P55 and P56. Injury site created at P86. Joints were collected at D2 and D7 post FOD, then processed for immunostaining and confocal imaging (N=3 for males and females at each timepoint D2 and D7).

We tried waiting for a longer period post multiple TAM injections; at day 90 post-TAM injections, FOD was created, and joint samples were collected at D2 and D7 post FOD induction. We only show images from D2 post FOD induction, however still no participation of tdT+ cells in tissue repair was observed (figure 38).

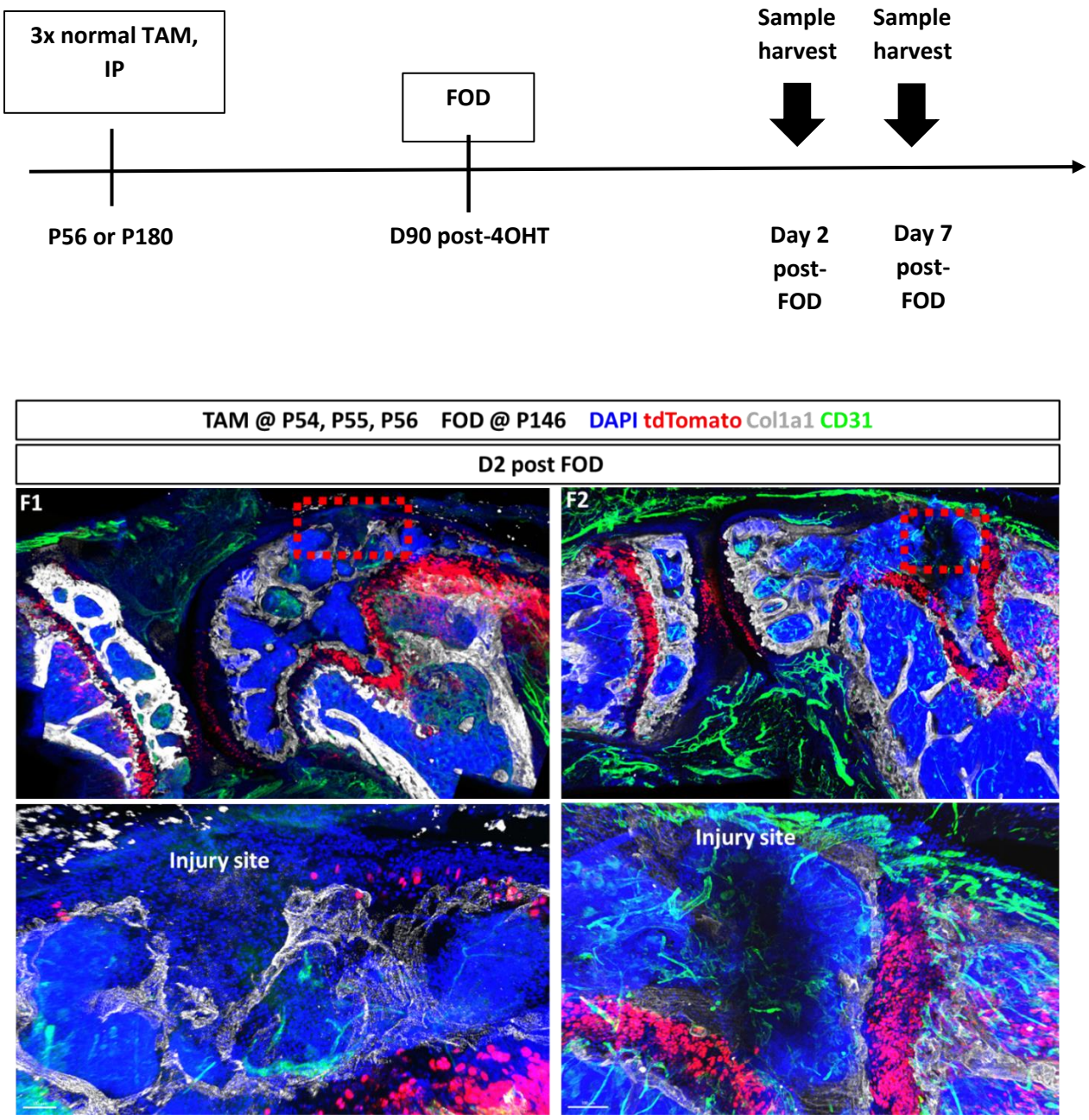

Figure 38: FOD performed three months after the last TAM injection in juvenile mice. Sox9-CreERT;Ai14 female mice were injected three times with TAM at P54, P55 and P56. Injury site created at P146. Joints were collected at D2 post FOD, then processed for immunostaining and confocal imaging (N=3 for males and females).

5.4 Summary

In this chapter, after developing and optimizing the FOD model, our data showed no contribution of tdT+ cells in tissue repair in all animals (young, adult, males, and females) and all the different conditions of the experimental plan (one versus three tamoxifen injections and creating the FOD injury 30 or 90 days post injections). However, other studies have previously shown that Sox9+ cells have a regenerative capacity in femurs and ribs[202,203]. In addition, it has been shown that Sox9+ periosteal cells regenerate a fracture injury[202], thus, it is already established that Sox9+ cells have a regenerative potential. These experiments gave us information about the proliferation and differentiation kinetics of Sox9+ cells. Combined with our EdU experiments (presented in chapter 3), several optimizations are being performed currently to study these cells in our developed FOD model; these include performing intra-articular injections instead of ip, inject our mice at an earlier age and for longer period of times (2-3 weeks of constant TAM injections) and do even longer chases.

Chapter 6: Discussion, limitations, future directions, and conclusion

6.1 Discussion

To prove the existence of stem cells and study the molecular mechanisms behind their fate decisions such as self-renewal, differentiation, proliferation, quiescence, and others, requires detailed analysis of stem cells throughout prenatal and postnatal development, as well as during adulthood and aging. Lineage tracing in vivo is the gold standard assay to identify populations of putative somatic stem cells during embryonic and postnatal development[95,96,170]. In the postnatal skeleton, the identification of *bona fide* SSCs using lineage tracing has been hindered by technical limitations associated with processing of hard tissues for immune- and histological analysis, the autofluorescence of skeletal tissues, and the lack of computational tools to quantify various and abundant subpopulations of cells in entire organs. However, these hurdles were recently addressed by novel techniques enabling multiplexed 3D fluorescence imaging of large skeletal tissues and computational tools allowing fast and reproducible imaging cytometry of large imaging datasets[109,186,194]. Our lab is the only one with the required technical expertise to perform these assays, and one of few labs worldwide studying the fundamental biology of SSCs. Therefore, we are especially well positioned to perform these studies.

In our study, we used Sox9-CreERT;Ai14 mice in which tamoxifen administration leads to constitutive expression of the tdT fluorescent reporter in Sox9-expressing cells and their progeny. We pulsed the mice with tamoxifen and EdU for three consecutive days to perform dual lineage tracing (of Sox9+ cells and proliferating cells). This allowed us to track the fate of Sox9+ cells and their progeny based on tdT expression, to quantify proliferative cells and track their fate based on EdU incorporation, and to measure cell turnover rate based on tdT and EdU label

retention. Femurs were harvested at day two, 30 and 90 post-labeling, fixed, decalcified, sectioned as coronal thick section of 250 µm in thickness on a vibratome, probed with an antibody against Sox9 and counterstained with DAPI. After optical clearing with histodenz, the entire sections were scanned with a spectral confocal microscope, and the lasers and detectors settings adjusted with staining controls. Each section represented approximately 30-50% of the entire femur, requiring 12-15 hours of acquisition time at the microscope each, and the resulting datasets consist of 10^{11} individual voxels (3D pixels) each acquired at 8-bits (totalling roughly 150 gigabytes per dataset). The data was transferred, converted, compressed (lossless), and backed-up. We then used a machine learning algorithm (within Imaris software) to identify tdT+ cells within the images (3D segmentation), exported the segmentation data into an unbiased self-developed software (XiT)[194]. Using XiT, we excluded cells without detectable DAPI signal as well as large cells (representing doublets not split during segmentation), and using staining controls, we then selected gating thresholds to quantify the number of tdT+ cells that are also positive for Sox9 protein and/or EdU.

Using these techniques and the dual lineage tracing approach, we demonstrated that the resting zone of the postnatal mouse physis harbors multipotent osteochondral Sox9+ cells that self-renew over the lifespan of the animal driving postnatal bone growth and persist in skeletally mature mice to maintain skeletal tissue homeostasis. These cells are either the progenitors of recently identified putative SSCs in the physeal cartilage or represent a subpopulation of these cells. Our data also builds on and supports previous studies demonstrating that Sox9 labels osteochondral progenitors, and that Sox9+ cells in the periosteum participate in injury repair [202]. We hypothesize that Sox9+ SSCs in the periphery of the physis are seeded or left behind in the periosteum as the bone elongates, where they remain mostly quiescent until they are activated to proliferate and participate in tissue maintenance or regeneration. Whether these periosteal Sox9+ cells retain their

self-renewal potential is currently unknown. To test this hypothesis would likely require more sophisticated lineage tracing using dual inducible recombinases and/or multiple thymidine analogues incorporation and retention assays.

Indeed, our EdU labeling experiments indicate that periosteal cells are actively dividing in growing, postnatal bones, since many of them incorporated EdU during a short, three-day pulse. However, they probably underwent only one or two rounds of division during that time, after which they stopped proliferating and became postmitotic cortical osteocytes that retained EdU for over 30 days. However, no EdU+ cortical osteocytes were observed in longer chase (90 days), suggesting that these osteocytes had either turnover and been replaced by non-labeled cells. On the other hand, tdT+ cells derived from Sox9+ SSCs were detected less in periosteum and cortical bone, but their number increased with time, replacing the cells that had incorporated EdU. This strongly suggests that Sox9+ are the upstream progenitors of the proliferative periosteal cells and that cortical bone tissue in growing mouse bones exhibits a high rate of tissue turnover (with a suggested half-life of 20 to 30 days).

Our lineage tracing of Sox9-CreERT expressing cells combined with analysis of Sox9 protein expression and EdU incorporation/retention is the first experimental evidence that strongly suggests self-renewal in any type of SSCs identified to date *in vivo*. However, we were not able to demonstrate self-renewal and multipotency at the single cell level. Therefore, it remains possible that Sox9+ cells in the resting zone could be further divided in several subpopulation of cells that display features of SSCs only at the population level.

Another intriguing finding resides in the population kinetics of tdT+ and tdT+Sox9+ cells we observed. In growing bones, we observed a biphasic population kinetics of tdT+ cells, where their number increased within the first 30 days and then decreased back to their initial numbers in

longer chases (180 days later), mainly in young animals and not the adult. The number of tdT+Sox9+ cells (putative self-renewing SSCs) did not follow the same kinetics, they decreased after day two chase but remained stable the entire chase period till day 180). In addition, the population kinetics of these double positive cells was also different in mature bones. It is likely that the number of transiently amplifying clones that expressed Sox9 protein, such as proliferative chondrocytes and pre-osteoblasts, in growing bones combined with the increasing tissue volume and mass over time makes the interpretation of this data challenging. Moreover, it is unclear what fraction of the total Sox9+ SSCs we labeled using such short labeling pulses, adding the challenge of interpreting this type of data.

As sexual dimorphism in skeletal tissues during development is established[16,18,19,21], we investigated the differences between male and female mice during our lineage tracing studies. In growing bones (young animals), almost double the number of tdT+ cells was detected in females than males at day 30 post labeling, whereas in adulthood, tdT+ cells were significantly higher in males at day 180 post labelling. Given the fact that sex steroids affect bone growth and development, we hypothesized that the high levels of estrogen in females is the main reason behind these differences. Female skeletal tissue is known to grow earlier and faster than males, which also includes an earlier closure of the femur growth plates in females. This could explain the slower growth rate in males, hence the higher number of tdT+ cells detected in mature femurs in longer chases (potentially are still proliferating and differentiating). The higher percentage of tdT+Sox9+ double positive cells detected at day-two short chase in young males suggests a slower proliferation rate of these SSCs than females that have high estrogen levels. However, during skeletal maturity, these double positive cells were constant and non-significantly different between both sexes. In addition, tdT+ adipocytes were only observed in young females at day two, then

these cells turnover and were replaced by non-labeled adipocytes in long chases and adulthood. This suggests that Sox9+ SSCs do not contribute long-term to bone marrow adipose tissue and that most probably a separate subpopulation of non-self-renewing Sox9+ cells gives rise to these adipocytes. In young male mice, no fat tissue was detected in the marrow until P86, which can be explained by the fact that the male skeleton matures slower than the female skeleton during postnatal development. Skeletal development, growth and maintenance is sexually dimorphic and women are more prone to some skeletal conditions such as osteoporosis, for instance. We have observed differences in bone mass, size, and number of cells obtained after bone digestion between male and female animals. But the ratio between cell subtypes was never significantly different (based on extensive flow cytometry analyses) nor were their abundance or anatomical localization.

When femurs were enzymatically and mechanically dissociated to isolate skeletal cells two days post-labeling in young animals, about 4% of the colonies expressed tdT in females, and around 8% in males. Although our data clearly shows that Sox9+ SSCs are maintained in skeletally mature animals and continue to contribute to bone homeostasis, however, isolating these SSCs from older animals proved to be challenging and it is possible that their growth requirement changed, such as these older SSCs are more prone to cellular senescence, or that we observed an age-related stem cell exhaustion or loss of function. Further studies will be required to address these issues. These isolated SSCs, when placed in differentiation conditions, we observed tdT+ chondrocytes, osteoblasts, and adipocytes in vitro, suggesting their multipotency differentiation potential in cell culture, at the population level.

Also, we also performed pseudotime analysis on a published single cell RNAseq dataset[190] of skeletal cells in collaboration with another lab in OHRI. This preliminary analysis confirmed

that Sox9^{high} cells could give rise to chondrocytes and osteoblasts. Further analysis and single cell transcriptomics need to be performed.

We showed that Sox9+ cells are relatively rare in postnatal human bones, but when purified by flow cytometry they formed colonies in vitro which could be differentiated into chondrocytes, osteoblasts, and adipocytes. These data are preliminary evidence where we showed that postnatal human bones contain Sox9+ cells with a similar phenotype as mouse Sox9+ putative osteochondral SSCs. Hence, we hypothesize that postnatal human bones also harbour Sox9+ SSCs. A more detailed characterization of these cells needs to be performed using the assays we established for mouse cells.

Finally, when we tried characterizing Sox9+ SSCs regenerative potential. However, we have been unable to observe contribution of Sox9+ in skeletal regeneration in our FOD model, although their contribution to skeletal injury repair has already been demonstrated[202,203]. We hypothesize that this is due to the short tamoxifen pulses we used; it has a bioavailability of only two hours in vivo and may have failed to reach the avascular cartilage where Sox9 is detected in tdT negative cells, which can be addressed by injecting repeatedly the mice with tamoxifen for a longer period of time (2-3 weeks) and/or feed them chow tamoxifen. Another explanation is that our experimental design, such as timing of tamoxifen administration, FOD injury creation, and chase lengths, was out of phase with the kinetics of tissue deposition during normal growth and regeneration. We are still testing various experimental designs to account for our observations of proliferation kinetics and tissue turnover rates, by doing longer pulses at an earlier age, and intra-articular injection of tamoxifen instead of intraperitoneal. We have shown in chapter 3 that these cells give rise to most bone and growth plate cartilage produced after tamoxifen injection as well as to subchondral bone, in addition studies have previously shown that Sox9+ cells have a

regenerative capacity in femurs and ribs[202,203], and that Sox9+ periosteal cells regenerate a fracture injury[202]. Thus, the fact that we did not observe contribution of Sox9+ cells in the regeneration of subchondral bone is intriguing, since we observe subchondral tdT+ cells in our lineage tracing experiments. By optimizing our experimental conditions, we expect to see a participation of Sox9+ cells in skeletal tissue repair.

Overall, the data of my project focuses on a population of putative SSCs in the resting zone of the growth plate, labeled by Sox9 protein. This is in accordance with two recent publications suggesting that the skeletal stem cells are also located in the resting zone of the growth plate[107,120], however these studies only focus on embryos and perinatal animals. In my study, extensive characterisation of the putative Sox9+ SSCs was performed on young and adult animals to determine their stemness, but only at the population level. This study is the first to prove self-renewal and multipotency in vivo in postnatal animals. Most importantly, parallel experiments between males and females were performed in this thesis to consider sexual dimorphism as an important factor when studying postnatal SSCs, unlike most published SSCs studies[106,107,120,122–126,204,108,111,113–117,119]. Moreover, as explained in Chapter 1, section 4.2, the majority of the markers used for lineage tracing labeled unspecific and differentiated lineages, and although Sox9 labeled multiple types of skeletal cells (resting zone chondrocytes, progenitor chondrocytes, proliferative chondrocytes, hypertrophic chondrocytes, periosteal cells, trabecular and compact bone osteoblasts), it is by far the most specific marker to SSCs compared to the previously published markers, in addition to the low resolution and autofluorescent images and the biased quantitative methods used. The results and images of this project were obtained by using a cutting-edge technique that preserves the integrity of the skeletal tissue and does not disrupt its native organisation, while reducing the autofluorescence problem by optical clearing, enhancing the

resolution of the 3D images, and most importantly using unbiased computational methods for proper quantification and analysis of the different markers co-expression levels. Finally, these putative Sox9+ SSCs were identified in both murine and human skeletal tissue using similar techniques and analysis tools, another advantage presented in this thesis compared to the literature[106,107,120,122–126,204,108,111,113–117,119].

6.2 Limitations

Our lineage tracing experiments, showed some discrepancies between the expression of tdT and Sox9 protein at two days post-labeling. Indeed, several osteogenic tdT+ cells had no detectable Sox9 protein whereas some Sox9+ proliferative chondrocytes did not get labeled with tdT (although it is known that proliferative chondrocyte express Sox9 protein). One explanation could be that the short two-day chase was enough for some Sox9+ cells to commit to the osteoblast lineage and downregulate Sox9. Similarly, it is possible that proliferative chondrocytes stopped transcribing the Sox9 gene but still contained detectable Sox9 protein. An alternative explanation would involve a combination of differential transcriptional bursting pattern, protein maturation, and protein stability between the endogenous Sox9 gene, the Sox9-CreERT transgene, and the Rosa26 tdTomato Cre-reporter and their respective encoded proteins. It is also possible that given the short tamoxifen pulses used and the short bioavailability of its active metabolites, cells located deep within the avascular cartilage were not exposed to sufficient levels of tamoxifen. Fortunately, none of these limitations and explanations alter our interpretation of the lineage tracing data.

6.3 Future directions

In this thesis study, we showed that, at the population level, a subtype of epiphyseal Sox9+ cells possess self-renewing osteochondral stem cells. We also showed that these cells persist in adulthood. Additional studies are required to determine if these cells are indeed SSCs or early skeletal progenitors through single cell assays. To do so, clonal lineage tracing analysis at the single cell level in vivo needs to be performed. One method would be by using the Confetti fluorescent Cre-reporter allele and crossing it with our Sox9-CreERT2 line to obtain the Sox9-CreERT;Confetti double mutant line. Then, these mice will be pulsed with tamoxifen at P56 for three consecutive days and femurs will be harvested at day 2, 30, and 90 post-labeling, with additional time points added if required for higher temporal resolution. By using similar techniques (lineage tracing, confocal microscopy and imaging cytometry), we can quantify the number of clones of each color, how many labelled cells maintain Sox9 expression over time, and how many give rise to both chondrocytes and osteoblasts.

For an *in vitro* single cell analysis, to clonally determine the expansion and differentiation potential of Sox9+ SSCs, an *in vitro* colony forming (CFU-f) at clonal density can be performed, as well as clonal osteo-, chondro- and adipocytic differentiation assays on single colony-derived cells. Briefly, Sox9-CreERT;Ai14 mice will be pulsed with tamoxifen at P56. Two days post-labeling, femurs will be harvested and dissociated enzymatically and mechanically. Flow cytometry will be used to isolate tdT+ cells from numerous animals to have enough. Single cells will be seeded in individual wells on a layer of non-labelled primary skeletal feeder cells derived from C57Bl/6 mice and cultured in appropriate medium. Wells will be inspected for the development of tdT+ colonies, which will then be expanded and subjected to differentiation assays to assess osteogenic and chondrogenic potential.

To confirm the number of self-renewing, multipotent Sox9+ SSCs in vivo at the single cell level, we are developing a limiting dilution ossicle transplantation assay. Briefly, tdT+ cells from Sox9-CreERT;Ai14 mice will be purified by flow cytometry at D2 post-4OHT and then mixed with wildtype mesenchymal stromal cells[187,205] using limiting dilution assay. These will be seeded on Gelfoam collagen sponges or directly placed in micropellet cultures in a chondrogenic medium for three weeks, followed by two weeks in a hypertrophic medium. This will induce hypertrophic chondrocyte differentiation of the cells and then subcutaneously transplant them in wild type C57Bl/6 mice for 8 weeks to induce endochondral ossification[187,205–208]. Some samples will then be harvested and immunostained to assess multilineage contribution of Sox9+ cells, as well as their self-renewal by staining them with a Sox9 antibody, others will be dissociated to perform a secondary transplantation assay.

In addition, to confirm our lineage tracing observations, a different Sox9 mouse line can be used, the IRES knock-in Sox9 mouse model (C57BL6/-*Sox9*$^{em1(cre/ERT2)Tchn}$ MGI:035092)[209] , to reflect better the expression of Sox9 since one of the limitations of this study was the discrepancies observed between tdT and Sox9 protein in the lineage tracing experiments. Also, it is important to examine in more details how aging affects the number and phenotype of these cells, by repeating all the described experiment above and in the thesis but in older animals (aged around one year old).

A single cell transcriptomics would be essential for a better understanding of the genetic profile of these Sox9+ SSCs. The data will be analyzed to identify gene differentially expressed between cell types, age groups and sex. RNA Velocity or pseudotime analysis will be used to reconstruct/infer lineage trajectories based on gene expression, as described in the thesis[210–212]. By comparing the phenotype and gene expression profiles between cells of different sex, at different

ages, we will better understand how aging affects the molecular phenotype of Sox9+ putative SSCs. Also, by gaining a better understanding of their molecular regulation of fate decision, we can test it by using pharmacological activators and inhibitors of the genes identified, or conditional knockout mouse lines.

In addition, we need to assess the endogenous regenerative potential of these Sox9+ cells. This can be performed by either pulsing the animals more frequently and for longer chases with tamoxifen, also feeding the animals with chow tamoxifen. In addition, to testing the femoral fracture model as mentioned earlier. Following the injury, femurs of joints will be collected at day two, seven, 14 and 30 post-FOD, and a normal lineage tracing experiment with the addition of an injury will be performed. The number and phenotype of tdT+ cells over time will be quantified and compared between groups (age, sex, injured or sham). We will also isolate skeletal cells from mice two days post-injury and process them for scRNAseq as described above for the healthy samples, to determine the molecular pathways activated during tissue regeneration and compare.

Finally, since we have showed in this study preliminary data that postnatal human bones contain Sox9+ cells with a similar phenotype as mouse Sox9+ putative osteochondral SSCs, we hypothesize that postnatal human bones also harbour Sox9+ SSCs. A more detailed characterization of these cells using the same assays we established for mouse cells will be performed. We will obtaining our human samples from several sources; physeal cartilage samples will be provided from adolescent patients undergoing elective epiphysiodesis for limb length discrepancies without underlying genetic or metabolic disease, or post-traumatic contralateral growth plate closure, and adult samples from trauma patients undergoing arthroscopic surgery or hemi-/total arthroplasty (epiphyseal scars, trabecular bone, cortical bone and/or periosteum) to test for the persistence of these stem cells into adulthood. Samples will be received from the OR and

either fixed or processed for cell isolation. Fixed tissues are processed from confocal analysis as per our mouse protocol. Other samples are enzymatically and mechanically dissociated, the single cell suspension is then placed in culture for clonal *in vitro* and/or transplantation assays or processed for scRNAseq.

6.4 Conclusion

In this thesis, we demonstrated that the resting zone of the postnatal mouse physis harbors multipotent osteochondral Sox9+ cells that self-renew over the lifespan of the animal driving postnatal bone growth. They also persist in skeletally mature mice to maintain skeletal tissue homeostasis. These cells are either the progenitors of recently identified putative SSCs in the physeal cartilage or represent a subpopulation of these cells. Our data is consistent with recent studies suggesting the existence of SSCs residing in an epiphyseal stem cell niche[213] and provides additional information about the multipotentiality, self-renewal capacity and proliferation kinetics of these SSCs. Also, our data builds on and supports previous studies demonstrating that Sox9 labels osteochondral progenitors, and that Sox9+ cells in the periosteum participate in injury repair[196]. Overall, our study provides a strong basis to further characterize this novel population of self-renewing osteochondral SSCs in the postnatal skeleton, and those further studies will help in the design of innovative stem cell-based regenerative therapies for various orthopedic conditions.

Chapter 7: References

1. Ono, N., Balani, D. H. & Kronenberg, H. M. *Stem and progenitor cells in skeletal development*. *Vertebrate Skeletal Development* vol. 133 (Elsevier Inc., 2019).

2. Ono, N. & Kronenberg, H. M. *Developmental Biology of Musculoskeletal Tissues for Tissue Engineers*. *Developmental Biology and Musculoskeletal Tissue Engineering* (Elsevier Inc., 2018). doi:10.1016/b978-0-12-811467-4.00001-2.

3. Berendsen, A. D. & Olsen, B. R. Bone development Agnes. 14–18 (2015) doi:10.1016/j.bone.2015.04.035.Bone.

4. Fleming, A., Kishida, M. G., Kimmel, C. B. & Keynes, R. J. Building the backbone: the development and evolution of vertebral patterning. *Development* **142**, 1733–1744 (2015).

5. Mariani, F. V & Martin, G. R. clues from the limb. **423**, 319–325 (2003).

6. Karsenty, G., Kronenberg, H. M. & Settembre, C. Genetic Control of Bone Formation. (2009) doi:10.1146/annurev.cellbio.042308.113308.

7. Bi, W., Deng, J. M., Zhang, Z., Behringer, R. R. & Crombrugghe, B. De. Sox9 is required for cartilage formation. **22**, 85–89 (1999).

8. Crombrugghe, B. De. The transcription factor Sox9 has essential roles in successive steps of the chondrocyte differentiation pathway and is required for expression of Sox5 and Sox6. 2813–2828 (2002) doi:10.1101/gad.1017802.overt.

9. Yang, J., Andre, P., Ye, L. & Yang, Y. Z. The Hedgehog signalling pathway in bone formation. *Int. J. Oral Sci.* **7**, 73–79 (2015).

10. Maes, C. *et al.* Osteoblast precursors, but not mature osteoblasts, move into developing

and fractured bones along with invading blood vessels. *Dev. Cell* **19**, 329–344 (2010).

11. Coutu, D. L., Kokkaliaris, K. D., Kunz, L. & Schroeder, T. Three-dimensional map of nonhematopoietic bone and bone-marrow cells and molecules. *Nat. Biotechnol.* **35**, 1202–1210 (2017).

12. De Bruyn, P. P. H., Breen, P. C. & Thomas, T. B. The microcirculation of the bone marrow. *Anat. Rec.* **168**, 55–68 (1970).

13. Abad, V. *et al.* The Role of the Resting Zone in Growth Plate Chondrogenesis. *Endocrinology* **143**, 1851–1857 (2002).

14. Callewaert, F. *et al.* Sexual dimorphism in cortical bone size and strength but not density is determined by independent and time-specific actions of sex steroids and IGF-1: Evidence from pubertal mouse models. *J. Bone Miner. Res.* **25**, 617–626 (2010).

15. Callewaert, F., Boonen, S. & Vanderschueren, D. Sex steroids and the male skeleton: a tale of two hormones. *Trends Endocrinol. Metab.* **21**, 89–95 (2010).

16. Callewaert, F., Sinnesael, M., Gielen, E., Boonen, S. & Vanderschueren, D. Skeletal sexual dimorphism: Relative contribution of sex steroids, GH-IGF1, and mechanical loading. *J. Endocrinol.* **207**, 127–134 (2010).

17. E, S. Pathogenesis of bone fragility in women and men. *Lancet* **359**, 1841–50 (2002).

18. Seeman, E. Clinical review 137: Sexual dimorphism in skeletal size, density, and strength. *J. Clin. Endocrinol. Metab.* **86**, 4576–4584 (2001).

19. Lorenzo, J. Sexual Dimorphism in Osteoclasts. *Cells* **9**, 1–7 (2020).

20. Zamberlan, N. *et al.* Evaluation of cortical thickness and bone density by roentgen

microdensitometry in growing males and females. *Eur. J. Pediatr.* **155**, 377–382 (1996).

21. Mun, S. H. *et al.* Sexual Dimorphism in Differentiating Osteoclast Precursors Demonstrates Enhanced Inflammatory Pathway Activation in Female Cells. *J. Bone Miner. Res.* **36**, 1104–1116 (2021).

22. Vanderschueren, D. *et al.* Androgens and bone. *Endocr. Rev.* **25**, 389–425 (2004).

23. Nilsson, O. *et al.* Evidence that estrogen hastens epiphyseal fusion and cessation of longitudinal bone growth by irreversibly depleting the number of resting zone progenitor cells in female rabbits. *Endocrinology* **155**, 2892–2899 (2014).

24. Callewaert, F. *et al.* Differential regulation of bone and body composition in male mice with combined inactivation of androgen and estrogen receptor-α. *FASEB J.* **23**, 232–240 (2009).

25. Cole, T. J., Ahmed, M. L., Preece, M. A., Hindmarsh, P. & Dunger, D. B. The relationship between Insulin-like Growth Factor 1, sex steroids and timing of the pubertal growth spurt. *Clin. Endocrinol. (Oxf).* **82**, 862–869 (2015).

26. Lupu, F., Terwilliger, J. D., Lee, K., Segre, G. V. & Efstratiadis, A. Roles of growth hormone and insulin-like growth factor 1 in mouse postnatal growth. *Dev. Biol.* **229**, 141–162 (2001).

27. Laron, Z. The essential role of IGF-I: Lessons from the long-term study and treatment of children and adults with Laron syndrome. *J. Clin. Endocrinol. Metab.* **84**, 4397–4404 (1999).

28. Sims, N. A. *et al.* Bone homeostasis in growth hormone receptor-null mice is restored by IGF-I but independent of Stat5. *J. Clin. Invest.* **106**, 1095–1103 (2000).

29. Juul, A. The effects of oestrogens on linear bone growth. *Hum. Reprod. Update* **7**, 303–313 (2001).

30. Venken, K. *et al.* Growth without growth hormone receptor: Estradiol is a major growth hormone-independent regulator of hepatic IGF-I synthesis. *J. Bone Miner. Res.* **20**, 2138–2149 (2005).

31. Vanderschueren, D. *et al.* Aromatase inhibition impairs skeletal modeling and decreases bone mineral density in growing male rats. *Endocrinology* **138**, 2301–2307 (1997).

32. Vidal, O. *et al.* Estrogen receptor specificity in the regulation of skeletal growth and maturation in male mice. *Proc. Natl. Acad. Sci. U. S. A.* **97**, 5474–5479 (2000).

33. Börjesson, A. E. *et al.* The role of estrogen receptor α in growth plate cartilage for longitudinal bone growth. *J. Bone Miner. Res.* **25**, 2690–2700 (2010).

34. Mosley, J. R. & Lanyon, L. E. Strain rate as a controlling influence on adaptive modeling in response to dynamic loading of the ulna in growing male rats. *Bone* **23**, 313–318 (1998).

35. Mosley, J. R., March, B. M., Lynch, J. & Lanyon, L. E. Strain magnitude related changes in whole bone architecture in growing rats. *Bone* **20**, 191–198 (1997).

36. Hsieh, Y. F. & Turner, C. H. Effects of loading frequency on mechanically induced bone formation. *J. Bone Miner. Res.* **16**, 918–924 (2001).

37. Srinivasan, S., Weimer, D. A., Agans, S. C., Bain, S. D. & Gross, T. S. Low-magnitude mechanical loading becomes osteogenic when rest is inserted between each load cycle. *J. Bone Miner. Res.* **17**, 1613–1620 (2002).

38. Frost, H. M. Bone's Mechanostat: A 2003 Update. *Anat. Rec. - Part A Discov. Mol. Cell.*

Evol. Biol. **275**, 1081–1101 (2003).

39. Bass, S. L. *et al.* The effect of mechanical loading on the size and shape of bone in pre-, peri-, and postpubertal girls: A study in tennis players. *J. Bone Miner. Res.* **17**, 2274–2280 (2002).

40. Ducher, G., Daly, R. M. & Bass, S. L. Effects of repetitive loading on bone mass and geometry in young male tennis players: A quantitative study using MRI. *J. Bone Miner. Res.* **24**, 1686–1692 (2009).

41. Colnot, C. Skeletal cell fate decisions within periosteum and bone marrow during bone regeneration. *J. Bone Miner. Res.* **24**, 274–282 (2009).

42. Zhou, B. O. Leptin Receptor-expressing mesenchymal stromal cells represent the main source of bone formed by adult bone marrow. **15**, 154–168 (2014).

43. Duchamp De Lageneste, O. *et al.* Periosteum contains skeletal stem cells with high bone regenerative potential controlled by Periostin. *Nat. Commun.* **9**, 1–15 (2018).

44. Aya Kawanami, Takehiko Matsushita, Yuk Yu Chan, S. M. Mice expressing GFP and CreER in osteochondro progenitor cells in the periosteum. **386**, 477–482 (2009).

45. Matsushita, Y. *et al.* A Wnt-mediated transformation of the bone marrow stromal cell identity orchestrates skeletal regeneration. *Nat. Commun.* **11**, (2020).

46. Simon, T. M. & Jackson, D. W. Articular Cartilage: Injury Pathways and Treatment Options. *Sports Med. Arthrosc.* **26**, 146–154 (2018).

47. Borrelli, J. *et al.* Understanding Articular Cartilage Injury and Potential Treatments. *J. Orthop. Trauma* **33**, S6–S12 (2019).

48. Simon, T. Articular Cartilage- Injury Pathways and Treatment Options. 63482 (2006).

49. Apostolakos, J. *et al.* The enthesis: A review of the tendon-to-bone insertion. *Muscles. Ligaments Tendons J.* **4**, 333–342 (2014).

50. Howell, K. *et al.* Novel Model of Tendon Regeneration Reveals Distinct Cell Mechanisms Underlying Regenerative and Fibrotic Tendon Healing. *Sci. Rep.* **7**, 1–14 (2017).

51. Korpershoek, J. V., De Windt, T. S., Hagmeijer, M. H., Vonk, L. A. & Saris, D. B. F. Cell-based meniscus repair and regeneration: At the brink of clinical translation?: A systematic review of preclinical studies. *Orthop. J. Sport. Med.* **5**, 1–15 (2017).

52. Nepple, J. J., Dunn, W. R. & Wright, R. W. Meniscal repair outcomes at greater than five years: A systematic literature review and meta-analysis. *J. Bone Jt. Surg.* **94**, 2222–2227 (2012).

53. Golz, A. G., Mandelbaum, B. & Pace, J. L. All-Inside Meniscus Repair. 252–258 (2022).

54. Ollier, L. Du périoste au point de vue physiologique et chirurgical. in *Congrès Médical de Lyon* 69 (1864).

55. Goujon, E. Recherches expérimentales sur les propriétés physiologiques de la moelle des os. *J. l'anatomie la Physiol. Norm. Pathol. l'homme des animaux* **6**, 399–412 (1868).

56. L. SIMINOVITCH, J. E. T. A. E. A. M. Decline in colony-forming ability of marrow cells subjected to serial transplantation into irradiated mice. *Transplantation* **3**, 289 (1964).

57. Friedenstein, A. J., Piatetzky-Shapiro, I. I. & Petrakova, K. V. Osteogenesis in transplants of bone marrow cells. *J. Embryol. Exp. Morphol.* **16**, 381–90 (1966).

58. Friedenstein, A. J., Petrakova, K. V., Kurolesova, A. I. & Frolova, G. P. Heterotopic

transplants of bone marrow. *Transplantation* **6**, 230–47 (1968).

59. Crosby, M. T. and W. H. Transplantation of Marrow to Extramedullary Sites. **15**, 1–23 (1968).

60. Friedenstein, A., Chailakhjan, R. & Lalykina, K. THE DEVELOPMENT OF FIBROBLAST COLONIES IN MONOLAYER CULTURES OF GUINEA-PIG BONE MARROW AND SPLEEN CELLS. *Cell Tissue Kinet.* **3**, 393–403 (1970).

61. Friedenstein, A. Stromal cells responsible for transferring the microenvironment of the hemopoietic tissues- cloning in vitro and retransplantation in vivo. 63482 (1974).

62. Friedenstein, A. F., Chailakhjan, R. H. & Lalykina, K. S. THE DEVELOPMENT OF FIBROBLAST COLONIES IN MONOLAYER CULTURES OF GUINEA-PIG BONE MARROW AND SPLEEN CELLS. *Development* **38**, 1–6 (1897).

63. Friedenstein, A. & Kuralesova, A. I. Osteogenic precursor cells of bone marrow in radiation chimeras. *Transplantation* **12**, 99–108 (1971).

64. Bianco, P., Robey, P. G. & Simmons, P. J. Mesenchymal Stem Cells: Revisiting History, Concepts, and Assays. *Cell Stem Cell* **2**, 313–319 (2008).

65. Arnold I. Caplan. Mesenchymal Stem Cells* Arnold. *Chem. Phys. Lett.* **7**, 581–582 (1991).

66. Caplan, A. I. Mesenchymal stem cells: Time to change the name! *Stem Cells Transl. Med.* **6**, 1445–1451 (2017).

67. Pamela Gehron Robey, Sergei A. Kuznetsov, Mara Riminucci, and P. B. Bone marrow stromal cell assays – in vitro and in vivo. *Methods Mol. Biol.* **1130**, 233–243 (2014).

68. Robey, P. ‘Mesenchymal stem cells’: Fact or fiction, and implications in their therapeutic use. *F1000Research* **6**, 1–8 (2017).

69. Phinney, D. G. Functional heterogeneity of mesenchymal stem cells: Implications for cell therapy. *J. Cell. Biochem.* **113**, 2806–2812 (2012).

70. Pittenger, M. F. *et al.* Multilineage potential of adult human mesenchymal stem cells. *Science (80-.).* **284**, 143–147 (1999).

71. Viswanathan, S. *et al.* Mesenchymal stem versus stromal cells: International Society for Cell & Gene Therapy (ISCT®) Mesenchymal Stromal Cell committee position statement on nomenclature. *Cytotherapy* **21**, 1019–1024 (2019).

72. Prockop, D. J. Marrow stromal cells as stem cells for nonhematopoietic tissues. *Science (80-.).* **276**, 71–74 (1997).

73. View, E. & Phinney, D. G. Biochemical Heterogeneity of Mesenchymal Stem Cell Populations Clues to their Therapeutic Efficacy ND ES SC RIB ND ES SC RIB. **6**, 2884–2889 (2007).

74. Ibberson, D., Tremain, N., Gray, A. & Phinney, D. G. What is in a name? Defining the molecular phenotype of marrow stromal cells and their relationship to other stem/progenitor cells. *Cytotherapy* **3**, 409–411 (2001).

75. Russell, K. C. *et al.* In vitro high-capacity assay to quantify the clonal heterogeneity in trilineage potential of mesenchymal stem cells reveals a complex hierarchy of lineage commitment. *Stem Cells* **28**, 788–798 (2010).

76. Russell, K. C. *et al.* Clonal analysis of the proliferation potential of human bone marrow mesenchymal stem cells as a function of potency. *Biotechnol. Bioeng.* **108**, 2716–2726

(2011).

77. O'Connor, K. C. *et al.* High-capacity assay to quantify the clonal heterogeneity in potency of mesenchymal stem cells. *BMC Proc.* **5**, O14 (2011).

78. Dj, P. Marrow stromal cells as stem cells for nonhematopoietic tissues. (1997).

79. Alice, M. Origin of osteogenic Precursor Cell in Extramedullary Marrow Implants. **38**, 569–576 (1971).

80. Tavassoli, M. & Takahashi, K. Morphological studies on long-term culture of marrow cells: Characterization of the adherent stromal cells and their interactions in maintaining the proliferation of hemopoietic stem cells. *Am. J. Anat.* **164**, 91–111 (1982).

81. Tavassoli, M. & Friedenstein, A. Hemopoietic stromal microenvironment. *Am. J. Hematol.* **15**, 195–203 (1983).

82. Friedenstein, A. J., Chailakhyan, R. K., Latsinik, N. V., Panasyuk, A. F. & Keiliss-Borok, I. V. Stromal cells responsible for transferring the microenvironment of the hemopoietic tissues: cloning in vitro and retransplantation in vivo. *Transplantation* **17**, 331 (1974).

83. Weiss, L. The hematopoietic microenvironment of the bone marrow: An ultrastructural study of the stroma in rats. *Anat. Rec.* **186**, 161–184 (1976).

84. Ara, T. *et al.* Long-term hematopoietic stem cells require stromal cell-derived factor-1 for colonizing bone marrow during ontogeny. *Immunity* **19**, 257–67 (2003).

85. Tokoyoda, K., Egawa, T., Sugiyama, T., Choi, B. Il & Nagasawa, T. Cellular niches controlling B lymphocyte behavior within bone marrow during development. *Immunity* **20**, 707–718 (2004).

86. Crisan, M. *et al.* A Perivascular Origin for Mesenchymal Stem Cells in Multiple Human Organs. *Cell Stem Cell* **3**, 301–313 (2008).

87. Diaz-Flores, L. *et al.* Pericytes. Morphofunction, interactions and pathology in a quiescent and activated mesenchymal cell niche. *Histol. Histopathol.* **24**, 909–69 (2009).

88. Guimarães-Camboa, N. *et al.* Pericytes of Multiple Organs Do Not Behave as Mesenchymal Stem Cells In Vivo. *Cell Stem Cell* **20**, 345–359 (2017).

89. Ding, L., Saunders, T. L., Enikolopov, G. & Morrison, S. J. Endothelial and perivascular cells maintain haematopoietic stem cells. *Nature* **481**, 457–462 (2012).

90. Kunisaki, Y. *et al.* Arteriolar niches maintain haematopoietic stem cell quiescence. *Nature* **502**, 637–643 (2013).

91. Campagnolo, P., Katare, R. & Madeddu, P. Realities and misconceptions on the pericytes role in tissue repair. *Regen. Med.* **13**, 119–122 (2018).

92. Caplan, A. I. & Correa, D. Perspective The MSC : An Injury Drugstore. *Stem Cell* **9**, 11–15 (2011).

93. Caplan, A. I. & Dennis, J. E. Mesenchymal stem cells as trophic mediators. *J. Cell. Biochem.* **98**, 1076–84 (2006).

94. Caplan, A. I. All MSCs are pericytes? *Cell Stem Cell* **3**, 229–30 (2008).

95. Fox, D. T., Morris, L. X., Nystul, T. & Spradling, A. C. Lineage analysis of stem cells. in *StemBook [Internet]* 1–18 (2009). doi:10.3824/stembook.1.33.1.

96. Blanpain, C. & Simons, B. D. Unravelling stem cell dynamics by lineage tracing. *Nat. Rev. Mol. Cell Biol.* **14**, 489–502 (2013).

97. Madisen, L. *et al.* A robust and high-throughput Cre Repooting and characterization. *Nat Neurosci* **13**, 133–140 (2010).

98. Gonen, N., Quinn, A., O'Neill, H. C., Koopman, P. & Lovell-Badge, R. Normal Levels of Sox9 Expression in the Developing Mouse Testis Depend on the TES/TESCO Enhancer, but This Does Not Act Alone. *PLoS Genet.* **13**, 1–24 (2017).

99. Solius, G. M., Maltsev, D. I., Belousov, V. V & Podgorny, O. V. Recent advances in nucleotide analogue-based techniques for tracking dividing stem cells : An overview. *J. Biol. Chem.* **297**, 101345 (2021).

100. Salic, A. & Mitchison, T. J. A chemical method for fast and sensitive detection of DNA synthesis in vivo. (2007) doi:10.1073/pnas.0712168105.

101. Kim, H., Kim, M., Im, S.-K. & Fang, S. Mouse Cre-LoxP system: general principles to determine tissue-specific roles of target genes. *Lab. Anim. Res.* **34**, 147 (2018).

102. McLellan, M. A., Rosenthal, N. A. & Pinto, A. R. Cre-loxP-Mediated Recombination: General Principles and Experimental Considerations. *Curr. Protoc. Mouse Biol.* **7**, 1–12 (2017).

103. Hayashi, S. & McMahon, A. P. Efficient recombination in diverse tissues by a tamoxifen-inducible form of Cre: A tool for temporally regulated gene activation/inactivation in the mouse. *Dev. Biol.* **244**, 305–318 (2002).

104. Kristianto, J., Johnson, M. G., Zastrow, R. K., Radcliff, A. B. & Blank, R. D. Spontaneous recombinase activity of Cre–ERT2 in vivo. *Transgenic Res.* **26**, 411–417 (2017).

105. Indra, A. K. *et al.* Temporally-controlled site-specific mutagenesis in the basal layer of the epidermis: Comparison of the recombinase activity of the tamoxifen-inducible Cre-ER(T)

and Cre-ER(T2) recombinases. *Nucleic Acids Res.* **27**, 4324–4327 (1999).

106. Park, D. *et al.* Endogenous Bone Marrow MSCs Are Dynamic, Fate-Restricted Participants in Bone Maintenance and Regeneration. **10**, 259–272 (2012).

107. Chan, C. K. F. *et al.* Identification and specification of the mouse skeletal stem cell. *Cell* **160**, 285–298 (2015).

108. Méndez-Ferrer, S. *et al.* Mesenchymal and haematopoietic stem cells form a unique bone marrow niche. *Nature* **466**, 829–834 (2010).

109. Coutu, D. L., Kokkaliaris, K. D., Kunz, L. & Schroeder, T. Three-dimensional map of nonhematopoietic bone and bone-marrow cells and molecules. *Nat. Biotechnol.* **35**, 1202–1210 (2017).

110. Zhou, B. O., Yue, R., Murphy, M. M., Peyer, J. & Morrison, S. J. Leptin Receptor-expressing mesenchymal stromal cells represent the main source of bone formed by adult bone marrow. *Cell Stem Cell* **15**, 156–168 (2014).

111. Debnath, S. *et al.* Discovery of a periosteal stem cell mediating intramembranous bone formation. *Nature* **562**, 133–9 (2018).

112. Zhou, X. *et al.* Chondrocytes Transdifferentiate into Osteoblasts in Endochondral Bone during Development, Postnatal Growth and Fracture Healing in Mice. *PLoS Genet.* **10**, e1004820 (2014).

113. Yang, L., Tsang, K. Y., Tang, H. C., Chan, D. & Cheah, K. S. E. Hypertrophic chondrocytes can become osteoblasts and osteocytes in endochondral bone formation. *World Rev. Nutr. Diet.* **114**, 13 (2014).

114. Logan, M. *et al.* Expression of Cre Recombinase in the developing mouse limb bud driven

by a Prxl enhancer. *Genesis* **33**, 77–80 (2002).

115. Mizoguchi, T. *et al.* Osterix marks distinct waves of primitive and definitive stromal progenitors during bone marrow development. *Dev. Cell* **29**, 340–349 (2014).

116. Chen, J. *et al.* Osx-Cre targets multiple cell types besides osteoblast lineage in postnatal mice. *PLoS One* **9**, 1–6 (2014).

117. Liu, Y. *et al.* Osterix-Cre Labeled Progenitor Cells Contribute to the Formation and Maintenance of the Bone Marrow Stroma. *PLoS One* **8**, (2013).

118. Ono, N. A Subset of Chondrogenic Cells Provides Early Mesenchymal Progenitors in Growing Bones. **40**, 1291–1296 (2014).

119. Worthley, D. L. Gremlin 1 Identifies a Skeletal Stem Cell with Bone, Cartilage, and Reticular Stromal Potential. **40**, 1291–1296 (2015).

120. Mizuhashi, K. *et al.* Resting zone of the growth plate houses a unique class of skeletal stem cells. *Nature* **563**, 254–258 (2018).

121. Hoppe, P. S. *et al.* Early myeloid lineage choice is not initiated by random PU.1 to GATA1 protein ratios. *Nature* **535**, 299–302 (2016).

122. Lu, W.-J. *et al.* Identification of the Human Skeletal Stem Cell. *Cell* **175**, 43-56.e21 (2018).

123. Balani, D. H., Ono, N. & Kronenberg, H. M. Parathyroid hormone regulates fates of murine osteoblast precursors in vivo. *J. Clin. Invest.* **127**, 3327–3338 (2017).

124. Ono, N., Ono, W., Nagasawa, T. & Kronenberg, H. M. A subset of chondrogenic cells provides early mesenchymal progenitors in growing bones. *Nat. Cell Biol.* **16**, 1157–1167

(2014).

125. Guimarães-Camboa, N. *et al.* Pericytes of Multiple Organs Do Not Behave as Mesenchymal Stem Cells In Vivo. *Cell Stem Cell* **20**, 345-359.e5 (2017).

126. Tsukasaki, M. *et al.* Periosteal stem cells control growth plate stem cells during postnatal skeletal growth. 1–8 (2022) doi:10.1038/s41467-022-31592-x.

127. Symon, A. & Harley, V. SOX9: A genomic view of tissue specific expression and action. *Int. J. Biochem. Cell Biol.* **87**, 18–22 (2017).

128. Jo, A. *et al.* The versatile functions of Sox9 in development, stem cells, and human diseases. *Genes Dis.* **1**, 149–161 (2014).

129. Determination, V. S. Vertebrate Sex Determination. *Vertebr. Sex Determ.* (2003) doi:10.1159/isbn.978-3-318-01054-1.

130. Panda, M., Tripathi, S. K. & Biswal, B. K. SOX9: An emerging driving factor from cancer progression to drug resistance. *Biochim. Biophys. Acta - Rev. Cancer* **1875**, (2021).

131. Aguilar-Medina, M. *et al.* SOX9 Stem-Cell Factor: Clinical and Functional Relevance in Cancer. *J. Oncol.* **2019**, (2019).

132. Wegner, M., Neurobiologie, M., Hamburg, U. & Hamburg, D.-. From head to toes : the multiple facets of Sox proteins. **27**, 1409–1420 (1999).

133. Kamachi, Y., Uchikawa, M., Kondoh, H. & Biology, C. Pairing SOX off with partners in the regulation of embryonic development. **9525**, 2–7 (2000).

134. Leung, V. Y. L. *et al.* SOX9 Governs Differentiation Stage-Specific Gene Expression in Growth Plate Chondrocytes via Direct Concomitant Transactivation and Repression. **7**, 1–

16 (2011).

135. Ikeda, T. *et al.* The Combination of SOX5 , SOX6 , and SOX9 (the SOX Trio) Provides Signals Sufficient for Induction of Permanent Cartilage. **50**, 3561–3573 (2004).

136. Martini, S. *et al.* A critical role for Sox9 in Notch-induced astrogliogenesis and stem cell maintenance. *Stem Cells* **31**, 741–751 (2013).

137. Scott, C. E. *et al.* SOX9 induces and maintains neural stem cells. *Nat. Neurosci.* **13**, 1181–1189 (2010).

138. Seymour, P. A. *et al.* SOX9 is required for maintenance of the pancreatic progenitor cell pool. *Proc. Natl. Acad. Sci. U. S. A.* **104**, 1865–1870 (2007).

139. Kopp, J. L. *et al.* Sox9+ ductal cells are multipotent progenitors throughout development but do not produce new endocrine cells in the normal or injured adult pancreas. *Development* **138**, 653–665 (2011).

140. Furuyama, K. *et al.* Continuous cell supply from a Sox9-expressing progenitor zone in adult liver, exocrine pancreas and intestine. *Nat. Genet.* **43**, 34–41 (2011).

141. Belo, J., Krishnamurthy, M., Oakie, A. & Wang, R. The role of SOX9 transcription factor in pancreatic and duodenal development. *Stem Cells Dev.* **22**, 2935–2943 (2013).

142. Bastide, P. *et al.* Sox9 regulates cell proliferation and is required for Paneth cell differentiation in the intestinal epithelium. *J. Cell Biol.* **178**, 635–648 (2007).

143. Mori-Akiyama, Y. *et al.* SOX9 Is Required for the Differentiation of Paneth Cells in the Intestinal Epithelium. *Gastroenterology* **133**, 539–546 (2007).

144. Kawaguchi, Y. Sox9 and programming of liver and pancreatic progenitors Find the latest

version : Review series Sox9 and programming of liver and pancreatic progenitors. *J. Invest Clin* **123**, 1881–1886 (2013).

145. Akiyama, H. *et al.* Essential role of Sox9 in the pathway that controls formation of cardiac valves and septa. *Proc. Natl. Acad. Sci. U. S. A.* **101**, 6502–6507 (2004).

146. Lin, F. R., Niparko, J. K. & Ferrucci, and L. Sox9 is required for precursor cell expansion and extracellular matrix organization during mouse heart valve development. *Bone* **23**, 1–7 (2014).

147. Foster, J. W. *et al.* Campomelic dysplasia and autosomal sex reversal caused by mutations in an SRY-related gene. *Nature* vol. 372 525–530 (1994).

148. Huang, B., Wang, S., Ning, Y., Lamb, A. N. & Bartley, J. Autosomal XX sex reversal caused by duplication of SOX9. *Am. J. Med. Genet.* **87**, 349–353 (1999).

149. Vidal, V. P. I. *et al.* Sox9 is essential for outer root sheath differentiation and the formation of the hair stem cell compartment. *Curr. Biol.* **15**, 1340–1351 (2005).

150. Blanpain, C. & Fuchs, E. Epidermal stem cells of the skin. *Annu. Rev. Cell Dev. Biol.* **22**, 339–373 (2006).

151. Ross A. Poché, Yasuhide Furuta3, Marie-Christine Chaboissier4, Andreas Schedl4, and R. R. B. Sox9 Is Expressed in Mouse Multipotent Retinal Progenitor Cells and Functions in Müller Glial Cell Development. *Physiol. Behav.* **176**, 139–148 (2008).

152. Zhu, M. Y., Gasperowicz, M. & Chow, R. L. The expression of NOTCH2, HES1 and SOX9 during mouse retinal development. *Gene Expr. Patterns* **13**, 78–83 (2013).

153. Masuda, T. & Esumi, N. SOX9, through interaction with microphthalmia-associated transcription factor (MITF) and OTX2, regulates BEST1 expression in the retinal pigment

epithelium. *J. Biol. Chem.* **285**, 26933–26944 (2010).

154. Lefebvre V, D.-G. M. SOX9 and the many facets of its regulation in the chondrocyte lineage. **58**, 2–14 (2017).

155. Lefebvre, V., Huang, W., Harley, V. R., Goodfellow, P. N. & de Crombrugghe, B. SOX9 is a potent activator of the chondrocyte-specific enhancer of the pro alpha1(II) collagen gene. *Mol. Cell. Biol.* **17**, 2336–2346 (1997).

156. Jana, S. *et al.* SOX9: The master regulator of cell fate in breast cancer. *Biochem. Pharmacol.* **174**, (2020).

157. Edelman, H. E. *et al.* SOX9 modulates cancer biomarker and cilia genes in pancreatic cancer. *Hum. Mol. Genet.* **30**, 485–499 (2021).

158. Ma, F. *et al.* SOX9 drives WNT pathway activation in prostate cancer. *J. Clin. Invest.* **126**, 1745–1758 (2016).

159. Huang, Z. *et al.* Sox9 is required for prostate development and prostate cancer initiation. *Oncotarget* **3**, 651–663 (2012).

160. Santos, J. C. *et al.* SOX9 elevation acts with canonical WNT signaling to drive gastric cancer progression. *Cancer Res.* **76**, 6735–6746 (2016).

161. Li, X. L. *et al.* SOX9 was involved in TKIs resistance in renal cell carcinoma via Raf/MEK/ERK signaling pathway. *Int. J. Clin. Exp. Pathol.* **8**, 3871–3881 (2015).

162. Wang, H. Y., Lian, P. & Zheng, P. S. SOX9, a potential tumor suppressor in cervical cancer, transactivates p21WAF1/CIP1 and suppresses cervical tumor growth. *Oncotarget* **6**, 20711–20722 (2015).

163. Prévostel, C. *et al.* SOX9 is an atypical intestinal tumor suppressor controlling the oncogenic Wnt/β-catenin signaling. *Oncotarget* **7**, 82228–82243 (2016).

164. Bagheri-Fam, S. *et al.* Sox9 gene regulation and the loss of the XY/XX sex-determining mechanism in the mole vole Ellobius lutescens. *Chromosom. Res.* **20**, 191–199 (2012).

165. Sekido, R. & Lovell-Badge, R. Sex determination involves synergistic action of SRY and SF1 on a specific Sox9 enhancer. *Nature* **453**, 930–934 (2008).

166. Croft, B. *et al.* Human sex reversal is caused by duplication or deletion of core enhancers upstream of SOX9. *Nat. Commun.* **9**, 1–10 (2018).

167. Barrionuevo, F. *et al.* Homozygous inactivation of Sox9 causes complete XY sex reversal in mice. *Biol. Reprod.* **74**, 195–201 (2006).

168. Bishop, C. E. *et al.* A transgenic insertion upstream of Sox9 is associated with dominant XX sex reversal in the mouse. *Nat. Genet.* **26**, 490–494 (2000).

169. Gregoire, E. P. *et al.* Transient development of ovotestes in XX Sox9 transgenic mice. *Dev. Biol.* **349**, 65–77 (2011).

170. Matsushita, Y., Ono, W. & Ono, N. Skeletal Stem Cells for Bone Development and Repair: Diversity Matters. *Curr. Osteoporos. Rep.* **18**, 189–198 (2020).

171. Karsenty, G., Kronenberg, H. M. & Settembre, C. Genetic control of bone formation. *Annu. Rev. Cell Dev. Biol.* **25**, 629–648 (2009).

172. H., A., M.-C., C., J.F., M., A., S. & B., D. C. The transcription factor Sox9 has essential roles in successive steps of the chondrocyte differentiation pathway and is required for expression of Sox5 and Sox6. *Genes Dev.* **16**, 2813–2828 (2002).

173. Wagner, T. *et al.* Autosomal sex reversal and campomelic dysplasia are caused by mutations in and around the SRY-related gene SOX9. *Cell* **79**, 1111–1120 (1994).

174. McDowall, S. *et al.* Functional and structural studies of wild SOX9 and mutations causing campomelic dysplasia. *J. Biol. Chem.* **274**, 24023–24030 (1999).

175. Eggers, S. *et al.* Disorders of sex development: Insights from targeted gene sequencing of a large international patient cohort. *Genome Biol.* **17**, 1–21 (2016).

176. Karaer, K., Yüksel, Z., Yalinbaş, E. & Scherer, G. A case of campomelic dysplasia in whom a new mutation was found in the SOX9 gene. *Turk Pediatr. Ars.* **49**, 154–156 (2014).

177. Mansour, S., Hall, C. M., Pembrey, M. E. & Young, I. D. A clinical and genetic study of campomelic dysplasia. *J. Med. Genet.* **32**, 415–420 (1995).

178. Hattori, T. *et al.* SOX9 is a major negative regulator of cartilage vascularization, bone marrow formation and endochondral ossification. *Development* **137**, 901–911 (2010).

179. Barna, M. & Niswander, L. Visualization of Cartilage Formation: Insight into Cellular Properties of Skeletal Progenitors and Chondrodysplasia Syndromes. *Dev. Cell* **12**, 931–941 (2007).

180. Akiyama, H. *et al.* Interactions between Sox9 and beta-catenin control chondrocyte differentiation. *Genes Dev.* 1072–1087 (2004) doi:10.1101/gad.1171104.Wagner.

181. Soeda, T. *et al.* Sox9-expressing precursors are the cellular origin of the cruciate ligament of the knee joint and the limb tendons. *Genesis* **48**, 635–644 (2010).

182. Sugimoto, Y. *et al.* Scx+/Sox9+ progenitors contribute to the establishment of the junction between cartilage and tendon/ligament. *Development* **140**, 2280–2288 (2013).

183. Blitz, E., Sharir, A., Akiyama, H. & Zelzer, E. Tendon-bone attachment unit is formed modularly by a distinct pool of Scx - and Sox9 -positive progenitors . *Development* **140**, 2680–2690 (2013).

184. Balani, D. H., Trinh, S., Xu, M. & Kronenberg, H. M. Sclerostin Antibody Administration Increases the Numbers of Sox9creER+ Skeletal Precursors and Their Progeny. *J. Bone Miner. Res.* (2021) doi:10.1002/jbmr.4238.

185. Coutu, D. L., Kokkaliaris, K. D., Kunz, L. & Schroeder, T. Multicolor quantitative confocal imaging cytometry. *Nat. Methods* **15**, 39–46 (2018).

186. Kunz, L. & Coutu, D. L. Multicolor 3D Confocal Imaging of Thick Tissue Sections. *Methods Mol. Biol.* **2350**, 95–104 (2021).

187. Coutu, D. L., François, M. & Galipeau, J. Inhibition of cellular senescence by developmentally regulated FGF receptors in mesenchymal stem cells. *Blood* **117**, 6801–6812 (2011).

188. https://www.jax.org/strain/018829. https://www.jax.org/strain/018829.

189. https://www.jax.org/strain/007909. https://www.jax.org/strain/007909.

190. Baryawno, N. *et al.* A Cellular Taxonomy of the Bone Marrow Stroma in Homeostasis and Leukemia. *Cell* **177**, 1915-1932.e16 (2019).

191. Coutu, D. L. *et al.* Hierarchical scaffold design for mesenchymal stem cell-based gene therapy of hemophilia B. *Biomaterials* **32**, 295–305 (2011).

192. Decker, R. S. *Cell origin, volume and arrangement are drivers of articular cartilage formation, morphogenesis and response to injury in mouse limbs*. vol. 426 (2017).

193. Fitzgerald, J. *et al.* Evidence for articular cartilage regeneration in MRL/MpJ mice. *Osteoarthr. Cartil.* **16**, 1319–1326 (2008).

194. Coutu, D. L., Kokkaliaris, K. D., Kunz, L. & Schroeder, T. Multicolor quantitative confocal imaging cytometry. *Nat. Methods* **15**, 39–46 (2018).

195. Yang, B. *et al.* Single-cell phenotyping within transparent intact tissue through whole-body clearing. *Cell* **158**, 945–958 (2014).

196. He, X. *et al.* Sox9 positive periosteal cells in fracture repair of the adult mammalian long bone. 12–19 (2019) doi:10.1016/j.bone.2017.06.008.Sox9.

197. Stöckl, S., Göttl, C., Grifka, J. & Grässel, S. Sox9 modulates proliferation and expression of osteogenic markers of adipose-derived stem cells (ASC). *Cell. Physiol. Biochem.* **31**, 703–717 (2013).

198. Ferguson, V. L., Ayers, R. A., Bateman, T. A. & Simske, S. J. Bone development and age-related bone loss in male C57BL/6J mice. *Bone* **33**, 387–398 (2003).

199. Park, J. *et al.* Dual pathways to endochondral osteoblasts: A novel chondrocytederived osteoprogenitor cell identified in hypertrophic cartilage. *Biol. Open* **4**, 608–621 (2015).

200. Weinstein, R. S., Jilka, R. L., Michael Parfitt, A. & Manolagas, S. C. Inhibition of osteoblastogenesis and promotion of apoptosis of osteoblasts end osteocytes by glucocorticoids potential mechanisms of their deleterious effects on bone. *J. Clin. Invest.* **102**, 274–282 (1998).

201. Newton, P. T. *et al.* A radical switch in clonality reveals a stem cell niche in the epiphyseal growth plate. *Nature* **567**, 234–238 (2019).

202. WANG, T. & , XINPING ZHANG, and D. D. B. Osteogenic Differentiation of Periosteal

Cells During Fracture Healing. *Physiol. Behav.* **176**, 139–148 (2017).

203. Kuwahara, S. T. *et al.* Sox9+ messenger cells orchestrate large-scale skeletal regeneration in the mammalian rib. *Elife* **8**, 1–21 (2019).

204. Zhou, B. O., Yue, R., Murphy, M. M., Peyer, J. G. & Morrison, S. J. Leptin-receptor-expressing mesenchymal stromal cells represent the main source of bone formed by adult bone marrow. *Cell Stem Cell* **15**, 154–168 (2014).

205. Paul E. Bourgine, Thibaut Klein, Anna M. Paczulla, Takafumi Shimizu, Leo Kunz, Konstantinos D. Kokkaliaris, Daniel L. Coutu, Claudia Lengerke, Radek Skoda, Timm Schroeder, and I. M. In vitro biomimetic engineering of a human hematopoietic niche with functional properties. *Proc. Natl. Acad. Sci.* **115**, E5688–E5695 (2018).

206. Scotti, C. *et al.* Engineering of a functional bone organ through endochondral ossification. *Proc. Natl. Acad. Sci. U. S. A.* **110**, 3997–4002 (2013).

207. Bourgine, P. E. *et al.* Fate Distribution and Regulatory Role of Human Mesenchymal Stromal Cells in Engineered Hematopoietic Bone Organs. *iScience* **19**, 504–513 (2019).

208. Bonnefoix, T. & Callanan, M. Accurate hematopoietic stem cell frequency estimates by fitting multicell Poisson models substituting to the single-hit Poisson model in limiting dilution transplantation assays. *Blood* **116**, 2472–2475 (2010).

209. Xu, Z. *et al.* Embryonic attenuated Wnt/β-catenin signaling defines niche location and long- term stem cell fate in hair follicle. *Elife* **4**, (2015).

210. Kester, L. & van Oudenaarden, A. Single-Cell Transcriptomics Meets Lineage Tracing. *Cell Stem Cell* **23**, 166–179 (2018).

211. Haghverdi, L., Büttner, M., Wolf, F. A., Buettner, F. & Theis, F. J. Diffusion pseudotime

robustly reconstructs lineage branching. *Nat. Methods* **13**, 845–848 (2016).

212. Manno, G. La *et al.* RNA velocity of single cells. **560**, 494–498 (2019).

213. Chagin, A. S. & Newton, P. T. Postnatal skeletal growth is driven by the epiphyseal stem cell niche : potential implications to pediatrics. *Pediatr. Res.* (2020) doi:10.1038/s41390-019-0722-z.